Physics – Uspekhi **54** (10) 1007 – 1059 (2011)

REVIEWS OF TOPICAL PROBLEMS PACS numbers: **72.10.–d**, **73.23.–b**, 73.50.Td, 74.25.F–, **74.45.+c**, 74.78.Na

Scattering matrix approach to the description of quantum electron transport

G B Lesovik, I A Sadovskyy

DOI: 10.3367/UFNe.0181.201110b.1041

Contents

G B Lesovik Landau Institute for Theoretical Physics, Russian Academy of Sciences, prosp. Akademika Semenova 1-A, 142432 Chernogolovka, Moscow region, Russian Federation
Tel. (7-495) 137 32 44. Fax (7-495) 938 20 77
E-mail: glesovik@yandex.ru
I A Sadovskyy Rutgers University, 136 Frelinghuysen Rd, Piscataway, NJ, 08854, USA. E-mail: ivan.sadovsky@gmail.com

Received 12 December 2010
Uspekhi Fizicheskikh Nauk **181** (10) 1041 – 1096 (2011)
DOI: 10.3367/UFNr.0181.201110b.1041
Translated by M N Sapozhnikov; edited by A M Semikhatov

Abstract. We consider the scattering matrix approach to quantum electron transport in meso- and nanoconductors. This approach is an alternative to the more conventional kinetic equation and Green's function approaches, and is often more efficient for coherent conductors (especially when proving general relations) and typically more transparent. We provide a description of both time-averaged quantities (for example, current–voltage characteristics) and current fluctuations in time — noise, as well as full counting statistics of charge transport in a finite time. In addition to normal con-

ductors, we consider contacts with superconductors and Josephson junctions.

1. Introduction

Over the past 30 years, the study of electrical conductors have evolved from considering of macroscopic objects, in which the quantum nature is mainly manifested at the level of band structure formation, to the study of mesoscopic objects [1] at a scale larger than the atomic one but smaller than the characteristic length at which quantum correlations already appear, and finally to nanophysics objects at even smaller scales, down to the atomic ones (quantum contacts and quantum dots, molecular and quantum contacts, carbon nanotubes, and graphene).

Electron transport in conductors of a size comparable to inelastic scattering lengths, such as the energy relaxation length or the dephasing length, or even to Fermi wavelengths, has a number of specific features, the most important of which is a considerable transport nonlocality. For such conductors, it is meaningless to consider quantities such as local conductivity, and the question is actually asked about the electron transport from point A (left reservoir) to point B (right reservoir). In this case, the electron transfer through the conductor is a purely quantum mechanical process. This process can be described by using the well-known approach from the particle and atom scattering theory which consider an initial state (in our case, electron state), a scatterer, and a final state (reservoir to which the electron arrives) and where the transition from one state to another is described by the scattering matrix.

Last years the scattering matrix approach has been widely and successfully used to describe quantum transport. The difference between this approach and more traditional methods based, for example, on the kinetic equation, the Kubo formula, Green's functions, or diagram techniques, is mainly as follows. The total conductivity (or the total current) of a system can be expressed in terms of the conductor quantum transparency (in the general case, in terms of the scattering matrix) and the occupation numbers of exact electron scattering states, which are determined by parameters at the boundaries (reservoirs).

At first glance, such a method for describing electron transport only replaces the problem of calculating the local or nonlocal conductivity with the calculation of transmission, which is no less complicated. But this is not the case. First, in many cases with a simple sample geometry and a simple scattering potential, transmission can be calculated analytically, which is simpler, e.g., than calculating the Green's function. Second, it is often possible to make a reasonable assumption about the scattering matrix to describe experiments adequately. For disordered (dirty) conductors with a complex scattering potential, the transmission probabilities can be efficiently described statistically, for example, by methods developed for random matrices.

In addition, due to the development of mesoscopics and nanophysics, new problems appeared, which either had not attracted special attention earlier or seemed unrealistic for systems under study. One such problem is the description of not only the mean current but also its fluctuations and the full counting statistics as a whole in quantum meso- and nanoconductors. It was found that these problems can be efficiently solved by the scattering matrix method. It is important that even if the scattering matrix is unknown, i.e., is not calculated for a particular scattering potential, the full counting statistics for large times can formally be described, as can the mean current. Therefore, if the transmission is known, then we know not only the conductance $G = 1/R$, where R is the resistance, but also the spectral density $S(\omega)$ of current fluctuations at low frequencies, the distribution function $P(Q)$ of the charge transferred for a certain fixed time, and so on. In some cases, it is possible to derive general relations like the fluctuation–dissipation theorem, for example, relating the mean current and nonequilibrium fluctuations. The traditional approach would require calculating S, P, and other quantities different from the mean current each time.

2. Scattering matrix approach to the description of transport: the Landauer formula

The scattering matrix, taking asymptotically free incoming states through an interaction region and providing the free outgoing states, plays a tremendous role in quantum physics. This matrix, first introduced by Born [1] and then by Wheeler [2] and independently by Heisenberg [3, 4] to describe the scattering of particles and atoms, has been extensively used since the late 20th century in the theory of electron transport in quantum conductors.

The best-known result in the theory of quantum transport obtained with the help of the scattering matrix is the famous Landauer formula,[2] which is also called the Landauer–Büttiker formula. In fact, this formula in the form conventionally used first appeared in [6–8]. The conductance of a quasi-one-dimensional (one-channel) conductor is given by the conductance quantum $G_0 = 2e^2/h$ (where e is the electron charge, h is Planck's constant, and the factor 2 appears due to the spin degeneracy), known from the quantum Hall effect [9], times the transparency T of the conduction channel. In the case of several channels, the expression for the conductance

$$G = \frac{2e^2}{h} \sum_{n,m} T_{nm} \tag{1}$$

contains the sum of transmission probabilities T_{nm} from one mode (channel) to another (see the details in Section 3).

The Landauer approach was better understood in subsequent papers (for example, Imry [10] pointed out the role of a voltage drop at the input to the conductor) and extended to more complicated systems with many reservoirs, the quantum Hall effect regime [11–14], and hybrid superconducting systems [15–20], and was also used to describe current fluctuations in time [21–24]. Currently, this method has become very clear and functional. As a whole, this approach can be applied to the description of coherent mesoscopic conductors in which the characteristic size L of the voltage drop region is much smaller than all inelastic lengths.

[1] That is, objects with properties intermediate between microscopic and macroscopic. *Mesoscopic* translated from Greek means *intermediate scopic* or *mean scopic*.

[2] This formula is called this because Landauer [5] was the first to use scattering matrices to describe transport problems.

2.1 Conductance in a one-dimensional contact

To describe a quasi-one-dimensional conductor, we first consider a purely one-dimensional problem[3] for a system in which electron reservoirs are located to the left and to the right, far away from an obstacle located at the center, and emit electrons in the direction of this obstacle.

We assume that the left electron reservoir emits electrons in the direction of the obstacle (we forget about spin for the moment) with energies up to μ (experimentally, this may correspond to the presence of the bias voltage $V = \mu/e$). The conductor is coherent and the states are the Lippmann–Schwinger scattering states.

For such states belonging to the continuous spectrum, the problem of counting their number appears. For the continuous spectrum, 'box normalization' is often used, i.e., periodic boundary conditions are imposed and the conductor is closed to a circle with length L to make the spectrum discrete, after which the limit $L \to \infty$ is taken. But it is difficult to rigorously perform this procedure for scattering states, and we here solve this problem differently, by forming normalized wave packets from continuous-spectrum states.

By dividing the energy interval $[0, \mu]$ into N segments with size $\Delta = \mu/N$, we form the wave packets

$$\Psi_n(x,t) = c_n \int_{(n-1)\Delta}^{n\Delta} \mathrm{d}E\, \Psi_{\mathrm{L},E}(x) \exp\left(-\frac{\mathrm{i}Et}{\hbar}\right), \tag{2}$$

where $n = 1, \ldots, N$ and $\Psi_{\mathrm{L},E}(x)$ is the Lippmann–Schwinger scattering (left) state with energy E, having the asymptotic forms

$$\Psi_{\mathrm{L},E}(x) = \begin{cases} \exp(\mathrm{i}kx) + r(E)\exp(-\mathrm{i}kx), & x \to -\infty, \\ t(E)\exp(\mathrm{i}kx), & x \to \infty. \end{cases} \tag{3}$$

The normalization constant can be calculated from the relation

$$\int \mathrm{d}x\, \Psi^*_{\mathrm{L},E'}(x)\, \Psi_{\mathrm{L},E}(x) = 2\pi\delta(k' - k), \tag{4}$$

where $k = \sqrt{2mE}/\hbar$. Calculating the integral $\int \mathrm{d}x\, |\Psi_n(x,t)|^2$ and equating it to unity for the correct normalization of wave packets, we obtain

$$c_n = \frac{1}{\sqrt{hv_n\Delta}}, \tag{5}$$

where $v_n = \sqrt{2n\Delta/m}$ is the velocity of the nth packet; we assume that Δ is small.

The wave packets described by expressions (2) are localized in the vicinity of $x = 0$ at the instant $t = 0$ and have the characteristic size hv_n/Δ. These packets move at the speed v_n. As $\Delta \to 0$ (i.e., $N \to \infty$), the wave packets become broader, their shape approaching the shape of scattering states (3).

We now calculate the current I carried by a given orthonormalized set of wave packets. The current for them is additive (because, according to Pauli's principle, only one electron can occupy each state), and we can first calculate the contribution I_n to the current from each nth packet and then sum the contributions. For scattering states (as for any stationary states), the current is independent of the point at which we calculate it, and hence in the limit $\Delta \to 0$, the contribution to the current from each packet at $t = 0$,

$$I_n = -\mathrm{i}\,\frac{e\hbar}{2m}\left[\Psi^*_n(x)\Psi'_n(x) - \Psi'^*_n(x)\Psi_n(x)\right], \tag{6}$$

can be calculated, for example, to the right of the barrier, where the wave function has the known form $\Psi_{\mathrm{L}}(x) = t(E)\exp(\mathrm{i}kx)$. This gives

$$I_n = c_n^2\Delta^2 e v_n T(n\Delta) = \frac{e}{h}\,\Delta T(n\Delta), \tag{7}$$

where $T(E) = |t(E)|^2$ is the transparency at the energy E. Summing the contributions of all packets, we find

$$I = \sum_{n=1}^{N} I_n = \frac{e}{h}\,\Delta \sum_{n=1}^{N} T(n\Delta) \overset{(\Delta\to 0)}{\to} \frac{e}{h}\int_0^{\mu} \mathrm{d}E\, T(E), \tag{8}$$

where the sum over n transforms to the usual (Riemann) integral in the limit as $\Delta \to 0$. The conductance, defined as the ratio of the current I to the voltage $V = \mu/e$, is written in the form

$$G = \frac{I}{V} = \frac{e^2}{h}\int_0^{\mu} \frac{\mathrm{d}E}{\mu}\, T(E). \tag{9}$$

Expression (9) is a simple variant of the Landauer formula for the conductance [7, 25].

Because the wave functions of the continuous spectrum cannot be normalized in the usual way as the states of the discrete spectrum, it is not clear beforehand in the construction of a many-particle state from arbitrary states of the continuous spectrum which current is carried by each state. This question can be solved by dividing into wave packets and passing to the limit, as we did above. Such a procedure can be used in an explicit form to analyze intricate problems, for example, to describe the full transport statistics, as was done in [26]. The current can be calculated using the rule (which can also be derived by the method indicated above) allowing the summation of the contributions to the current from continuous-spectrum states: if $\psi_\xi(x)$ satisfies a normalization condition generalizing (4),

$$\int \mathrm{d}x\, \psi^*_\xi(x)\, \psi_{\xi'}(x) = c(\xi)\, \delta(\xi - \xi'), \tag{10}$$

then the mean of the current operator is given by

$$I = \int \frac{\mathrm{d}\xi}{c(\xi)}\, n(\xi) I_\xi, \tag{11}$$

where I_ξ is the current from the particle in the state $\psi_\xi(x)$ and $n(\xi)$ is the occupation number, equal to 1 if the state with the subscript ξ is present in the many-particle wave function (Slater determinant) and to 0 otherwise (at finite temperatures $\Theta > 0$, the number $n(\xi)$ can take values between 0 and 1). In the case discussed here, $\xi = k$, $I_k = -e\hbar k T(E)/m$, $c(k) = 2\pi$, and

$$n(k) = \begin{cases} 1, & \dfrac{\hbar^2 k^2}{2m} < \mu, \\ 0, & \dfrac{\hbar^2 k^2}{2m} > \mu. \end{cases}$$

[3] It is this problem that Landauer initially considered in [5]. The problem was solved by using an impressively small amount of knowledge: information on the setup and solution of scattering problems in the one-dimensional case in quantum mechanics and basic concepts about the degenerate electron gas at the general physics level.

Substituting these expressions in (11), we obtain

$$I = \frac{e\hbar}{m}\int_0^{k(\mu)} \frac{\mathrm{d}k}{2\pi}\, k\, T(E) = \frac{e}{h}\int_0^{\mu} \mathrm{d}E\, T(E)\,, \tag{12}$$

which corresponds to (8). At the last calculation step, we switched from integration over the wave vector k to integration over energy E, using the one-dimensional density of states

$$v(E) = \frac{\mathrm{d}k}{\mathrm{d}E} = \frac{m}{\hbar^2 k}\,. \tag{13}$$

This leads to the cancelation of the factor k in the integrand in (12), and it then follows that each energy interval (in the absence of scattering) carries the same current

$$i_0 = \frac{\delta I}{\delta E} = \frac{e}{h}\,, \tag{14}$$

which is a characteristic feature of the one-dimensional ballistic transport.

2.2 Two reservoirs

In Section 2.1, we discussed the case where spinless electrons were emitted by one reservoir. We now consider the more realistic case where spin-1/2 electrons are emitted by both reservoirs. We assume that the left reservoir with the electrochemical potential[4] μ_{L} emits the 'left' scattering states $\Psi_{\mathrm{L}}(x)$ and the right reservoir with the electrochemical potential μ_{R} emits the 'right' scattering states $\Psi_{\mathrm{R}}(x)$ (Fig. 1). Then the total current is determined by contributions from both reservoirs:

$$I_{\mathrm{L}} = \frac{2e}{h}\int_0^{\mu_{\mathrm{L}}} \mathrm{d}E\, T(E)\,, \tag{15}$$

$$I_{\mathrm{R}} = -\frac{2e}{h}\int_0^{\mu_{\mathrm{R}}} \mathrm{d}E\, T(E)\,, \tag{16}$$

where the factor 2 appears due to the spin degeneracy, and in contrast to I_{L}, the current I_{R} determined by the right states acquires a minus sign because the wave vector and velocity for $\Psi_{\mathrm{R}}(x)$ are opposite to those for $\Psi_{\mathrm{L}}(x)$. Here, we used the important property of the scattering matrix following from its unitarity and symmetry under time reversal, namely, that the transmission probabilities for mutually inverse processes are equal.[5] In our case, the transmission probability from left to right, $T = |t|^2$, is equal to the transmission probability from right to left, $T = T' = |t'|^2$. In the total current

$$I = I_{\mathrm{L}} + I_{\mathrm{R}} = \frac{2e}{h}\int_{\mu_{\mathrm{R}}}^{\mu_{\mathrm{L}}} \mathrm{d}E\, T(E)\,, \tag{17}$$

the contributions from energy intervals filled both on the left and on the right cancel, and only the states filled on one side make a contribution to the total current.

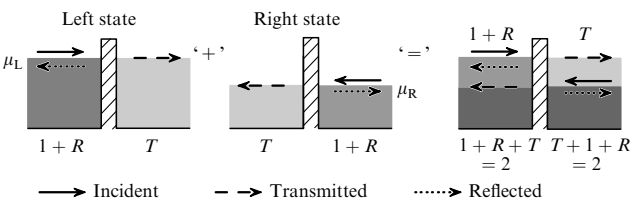

Figure 1. Charge density (shown by color gradation) caused by the left and right scattering states (we omit the details of Friedel oscillations and perform averaging over several wavelengths). The total densities of states with energies smaller than μ_{R} are equal (shown with dark grey). For the states with energies between μ_{R} and μ_{L}, the charge to the left of the scatterer is greater (for $T \neq 1$).

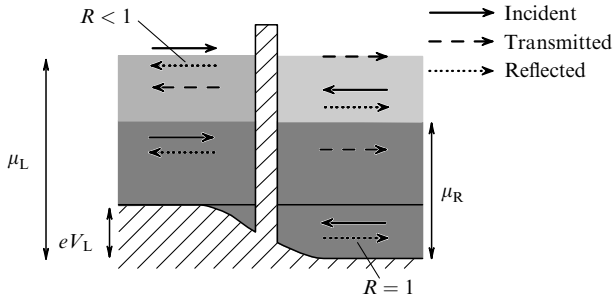

Figure 2. Occurrence of the Landauer voltage drop V_{L} on a barrier. Because of the bending of the conduction-band bottom caused by the voltage drop, the states emitted from the right reservoir with energies between 0 and eV_{L} are completely reflected. Here, $eV_{\mathrm{L}} > 0$, which corresponds to the negative voltage and electric current, but to the positive flow of particles (from left to right). This difference in signs appears because the electron charge is standardly assumed negative.

2.3 Landauer voltage drop

Having discussed the current caused by the difference in electrochemical potentials, we now address the question about the voltage drop on a scatterer. First, we determine the electron density produced in a nonequilibrium state, assuming that $\mu_{\mathrm{L}} > \mu_{\mathrm{R}}$ (Fig. 2). The left reservoir emits states (3) and the right reservoir emits the states $\Psi_{\mathrm{R},E}$. The total density to the right of the scatterer,

$$\rho_{\mathrm{R}} = 2\int_0^{k(\mu_{\mathrm{L}})} \frac{\mathrm{d}k}{2\pi}\, |\Psi_{\mathrm{L},E}(x)|^2 + 2\int_0^{k(\mu_{\mathrm{R}})} \frac{\mathrm{d}k}{2\pi}\, |\Psi_{\mathrm{R},E}(x)|^2$$
$$\approx 2\int_0^{k(\mu_{\mathrm{L}})} \frac{\mathrm{d}k}{2\pi}\, T(E) + 2\int_0^{k(\mu_{\mathrm{R}})} \frac{\mathrm{d}k}{2\pi}\, \left[1 + R(E)\right]\,, \tag{18}$$

is the sum of contributions from the left and right states (the factor 2 is due to spin degeneracy). (We do not consider the details of Friedel oscillations with the period $\pi/[k(\mu)]$ (see below) and perform averaging over several wavelengths $\propto \hbar/\sqrt{2m\mu}$.) Calculating the density on the left gives

$$\rho_{\mathrm{L}} \approx 2\int_0^{k(\mu_{\mathrm{L}})} \frac{\mathrm{d}k}{2\pi}\, \left[1 + R(E)\right] + 2\int_0^{k(\mu_{\mathrm{R}})} \frac{\mathrm{d}k}{2\pi}\, T(E)\,. \tag{19}$$

In the nonequilibrium situation, $\mu_{\mathrm{L}} \neq \mu_{\mathrm{R}}$, and if the transparency is not ideal, $T \neq 1$, then the density on the right of the scatterer does not coincide with that on the left (see Fig. 1).

[4] We recall that the electrochemical potential is the maximum total energy of one electron (at zero temperature), which is the sum of the kinetic (Fermi) energy and the potential energy (of a charge in the electrostatic potential).

[5] In the one-dimensional case, the equality of the transmission probabilities follows from the unitarity, even in the absence of the time reversal invariance.

The difference in densities is given by

$$\rho_{\mathrm{L}} - \rho_{\mathrm{R}} = 4 \int_{k(\mu_{\mathrm{R}})}^{k(\mu_{\mathrm{L}})} \frac{\mathrm{d}k}{2\pi} R(E)\,, \tag{20}$$

where we use the relation $R(E) + T(E) = 1$. If the quantum conductor is electrically neutral, then this density difference should be compensated by the voltage drop across the scatterer, which bends the conduction-band bottom. This (Landauer) voltage drop V_{L} in the stationary case can be obtained from the condition of electrical neutrality, which, as assumed, takes place in the equilibrium; in particular, the density should be the same on both sides of the barrier (see Fig. 2).

In the presence of a voltage drop V_{L}, the left states with the energy E (measured from the conduction band bottom in the right reservoir) have the form

$$\Psi_{\mathrm{L},E}(x) = \begin{cases} \exp(\mathrm{i}kx) + r(E)\exp(-\mathrm{i}kx)\,, & x \to -\infty\,, \\ \sqrt{\dfrac{k}{\tilde{k}}}\, t(E)\exp(\mathrm{i}\tilde{k}x)\,, & x \to \infty\,, \end{cases} \tag{21}$$

where $k(E) = \sqrt{2m(E - eV_{\mathrm{L}})}/\hbar$ and $\tilde{k}(E) = \sqrt{2mE}/\hbar$ are the wave vectors in the left and right asymptotic regions, respectively. Similarly, the right scattering states are

$$\Psi_{\mathrm{R},E}(x) = \begin{cases} \exp(-\mathrm{i}\tilde{k}x) + r'(E)\exp(\mathrm{i}\tilde{k}x)\,, & x \to \infty\,, \\ \sqrt{\dfrac{\tilde{k}}{k}}\, t'(E)\exp(-\mathrm{i}kx)\,, & x \to -\infty\,. \end{cases} \tag{22}$$

The factor $\sqrt{k/\tilde{k}}$ appears due to the unitarity of the scattering matrix. We also note that the scattering problem must be solved taking the bending of the conduction-band bottom due to the Landauer voltage V_{L} into account. For example, due to the appearance of this voltage, the right scattering states with energies $E < eV_{\mathrm{L}}$ are completely reflected and $R(E) = 1$. The averaged density on the left, caused by the left scattering states, is given by

$$\rho_{\mathrm{LL}} = 2 \int_0^{k(\mu_{\mathrm{L}})} \frac{\mathrm{d}k}{2\pi} \left[1 + R(E)\right], \tag{23}$$

where the factor 2 is due to spin degeneracy. The density on the left, caused by the right states, takes the form

$$\rho_{\mathrm{LR}} = 2 \int_{\tilde{k}(eV_{\mathrm{L}})}^{\tilde{k}(\mu_{\mathrm{R}})} \frac{\mathrm{d}\tilde{k}}{2\pi} \frac{\tilde{k}}{k}\, T(E)\,. \tag{24}$$

Similarly, calculating the density on the right, we find

$$\rho_{\mathrm{RL}} = 2 \int_0^{k(\mu_{\mathrm{L}})} \frac{\mathrm{d}k}{2\pi} \frac{k}{\tilde{k}}\, T(E)\,, \tag{25}$$

$$\rho_{\mathrm{RR}} = 2 \int_{\tilde{k}(eV_{\mathrm{L}})}^{\tilde{k}(\mu_{\mathrm{R}})} \frac{\mathrm{d}\tilde{k}}{2\pi} \left[1 + R(E)\right] + 2 \int_0^{\tilde{k}(eV_{\mathrm{L}})} \frac{\mathrm{d}\tilde{k}}{2\pi} (1 + 1)\,, \tag{26}$$

where the last term appears due to the right states completely reflected at the conduction-band bottom.

To simplify further calculations, we switch to integrals over energies. For ρ_{LL}, we then obtain ($\mathrm{d}k = (m/\hbar^2 k)\,\mathrm{d}E$)

$$\rho_{\mathrm{LL}} = \frac{2}{\hbar}\sqrt{\frac{m}{2}} \int_{eV_{\mathrm{L}}}^{\mu_{\mathrm{L}}} \frac{\mathrm{d}E}{2\pi} \frac{1 + R(E)}{\sqrt{E - eV_{\mathrm{L}}}}\,. \tag{27}$$

Similarly, for $\mathrm{d}\tilde{k} = (m/\hbar^2 \tilde{k})\,\mathrm{d}E$, we have

$$\rho_{\mathrm{LR}} = \frac{2}{\hbar}\sqrt{\frac{m}{2}} \int_{eV_{\mathrm{L}}}^{\mu_{\mathrm{R}}} \frac{\mathrm{d}E}{2\pi} \frac{T(E)}{\sqrt{E - eV_{\mathrm{L}}}}\,. \tag{28}$$

Calculations for ρ_{RL} and ρ_{RR} give

$$\rho_{\mathrm{RL}} = \frac{2}{\hbar}\sqrt{\frac{m}{2}} \int_{eV_{\mathrm{L}}}^{\mu_{\mathrm{L}}} \frac{\mathrm{d}E}{2\pi} \frac{T(E)}{\sqrt{E}}\,, \tag{29}$$

$$\rho_{\mathrm{RR}} = \frac{2}{\hbar}\sqrt{\frac{m}{2}} \int_{eV_{\mathrm{L}}}^{\mu_{\mathrm{R}}} \frac{\mathrm{d}E}{2\pi} \frac{1 + R(E)}{\sqrt{E}} + \frac{2}{\hbar}\sqrt{\frac{m}{2}} \int_0^{eV_{\mathrm{L}}} \frac{\mathrm{d}E}{2\pi} \frac{2}{\sqrt{E}}\,. \tag{30}$$

Summing the densities on the left, $\rho_{\mathrm{L}} = \rho_{\mathrm{LL}} + \rho_{\mathrm{LR}}$, and using the relation $T(E) + R(E) = 1$, we obtain

$$\rho_{\mathrm{L}} = \frac{2}{\hbar}\sqrt{\frac{m}{2}} \int_{eV_{\mathrm{L}}}^{\mu_{\mathrm{R}}} \frac{\mathrm{d}E}{2\pi} \frac{2}{\sqrt{E - eV_{\mathrm{L}}}} + \frac{2}{\hbar}\sqrt{\frac{m}{2}} \int_{\mu_{\mathrm{R}}}^{\mu_{\mathrm{L}}} \frac{\mathrm{d}E}{2\pi} \frac{1 + R(E)}{\sqrt{E - eV_{\mathrm{L}}}}\,, \tag{31}$$

while the total density on the right is given by

$$\rho_{\mathrm{R}} = \frac{2}{\hbar}\sqrt{\frac{m}{2}} \int_0^{\mu_{\mathrm{R}}} \frac{\mathrm{d}E}{2\pi} \frac{2}{\sqrt{E}} + \frac{2}{\hbar}\sqrt{\frac{m}{2}} \int_{\mu_{\mathrm{R}}}^{\mu_{\mathrm{L}}} \frac{\mathrm{d}E}{2\pi} \frac{T(E)}{\sqrt{E}}\,. \tag{32}$$

Assuming the electric neutrality, we should equate the densities:[6]

$$\int_{\mu_{\mathrm{R}}}^{\mu_{\mathrm{L}}} \frac{\mathrm{d}E}{2\pi} \frac{1 + R(E)}{\sqrt{E - eV_{\mathrm{L}}}} = \int_{\mu_{\mathrm{R}} + eV_{\mathrm{L}}}^{\mu_{\mathrm{R}}} \frac{\mathrm{d}E}{2\pi} \frac{2}{\sqrt{E}} + \int_{\mu_{\mathrm{R}}}^{\mu_{\mathrm{L}}} \frac{\mathrm{d}E}{2\pi} \frac{T(E)}{\sqrt{E}}\,. \tag{33}$$

Equation (33) allows calculating the voltage V_{L} for an arbitrary energy dependence of the transparency and an arbitrary difference of electrochemical potentials.

We consider a simple linear case and find V_{L} for a small difference $\Delta\mu \equiv \mu_{\mathrm{L}} - \mu_{\mathrm{R}} \ll \mu_{\mathrm{R}}$. Under such conditions, the voltage drop is also small, $|eV_{\mathrm{L}}| \ll \mu_{\mathrm{L}}$. We assume that $T(E)$ is constant on the interval $[\mu_{\mathrm{R}}, \mu_{\mathrm{L}}]$. Then replacing $\sqrt{E - eV_{\mathrm{L}}} \to \sqrt{E}$ in (33) and taking T and R out of the integrand, we express the Landauer voltage as

$$eV_{\mathrm{L}} = \Delta\mu R\,. \tag{34}$$

The voltage V_{L} is zero for an ideally transparent conductor and reaches the maximum $eV_{\mathrm{L}} = \Delta\mu$ when all the electrons are reflected. The current is [see expression (17)]

$$I = \frac{2e}{h}\, T\Delta\mu\,, \tag{35}$$

which gives the Landauer resistance

$$R_{\mathrm{L}} = \frac{V_{\mathrm{L}}}{I} = \frac{h}{2e^2}\frac{R}{T}\,. \tag{36}$$

The absence of the voltage drop in an ideal conductor was the object of intensive discussions for a long time. It finally became clear that the voltage drop occurs even in this case, but in joints with reservoirs rather than in the conductor itself (see the discussion in Section 2.4).

[6] In the nonlinear case, the additional requirement of the equality of densities to their equilibrium values gives the displacement of the barrier 'pedestal' with respect to electrochemical potentials at the boundaries.

2.4 Contact resistance

Equating $\Delta\mu$ in (35) to the value specified by the bias voltage eV, we obtain the conductance $G = I/V$ in the form[7]

$$G = \frac{2e^2}{h}\,T\,. \tag{37}$$

Resistance (36) is different from the inverse of G in 'Landauer formula' (37). We can assume that (37) is the conductance measured by the two-contact method, whereas (36) is the resistance measured by the four-contact method.[8] The Landauer resistance takes only the voltage drop directly across the barrier into account.[9] However, in a one-dimensional conductor, the voltage drop also appears in contacts with reservoirs, which is the reason for the discrepancy between the two Landauer formulas. Subtracting $V_{\rm L}$ from the bias voltage $\Delta\mu = eV$, we obtain the voltage drop $V_{\rm A}$ at the conductor entrances:

$$V_{\rm A} = \Delta\mu - eV_{\rm L} = \Delta\mu T\,.$$

The total voltage drop can be written as the sum

$$V = V_{\rm A} + V_{\rm LD} = IR_{\rm L} + IR_{\rm A}$$
$$= I\,\frac{h}{2e^2}\,\frac{1-T}{T} + I\,\frac{h}{2e^2} = I\,\frac{h}{2e^2 T} = \frac{I}{G}\,.$$

In the symmetric case, the voltage drop is distributed equally between contacts. The voltage drop $V_{\rm A}/2$ at each boundary (contact) corresponds to the resistance

$$R_{\rm S} = \frac{h}{4e^2}\,, \tag{38}$$

which is the quantum analogue of the known Sharvin resistance [28]. We can assume that this resistance is caused by the reflection of higher modes at the wire entrance (see Section 4).

Figure 3 shows the example of a ballistic conductor ($T = 1$). Applying a voltage, we obtain the nonzero current $I = 2e^2/hV$, although no voltage drop occurs in the one-dimensional conductor itself due to the absence of backward reflection. The distribution of the voltage equally between contacts has been studied theoretically in detail [29, 30] and verified experimentally [31, 32]. As a whole, the described situation is quite unusual from the standpoint of the classical local conduction: the electric field inside the conductor is absent (Fig. 4), although the total current is nonzero. It is also unusual that the Joule heat dissipates far from the reservoirs due to slow energy relaxation, whereas the electromagnetic energy, from the standpoint of classical electrodynamics, enters the electron system at much smaller scales, in voltage drop regions in contacts and at the barrier.

To conclude, we note that the oscillating part of the electron density (and its slowly changing part at a finite voltage), which we did not consider above, can lead to an additional scattering of electrons. Density oscillations

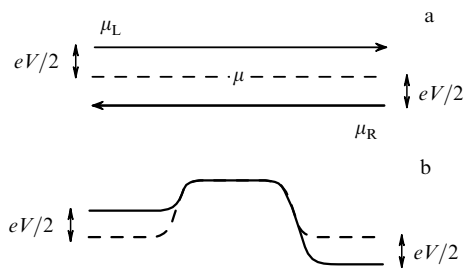

Figure 3. (a) Absence of the voltage drop in an ideal conductor. (b) Initial one-dimensional electrostatic potential (dashed curve) and its modification by the bias voltage (solid curve).

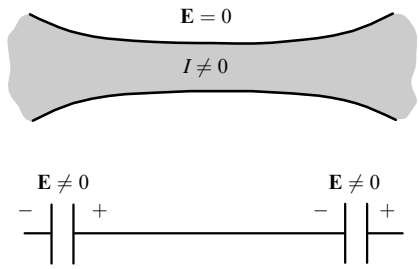

Figure 4. Input and output voltage drops in a ballistic one-channel conductor.

(Friedel oscillations) are not completely screened and produce a spatially dependent electrostatic potential. The oscillating part of the potential is especially important because the oscillation period is equal to $\pi/k_{\rm F}$ and backscattering from it (by $2k_{\rm F}$ in the momentum space) is strong [33]. Therefore, the transmission probability $T(E)$ taking the total scattering potential into account can strongly differ from the bare probability (determined on a local scatterer); in addition, this probability depends on the voltage V in principle. Assuming that the reflection amplitude is independent of energy, we can obtain the oscillating part of the density in equilibrium in the form

$$\delta n(x) = \frac{1}{|x|}\left\{\mathrm{Im}\,(r)\left[\cos\left(2k_{\rm F}x\right) - 1\right] + \mathrm{Re}\,(r)\sin\left(2k_{\rm F}|x|\right)\right\}.$$

The case of energy-independent r is realistic, for example, for almost complete reflection ($r \approx -1$), but similar oscillating dependences also appear for an arbitrary scatterer.

We once more emphasize the difference between our approach and more traditional methods: instead of the calculation of the nonlocal conductivity $\sigma(r, r')$ for use in the expression

$$j_\alpha(r) = \int \sigma(r, r')_{\alpha\beta}\, E_\beta(r')\,\mathrm{d}r'\,, \tag{39}$$

we calculate the total conductance determining the total current $I = GV$ as a function of voltage. The convenience of such an approach is obvious, because, instead of the self-consistent calculation of the field E for use in (39), only the total voltage drop V must be known. In this case, the conductance can be expressed in terms of the probability of transmission through the conductor. (Yet, to exactly solve the scattering problem in the nonlinear case, the electrostatic potential inside the conductor must also be known.)

[7] Below, we do not explicitly indicate the energy dependence of the transparency and elements of the scattering matrix, except in the cases where this dependence is being studied.

[8] We note that in this case, the actually measured resistance is also ill defined and depends on experimental conditions [27].

[9] Below, we will consider the case where such voltages can be summed in the usual way, as in an ohmic conductor.

In Section 3, to solve a broader class of problems, we consider a multichannel conductor as a waveguide for electrons.

3. Waveguides: the multichannel case

We describe a quantum conductor as a wire smoothly connected to reservoirs. More formally, we consider the geometry convenient for the description of such a system.

A quasi-one-dimensional system is formed as a constriction with infinitely high walls (or with a potential increasing at infinity) in transverse directions (y, z), such that transport is possible only along the x axis (Fig. 5). Along the x axis, plane waves can propagate that belong to different modes or, as is customarily said in mesoscopic physics, to channels having the spatial structure of bound states in transverse directions. The waveguide can transfer many modes. At low temperatures in a narrow waveguide, only the first mode is significant and the transport becomes effectively one-dimensional (we actually discussed this situation in Section 2). In the general case, the number of conducting modes (channels) involved in transport is finite.

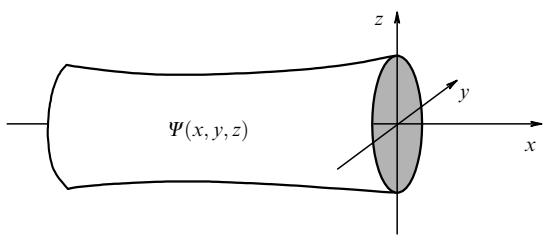

Figure 5. Waveguide elongated along the x axis with an adiabatically slowly varying cross section.

3.1 Quantized modes

We recall how in a simple case, in the presence of translational invariance (along the x axis), modes appear due to the transverse motion quantization. We must solve the Schrödinger equation

$$\left[-\frac{\hbar^2}{2m}\,\Delta + V(x,y,z)\right]\Psi(x,y,z) = E\Psi(x,y,z)\,, \tag{40}$$

where the potential $V(x,y,z) = V(y,z)$ and boundary conditions are temporarily considered independent of x. In this case, we can seek a solution of Eqn (40) in the form $\Psi(x,y,z) = \chi(y,z)\exp(\mathrm{i}kx)$. After the substitution of a function of this type in (40), the variables separate and we obtain the eigenvalue equation

$$\left[-\frac{\hbar^2}{2m}\,(\partial_y^2 + \partial_z^2) + V(y,z)\right]\chi_n(y,z) = E_n\chi_n(y,z)\,, \tag{41}$$

where n is the mode (channel) index, $\chi_n(y,z)$ is the corresponding wave function, and E_n is the transverse direction quantization energy. The functions $\chi_n(y,z)$ form a complete set,

$$\sum_n \chi_n(y,z)\,\chi_n^*(y',z') = \delta(y-y')\,\delta(z-z')\,, \tag{42}$$

which also orthonormalized,

$$\int \mathrm{d}y\,\mathrm{d}z\,\chi_m^*(y,z)\,\chi_n(y,z) = \delta_{mn}\,. \tag{43}$$

The general solution of Eqn (40) can be decomposed with respect to these functions as

$$\Psi(x,y,z) = \sum_n c_n\chi_n(y,z)\exp(\mathrm{i}k_n x)\,, \tag{44}$$

where $k_n = \sqrt{2m(E-E_n)}/\hbar$ is the wave vector in the nth mode (channel) and c_n are constants. Modes with energies $E < E_n$ decay as $\exp(-\varkappa_n x)$, where $\varkappa_n = \sqrt{2m(E_n - E)}/\hbar$.

3.2 Scattering problem in a waveguide

We consider a system that is a translation-invariant waveguide for $x \to \pm\infty$. Asymptotic solutions are described by expression (44). If an additional potential or a change in the boundary conditions exists in the vicinity of a finite $x \approx x_s$, then we can formulate a scattering problem. We assume that the incident (from left or right) wave has the form

$$\Psi^{\mathrm{in}}(x,y,z) = \chi_n(y,z)\exp\left(-\mathrm{i}k_n|x|\right). \tag{45}$$

Scattered waves can be written as

$$\Psi^{\mathrm{out}}(x,y,z) = \sum_m S_{mn}\sqrt{\frac{k_n}{k_m}}\,\chi_m(y,z)\exp\left(\mathrm{i}k_m|x|\right), \tag{46}$$

where the sum over m channels is taken for both transmitted $(S_{mn} = t_{mn})$ and reflected $(S_{mn} = r_{mn})$ states. The additional factor $\sqrt{k_n/k_m}$ is introduced to preserve the unitarity of the scattering matrix S_{mn}, and hence each of the asymptotic states $\chi_n(y,z)\exp(\mathrm{i}k_n x)/\sqrt{k_n}$ carries the unit current.

We calculate the electric current in the waveguide to the right of the scattering potential. Let μ_1 and μ_2 be electrochemical potentials of the reservoirs, and the electron distribution functions in them have the form

$$f_\alpha(E) = \frac{1}{\exp\left[(E-\mu_\alpha)/\Theta_\alpha\right]+1}\,, \quad \alpha = 1,2, \tag{47}$$

where Θ_α is the reservoir temperature in energy units. We assume here that the temperatures Θ_1 and Θ_2 are equal. Electrons with energy E emerging from the nth channel of the left reservoir $(\alpha = 1)$ make a contribution to the current in the unit energy interval to the left of the scattering potential (as in purely one-dimensional problems considered in Section 2), which is proportional to $f_1(E)(2e/h)$, while to the right, after scattering to the mth channel, they make a contribution proportional to $f_1(E)(2e/h)T_{nm}$. Electrons emerging to the right of the nth channel provide an initial current of the opposite sign $-f_2(E)(2e/h)$ and, after backscattering, also make the contribution $(2e/h)f_2(E)\sum_m R_{nm}$. As a result, after summation over channels, the current is given by

$$I = \frac{2e}{h}\sum_{n,m}\int_0^\infty \mathrm{d}E\left[f_1(E)T_{nm} - f_2(E)(\delta_{nm} - R_{nm})\right], \tag{48}$$

where $\delta_{nm} = 1$ for $n = m$ and $\delta_{nm} = 0$ for $n \neq m$. Similarly, we can formulate the scattering problem in the multilead case by replacing mode (channel) numbers by reservoir indices or by adding modes (channels) (Fig. 6). We now take the unitarity of the scattering matrix into account to simplify the expression for the current:

$$I = \frac{2e}{h}\sum_{n,m}\int_0^\infty \mathrm{d}E\,T_{nm}\left[f_1(E) - f_2(E)\right]. \tag{49}$$

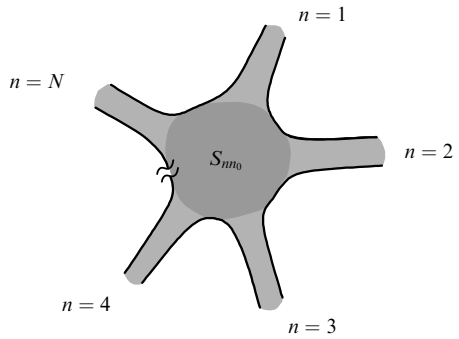

Figure 6. Multilead conductor.

The sum over the transparencies in (49) can sometimes be conveniently written as the trace of the scattering amplitude matrix. In this case, we obtain the conductance in the form

$$G = \frac{2e^2}{h}\,\mathrm{Tr}\,\{tt^\dagger\}\,. \tag{50}$$

In what follows, with the products of the transmission and reflection amplitude matrices of types $tt^\dagger$ and $1 - rr^\dagger$ appearing in expressions not only for current but also for noise and more complicated quantities, it is very important that due to the unitarity of S, such Hermitian matrices have the same set of eigenvalues $T_1, T_2, \ldots, T_N$, and the product of matrices such as $tt^\dagger tt^\dagger$ has the eigenvalues $T_1^2, T_2^2, \ldots, T_N^2$, and so on. Each of these transparency eigenvalues is a real number in the interval $[0, 1]$ (see [23, 34, 35]). In turn, such a diagonalization of the problem implies the presence of eigenmodes (channels) representing the superposition of states of type (44), which are no longer mixed after scattering. The conductance in the diagonal representation has the form

$$G = \frac{2e^2}{h}\,\mathrm{Tr}\,\{tt^\dagger\} = \frac{2e^2}{h}\sum_n T_n\,. \tag{51}$$

3.3 Waveguide with an adiabatically slowly changing cross section

In the general case, the boundary conditions and the potential in (4) are inhomogeneous. Nevertheless, changes are often rather slow and small at the wavelength scale. In this case, we can use the adiabatic approximation to separate rapid transverse motion in the waveguide and slow motion along it. The eigenvalue equation for rapid motion takes the form

$$\left[-\frac{\hbar^2}{2m}(\partial_y^2 + \partial_z^2) + V(x,y,z)\right]\chi_n(x,y,z) = E_n(x)\,\chi_n(x,y,z) \tag{52}$$

for each cross section (see Fig. 5). In this case, the transverse quantization energy $E_n(x)$ becomes slightly dependent on x. Assuming the adiabaticity, we substitute

$$\Psi(x,y,z) = \chi_n(x,y,z)\,\phi_n(x)\,, \tag{53}$$

where $\phi_n(x)$ is the solution of the equation

$$\left(-\frac{\hbar^2}{2m}\frac{\mathrm{d}^2}{\mathrm{d}x^2} + E_n(x)\right)\phi_n(x) = E\phi_n(x) \tag{54}$$

for motion along the wire. We note that the transverse quantization energy $E_n(x)$ serves as the effective potential $U(x)$ for slow motion along x. Expression (53) is an approximate solution of the Schrödinger equation with the mode mixing neglected. The approximation validity conditions are

$$\left|\frac{\partial_x\chi_n(x,y,z)}{\chi_n(x,y,z)}\right| \ll \left|\frac{\partial_x\phi_n(x)}{\phi_n(x)}\right| = \left|k(x)\right|\,, \tag{55}$$

$$\left|\frac{\partial_x^2\chi_n(x,y,z)}{\chi_n(x,y,z)}\right| \ll \left|\frac{\partial_x^2\phi_n(x)}{\phi_n(x)}\right| \approx \left|k^2(x)\right|\,. \tag{56}$$

We now consider the important example of a real waveguide, a microscopic constriction (a quantum point contact) in the two-dimensional electron gas.

4. Quantum contacts

4.1 Current through a quantum point contact

We consider a contact between two conductors. If the contact width W is so small that no more than a few electron wavelengths λ_F fit in it, such a contact is called a quantum point contact (QPC). The point contact can be realized in experiments in the following way [36, 37]: two massive electrodes are connected with a layer of the two-dimensional electron gas (2DEG) formed in the region of a semiconductor heterojunction (Fig. 7). Then two gates are brought to the 2DEG layer from above.[10] By applying a potential V_g to the gate, we can 'expel' electrons from regions near the gate, making them unavailable for electrons and thereby producing a constriction in the 2DEG (a point contact). The higher the voltage applied across the gate is, the larger the region forbidden for electrons and the stronger the narrowing.

We consider a system with connected reservoirs N_1 and N_2 (Fig. 8) and assume that the system is two-dimensional, corresponding to the standard experimental situation presented in Fig. 7.[11] We choose the direction of the x and y axes as shown in Fig. 8. The two-dimensional electron gas lying in the xy plane is additionally restricted in the y direction by means of voltages applied across the gates. We simulate the walls by the boundary condition

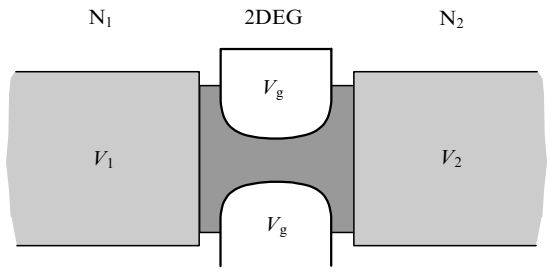

Figure 7. Diagram of the experimental realization of a point contact. Two massive electrodes are connected via a two-dimensional electron gas layer formed in a semiconductor heterostructure. A constriction is produced by the voltage V_g applied to the gates.

[10] This is the so-called *split gate technique* developed in [37, 38].

[11] More precisely, the size quantization along the z axis is so strong that under all standard experimental conditions, only the lowest mode is always filled.

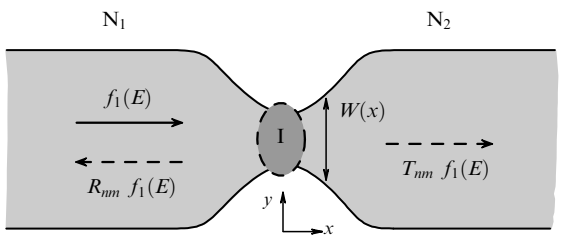

Figure 8. Point contact in the form of a constriction. The constriction width is described by a function $W(x)$ with a minimal value W_0. Inside the constriction, a scatterer I (for example, impurities) can be located.

$\Psi[x, \pm W(x)/2] = 0$, making motion possible only in a strip of the width $W(x)$ along the x axis. Assuming that $W(x)$ varies slowly and the mean free path in 2DEG greatly exceeds all the characteristic dimensions of the contact, we obtain

$$\chi_n(x, y) = \sqrt{\frac{2}{W(x)}}\, \sin\left(n\pi\, \frac{y + W(x)/2}{W(x)}\right) \tag{57}$$

for the transverse modes. The wave function $\phi_n(x)$ satisfies Eqn (54) describing motion in the effective potential $U(x) = E_n(x) = \hbar^2\pi^2 n^2/(2mW^2(x))$, $n \geqslant 1$. The applicability conditions for (55) and (56) now become $W'(x)/W(x) \ll k(x)$ and $W''(x)/W(x) \ll k^2(x)$. We let W_0 denote the minimal value of $W(x)$. Then the effective potential (depending on the transverse quantum number n) in the resultant Schrödinger equation has the form of a potential barrier with the height

$$E_n = \frac{(n\pi\hbar)^2}{2mW_0^2}\,, \tag{58}$$

decreasing to zero as $x \to \pm\infty$ (Fig. 9).

For a wave function with the mode number n, the transverse motion of an electron is specified by the condition that an integer number of half waves $\lambda_F/2$ fit in the contact width. Therefore, for electrons flowing through the contact, either one or two, or three, and so on half-waves fit in the contact width. These waveguide modes are called channels. For example, it is customary to say that an electron in the state with the wave function χ_n is in the nth channel.[12]

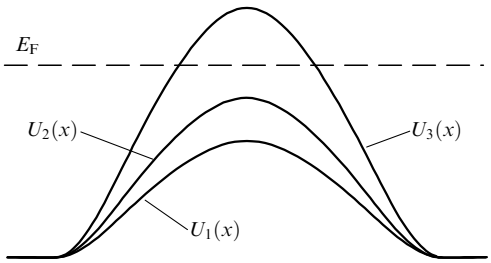

Figure 9. Example of the effective potential $U_n(x)$ appearing due to the effect of contact walls. For each n, the potential has the maximum value E_n determined by the smallest width. The current is provided by electrons with energies close to the Fermi energy E_F. The picture in the figure corresponds to two open channels (channels 1 and 2, because the relation $E_F > E_n$ is satisfied only for them).

[12] The terms 'channels' and 'leads' should be distinguished in multilead systems.

Since $W(x)$ changes slowly, Eqn (54) can be solved in the semiclassical approximation. In the leading approximation, only electrons with energies $E > E_n$ propagate through the throat. In the general case, the additional scattering of electrons in the narrowing, for example, from the impurity potential, must be taken into account. Such a scatterer is schematically shown by the dashed contour in Fig. 8.

4.2 Conductance quantization

We now consider the linear conductance $G = \mathrm{d}I/\mathrm{d}V$ at $V \to 0$. We assume that scattering by impurities in the constriction is absent and channels do not mix. Then expression (51) defines the conductance directly in terms of the transparencies T_n in each channel:

$$G = \frac{2e^2}{h} \sum_n T_n(E_F)\,. \tag{59}$$

The quantity $G_0 = 2e^2/h$, which is called the conductance quantum, is the natural unit for conductance measurements in mesoscopic systems. In the zeroth-order semiclassical approximation described in Section 2, $T_{nm} = \delta_{nm}$ for 'open' channels, whence

$$G = NG_0\,, \qquad N = \sum_n \theta(E_F - E_n)\,, \tag{60}$$

where N is the number of open channels and θ is the Heaviside function.

We consider how G changes when we change the QPC width W_0 by applying a voltage across the gate (see Fig. 9). If $W_0 \to 0$, we obtain $E_F < E_1$; therefore, $N = 0$ and electrons cannot pass through the QPC. This effect can be simply explained qualitatively: in a narrow QPC, due to the Heisenberg uncertainty principle, an electron should have a large quantization energy, and if this energy exceeds the specified energy, the presence of the electron in this region is forbidden. If $E_1 < E_F < E_2$, then one channel is open and $G = G_0$. If $E_2 < E_F < E_3$, then two channels are open; therefore, $G = 2G_0$, and so on. The QPC conductance is thus quantized in G_0 units (Fig. 10), similarly to the case of the integer quantum Hall effect (IQHE).[13] The analogy becomes even more direct in the presence of the Zeeman splitting (see Section 5.1), when the steps are split and the conductance is quantized in $G_0/2$ units, as in the IQHE.

The step height in the experimental plot in Fig. 10b obeys the quantization rule with good accuracy, whereas the step edges are smeared. This can be caused by different factors, such as a finite temperature, the finite probabilities of the underbarrier transmission and overbarrier reflection, and so on (see Section 4.3). It is interesting that the experimental constriction was rather small (Fig. 11), suggesting that quantization should not be so pronounced. This puzzle was solved in paper [40] (almost immediately after the publication of experimental results). It was found that the quantization conditions remained valid until the angle α was greater than $1/\pi^2$ rather than unity, as would be expected (the condition of

[13] For a waveguide with a two-dimensional effective cross section, the quantization picture can be much more intricate, because it depends on the energy level structure in a two-dimensional box formed by the cross section. When a certain spatial symmetry exists and a two-dimensional problem is integrable (for example, if the wire cross section is nearly circular), the levels are grouped and, when the parameters are changed, several channels can be 'switched on' at once, almost simultaneously [39].

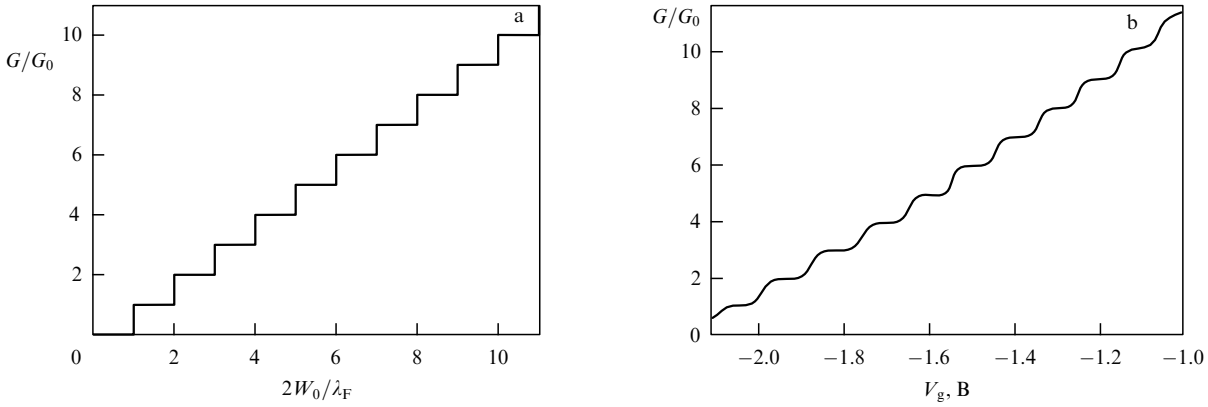

Figure 10. (a) Quantization of the conductance of a point contact under the variation in the constriction width W_0 due to a voltage applied to the gate (see Fig. 7). (b) Experimental dependences of the constriction conductance on the gate voltage V_g. It can be assumed with good accuracy that W_0 is a linear function of V_g. The plot is taken from the first experimental paper [36]. Similar results were presented at about the same time in [37].

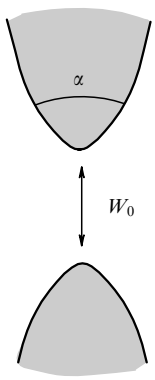

Figure 11. Quantization is observed for angles $\alpha \gg 1/\pi^2$.

the applicability of the adiabatic approximation proved to be more strict). The problem therefore has a specific numerical small parameter $1/\pi^2$. We consider this situation in more detail following [40].

4.3 Smearing of conductance steps caused by tunneling through the effective potential

To perform a more detailed analysis, we describe the shape of a QPC by the model dependence (see Figs 8 and 11)

$$W(x) = \frac{W_0}{L}\sqrt{x^2 + L^2}\,, \tag{61}$$

where W_0 and L are the QPC width and length. The opening angle of the contact walls is $\alpha = 2\arctan(W_0/2L)$. In this case, the effective potential

$$U_n(x) = \frac{\hbar^2\pi^2L^2n^2}{2mW_0^2(x^2+L^2)} \approx U_n(0) - \frac{m}{2}\,\Omega_n^2 x^2 \tag{62}$$

is approximately quadratic near the barrier top ($x = 0$), with the expansion coefficients

$$U_n(0) = E_n = \frac{\hbar^2\pi^2n^2}{2mW^2}\,, \qquad \Omega_n = \frac{\hbar\pi n}{mWL}\,.$$

The problem of tunneling through an inverted quadratic potential can be solved exactly. The probability of transmission through (62) is given by the Kemble formula [41, 42]

$$T_n(E) = \frac{1}{\exp\left[2\pi(E_n - E)/(\hbar\Omega_n)\right] + 1}\,, \tag{63}$$

in the form of a smeared step increasing from 0 for $E < E_n$ to 1 for $E > U_n(0)$; the crossover occurs at the scale $\hbar\Omega_n/(2\pi)$. To observe steps in the conductance as functions of W_0, the step width $\hbar\Omega_n/(2\pi)$ should be much smaller than the distance between steps: $U_{n+1}(0) - U_n(0) \approx \hbar^2\pi^2 n/mW_0^2$, i.e.,

$$\frac{L}{W} \gg \frac{1}{2\pi^2} \approx 0.051\,. \tag{64}$$

Good quantization is therefore observed even for a relatively short point contact [36, 37]. It is also important that the region of the potential responsible for scattering is sufficiently small, and therefore quadratic approximation (62) can be justified and the Kemble formula well describes the behavior of the transparency in the range from low transparencies $T \ll 1$ to high transparencies $T \approx 1$. The nonquadratic shape of the scattering potential would be manifested only in the description of very weak reflections or transmissions.

We consider the question of the possible mixing of channels. The condition for the absence of channel mixing in the constriction region is well satisfied. Away from the throat, in the banks, the situation for the first channels is the opposite: motion along the x axis in this region is faster, while transverse motion is slower and the distances between the transverse quantization levels are small. Therefore, even smooth inhomogeneities cause mode mixing. The mixing of transmitted modes does not affect the quantization picture, in particular, the transport remains reflectionless on a plateau. The point is that the eigenmodes diagonalizing the transmission amplitude matrix are important here. In the constriction, the eigenmodes look like usual transverse modes, which we already considered, whereas on the banks, they can be a complex mixture of transmitted modes. But if the transmitted modes are mixed with the reflected ones, then the conductance in the plateau can of course change and, moreover, the entire quantization picture can be smeared.

It is interesting that for the chosen boundary conditions (impenetrable walls), variables separate in the Schrödinger equations if the wall shape is described by a second-order curve such as a parabola or hyperbola [43]. In this case, the

absence of channel mixing is an exact fact rather than the result of approximation. In addition, variables are separated in the saddle potential [44], which is also used in simulations of QPCs [45]. Such a wall shape is also of interest because it allows solving the problem in a magnetic field.

The conductance quantization is observed not only in QPCs and a 2DEG but also in contacts of carbon nanotubes with metals [46–48] and in atomic point contacts [49–52], and it was predicted [53] and recently observed in graphene [54].

The nature of quantization in these systems is similar to that in QPCs; however, differences also exist. For example, the number of channels is related not only to the form of orbital transverse modes (in the case of atomic point contacts, they are caused by the electron wave functions of contacting atoms) but also to the physical amount of layers in nanotubes or atoms in the throat. The adiabaticity of the bottleneck–bank joining is also caused not by the smoothness of the conduction region opening, as in QPCs, but by a weak tunneling from a quasi-one-dimensional conductor to massive banks on a large effective contact area.

5. Electron waveguide in a magnetic field

A finite magnetic field in an electron waveguide, and in a QPC in particular, leads to two effects. First, Zeeman splitting appears. Second, orbital effects appear in two- and three-dimensional cases, which are absent in one-dimensional systems, where the vector potential leads simply to the phase accumulation and does not affect observables. In this case, the form of the wave functions of transverse modes (channels) changes considerably, and we consider these changes in Sections 5.1 and 5.2.

5.1 Zeeman effect in a quantum point contact

A QPC in a two-dimensional gas in the xy plane in a magnetic field with the vector lying in the same plane (Fig. 12a) is described by the Hamiltonian

$$\hat{H} = \frac{1}{2m}\left(\mathbf{p} - \frac{e}{c}\mathbf{A}\right)^2 + U(x,y) + \mu_{\mathrm{B}}\mathbf{B}\boldsymbol{\sigma}\,, \tag{65}$$

where e is the electron charge, μ_{B} is the Bohr magneton, $\boldsymbol{\sigma}$ are the Pauli matrices, and

$$\mathbf{B} = B\mathbf{e}_y\,. \tag{66}$$

We note that the in-plane magnetic field (66) does not affect the orbital motion of particles, and we can describe

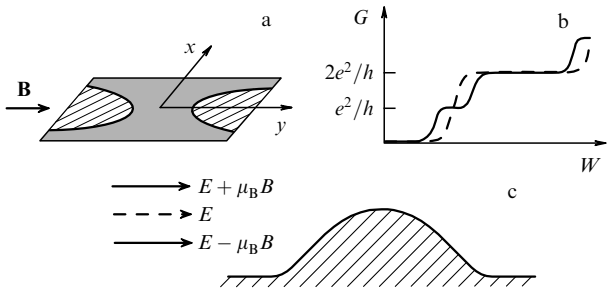

Figure 12. (a) Quantum point contact in a magnetic field collinear to the plane of a two-dimensional gas. (b) The solid curve shows conductance steps in the magnetic field, and the dashed curve does so in the absence of the magnetic field. (c) Each scattering state with an energy E is split into two with energies $E \pm \mu_{\mathrm{B}}B$.

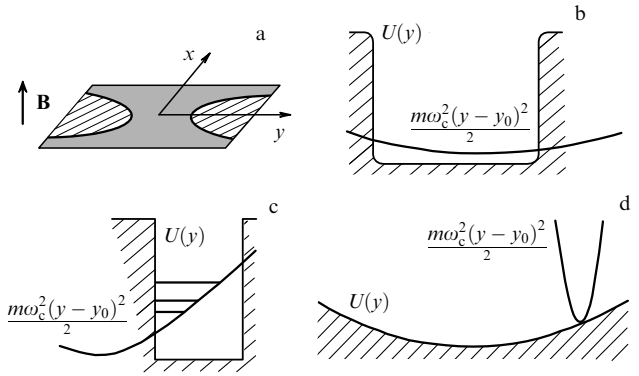

Figure 13. (a) Quantum point contact in a magnetic field perpendicular to a sample. (b) Weak magnetic field in a potential box. (c) Edge states in a strong magnetic field for a steep wall $U(y)$. (d) Edge states in a strong magnetic field for a smooth potential $U(y)$.

Hamiltonian (65) in the form

$$\hat{H} = \hat{H}_0 + \mu_{\mathrm{B}}B\sigma_y\,, \tag{67}$$

i.e., represent $\hat{H}$ as a sum of the Hamiltonian $\hat{H}_0 = p^2/2m + U(x,y)$ without a magnetic field and the Zeeman term. Two solutions with kinetic energies $E \pm \mu_{\mathrm{B}}B$ correspond to each scattering state or bound state of the Hamiltonian $\hat{H}_0$ with an energy E (see Fig. 12). As the throat width W increases, the spin degeneracy is lifted and the conductance of the system increases by steps e^2/h (Fig. 12b). Such a splitting was already observed in the pioneering paper [37] and was later investigated in detail in [55, 56]. This effect was considered theoretically in [57].

We note that in the plateau mode after odd steps, the spin-polarized current flows through the contact.

5.2 Edge states in a magnetic field

If the magnetic field $\mathbf{B}$ is perpendicular to the plane shown in Fig. 13a, then orbital effects appear along with the Zeeman effect. For simplicity, we consider only orbital effects in this section. We describe them by the Hamiltonian

$$\hat{H} = \frac{1}{2m}\left(\mathbf{p} - \frac{e}{c}\mathbf{A}\right)^2 + U(y)\,, \tag{68}$$

where the potential $U(y)$ is independent of the coordinate x along the wire. We still assume that the magnetic field is homogeneous, but this time it is perpendicular to the plane of the 2DEG,

$$\mathbf{B} = B\mathbf{e}_z\,. \tag{69}$$

The vector potential

$$\mathbf{A} = -By\,\mathbf{e}_x \tag{70}$$

corresponding to this magnetic field depends only on y (the Landau gauge). Hamiltonian (68) takes the form

$$\hat{H} = \frac{1}{2m}\left(p_x + \frac{eB}{c}\,y\right)^2 + \frac{p_y^2}{2m} + U(y)\,. \tag{71}$$

Variables in the Schrödinger equation with Hamiltonian (71) can be separated by the substitution

$$\Psi(x,y) = \exp\left(\mathrm{i}kx\right)\chi(y)\,. \tag{72}$$

The transverse modes $\chi(y)$ then satisfy the equation

$$\chi_n''(y) + \frac{2m}{\hbar^2}\left[E_n(k) - U(y) - \frac{m\omega_c^2}{2}\,(y-y_0)^2\right]\chi_n(y) = 0\,, \quad (73)$$

where $\omega_c = |e|B/mc$ is the cyclotron frequency, $y_0 = \ell_B^2 k$, and $\ell_B = \sqrt{c\hbar/|e|B}$ is the magnetic length. Solving Eqn (73), we can obtain the dispersion and $E_n(k)$ and the wave function in the presence of the magnetic field. In the absence of the additional potential, $U(y) = 0$, Eqn (73) reduces to the equation for a harmonic oscillator. The solution gives the Landau levels:

$$E_n(k) = \hbar\omega_c\left(n + \frac{1}{2}\right), \quad (74)$$

which form a flat dispersionless band [42].

In the case of a weak magnetic field in a QPC, we can regard the quadratic potential produced by B as a perturbation (Fig. 13b). The energy levels take the form

$$E_n(k) = E_n + \frac{\hbar^2 k^2}{2m} + \langle \chi_n^{(0)} | V(y) | \chi_n^{(0)} \rangle\,, \quad (75)$$

where E_n is the transverse quantization energy in the $\chi_n^{(0)}(y)$ state (in the absence of a magnetic field),

$$V(y) = \frac{m\omega_c^2}{2}\,(y^2 - 2y_0 y)\,. \quad (76)$$

Averaging over wave functions (57) gives

$$\langle \chi_n^{(0)} | V(y) | \chi_n^{(0)} \rangle = \frac{m\omega_c^2 W^2(x)}{24}\left(1 - \frac{6}{\pi^2 n^2}\right). \quad (77)$$

This addition to the transverse quantization energy shifts the steps and increases the plateau width [57]. An even more substantial effect is the narrowing of the step width due to a decrease in the curvature of the effective scattering potential $\tilde{\Omega}_n^2 = \Omega_n^2 - \Omega_H^2$, where

$$\Omega_H^2 = \frac{\omega_c^2 W^2(0)}{12L^2}\left(1 - \frac{6}{\pi^2 n^2}\right). \quad (78)$$

Both these effects improve quantization. But another contribution of the same order in the magnetic field exists, which can lead to the step broadening [57]. Taking the kinetic energy variation into account in the second-order perturbation theory [with a term linear in the magnetic field in (71)] complicates the picture: for the first step, it always provides a further increase in the quantization, whereas for the next steps, the effect can be the opposite due to the possible change in sign in the second-order perturbation theory.

At the same time, the magnetic field effect in [45] resulted only in the improvement of quantization. This difference can be caused by the use of different QPC models and the different choice of parameters (although the improvement of quantization in a magnetic field is intuitively the most natural result).

In the case of *a strong magnetic field and a steep wall*, transverse modes can change considerably for large k and B. Such a situation for a magnetic field in a potential box is shown in Fig. 13c, where the parabola of the quadratic potential is strongly displaced with respect to the center. The states formed at the boundaries, which are called edge states, play a key role in transport in the IQHE regime, when the magnetic film is so strong that only several modes contribute to the transport even in a wide contact, which are in fact edge states.

In a strong magnetic field for a smooth potential $U''(y_0)/m \ll \omega_c$, the wave function of the edge states is not deformed, $U(y)$ can be replaced with the potential $U(y_0)$, and the energy levels have the form

$$E_n(k) = \hbar\omega_c\left(n + \frac{1}{2}\right) + U(y_0)\,. \quad (79)$$

An exact solution can be obtained for parabolic walls, $U(y) = m\omega_0^2 y^2/2$, when the equation takes the form

$$\chi_n''(y) + \frac{2m}{\hbar^2}\left\{E_n(k) - \frac{m}{2}\left[\omega_0^2 y^2 + \omega_c^2 (y-y_0)^2\right]\right\}\chi_n(y) = 0\,. \quad (80)$$

Introducing the new variables

$$\tilde{\omega}^2 = \omega_c^2 + \omega_0^2\,, \qquad \tilde{y}_0 = y_0\,\frac{\omega_c^2}{\omega_c^2 + \omega_0^2}\,,$$

$$\tilde{E}_n(k) = E_n(k) - \frac{m\omega_c^2\omega_0^2}{2(\omega_c^2 + \omega_0^2)}\,y_0^2\,,$$

we can reduce (80) to the equation of a harmonic oscillator

$$\chi_n''(y) + \frac{2m}{\hbar^2}\left[\tilde{E}_n(k) - \frac{m\tilde{\omega}^2 (y - \tilde{y}_0)^2}{2}\right]\chi_n(y) = 0 \quad (81)$$

with the spectrum

$$\tilde{E}_n(k) = \hbar\tilde{\omega}\left(n + \frac{1}{2}\right). \quad (82)$$

Returning to the usual variables, we obtain

$$E_n(k) = \hbar\sqrt{\omega_c^2 + \omega_0^2}\left(n + \frac{1}{2}\right) + \frac{m\omega_c^2\omega_0^2}{2(\omega_c^2 + \omega_0^2)}\,y_0^2\,, \quad (83)$$

where the dependence on k enters through $y_0 = \ell_B^2 k$. In Eqn (81), $\tilde{y}_0$ indicates the edge state position. We fix the energy E and express $\tilde{y}_n$ in terms of E and n:

$$\tilde{y}_0^2 = \frac{2\omega_c^2}{m\omega_0^2(\omega_c^2 + \omega_0^2)}\left[E - \hbar\sqrt{\omega_c^2 + \omega_0^2}\left(n + \frac{1}{2}\right)\right]. \quad (84)$$

It follows from (84) that the higher the energy E is, the closer the edge state is to the sample boundary. The total excess nonequilibrium current in the IQHE mode is transferred just by these states. This is explained by the fact that the edge-state energy is higher than the energy of bulk states, and hence edge states are typically the first to touch the Fermi surface (level), making the contribution to transport. It is important that, as in the case of one-dimensional motion without a magnetic field, each channel (each Landau level in the strong-field approximation) carries the same current $i_0 = e/h$ per energy interval (for one spin direction) [see expression (14)]. This occurs because the current in the presence of a magnetic field can still be expressed in terms of the velocity, which cancels the velocity from the density of states, as in the normal case.

By analyzing the behavior of transverse modes, which are converted to edge states as the magnetic field increases, we can see that the quantization of the conductance both at the

QPC and in the IQHE has the same nature in a certain sense, namely, the switching on of new modes when changing parameters (width or magnetic field) upon passage from plateau to plateau through steps. As regards the transport on a plateau without reflection, this property is caused in the case of QPCs by motion without reflection in the semiclassical potential, while in the case of the IQHE, it is caused by a similar phenomenon of the suppression of scattering from boundary to boundary, because the edge states with opposite momenta are located near the opposite walls.

In pure conductors, the picture described above is clear and raises no doubts. In dirty conductors, the picture is more complicated and is commonly described by using quite different approaches. However, a similarity can be seen to exist between these pictures, which we discuss in Section 8, where we consider the transmission distribution function in dirty conductors.

The quantum Hall effect is an intricate and diverse phenomenon deserving a special discussion that is outside the scope of our review. Here, we only wanted to show that even a simple analysis of edge states based on the Landauer approach can give useful information. A more detailed analysis by means of scattering matrices was performed in [14] (after papers [58, 59], in which the nature of the IQHE was considered by using edge states). The theoretical and experimental aspects of edge states are discussed in detail in review [60].

6. Aharonov–Bohm effect

We consider one of the most interesting effects in which the nonlocality of quantum mechanics is manifested, the Aharonov–Bohm effect [61], which has been observed in mesoscopic quantum conductors [62]. Let a quantum wire (Fig. 14) with one open channel (one propagating mode) be connected at point 1 to a single-mode ring connected at point 2 to another quantum single-mode conductor. We consider the probability of propagation of a particle from one conductor to another in the case where the ring is in a magnetic field (for example, in a weak homogeneous magnetic field **B** perpendicular to its plane).

We calculate the scattering amplitude using the Feynman approach. The total scattering amplitude can then be found by summing the amplitudes of transmission of a particle from one conductor to another through the ring over all the possible paths. The shortest path is the propagation of the particle from the left conductor to the right one through the upper or lower part of the ring. We assume for simplicity that the ring and the contacts are symmetric, and hence, for $\mathbf{B} = 0$, the transmission amplitudes $t_{12}^{\mathrm{u(d)}}$ for the particle along these paths are the same and equal to t_{12}. If the magnetic field **B** is nonzero, the particle acquires different phases after propagation through the upper and lower parts of the ring:

$$t_{12}^{(\mathrm{u})} = t_{12} \exp(\mathrm{i}\chi_1)\,, \qquad t_{12}^{(\mathrm{d})} = t_{12} \exp(\mathrm{i}\chi_2)\,, \tag{85}$$

$$\chi_1 = \frac{e}{c\hbar}\int_{\mathrm{u}} \mathbf{A}\,\mathrm{d}\mathbf{l}\,, \qquad \chi_2 = \frac{e}{c\hbar}\int_{\mathrm{d}} \mathbf{A}\,\mathrm{d}\mathbf{l}\,, \tag{86}$$

where **A** is the vector potential and the integral is taken along the particle path between points 1 and 2. The difference between these phases can be expressed in terms of the ratio of the magnetic field flux $\Phi = \oint \mathbf{A}\,\mathrm{d}\mathbf{l}$ through the ring to the magnetic flux quantum $\Phi_0 = hc/e$,

$$\chi = \chi_1 - \chi_2 = \frac{e}{c\hbar}\oint \mathbf{A}\,\mathrm{d}\mathbf{l} = 2\pi\,\frac{\Phi}{\Phi_0}\,. \tag{87}$$

Then the total transmission amplitudes and the probability are

$$\tilde{t} = t_{12} \exp\left[\frac{\mathrm{i}(\chi_1+\chi_2)}{2}\right]\left[\exp\left(\frac{\mathrm{i}\chi}{2}\right) + \exp\left(-\frac{\mathrm{i}\chi}{2}\right)\right], \tag{88}$$

$$\tilde{t}' = t_{12} \exp\left[-\frac{\mathrm{i}(\chi_1+\chi_2)}{2}\right]\left[\exp\left(\frac{\mathrm{i}\chi}{2}\right) + \exp\left(-\frac{\mathrm{i}\chi}{2}\right)\right], \tag{89}$$

$$T = |\tilde{t}|^2 = 2T_{12} + 2T_{12}\cos\chi\,. \tag{90}$$

We note that the amplitude $\tilde{t}'$ of scattering from left to right, which can be found with the help of rule (359) (see Appendix A.3) from the expression for $\tilde{t}$, is not equal to $\tilde{t}$ in general, unlike that in problems with the symmetric ($t = t'$) scattering matrix considered in Sections 2–4. Here, this symmetry is broken [but the transmission probabilities are still equal because the scattering problem is effectively one-dimensional (see footnote 5 in Section 2.2)].

The periodic dependence of the transmission probability T on the magnetic field represents the Aharonov–Bohm effect. When the system shown in Fig. 14 is connected at the right and left to electron reservoirs, the conductance of such a contact is described by the Landauer formula $G = G_0 T$. If the motion of a particle were incoherent, we would obtain $T = 2T_{12}$. Due to interference, $T = 0$ when $\chi = \pi + 2\pi n$, $n = 0, \pm 1, \pm 2, \ldots$. The vanishing of the transmission indicates the presence of the so-called Fano resonance [63], which appears upon hybridization of the continuous and discrete spectra.[14] In the case $\chi = 2\pi n$, the conductance is twice that in the incoherent case.

We note that we did not take all the contributions to the scattering amplitude into account in (88), and considering only two amplitudes is, generally speaking, incorrect. A particle can tunnel at point 1 to the ring from the left conductor, pass several times along the ring, and only then enter the right conductor. Multiple reflections typical of a Fabry–Perot interferometer can be avoided by using a Mach–Zehnder interferometer in which only two amplitudes interfere (Fig. 15).[15] In this case, generally speaking, it is necessary to fabricate a reflectionless scatterer ('beamsplit-

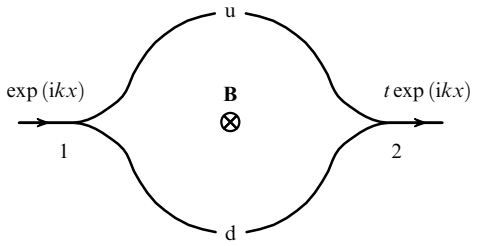

Figure 14. Aharonov–Bohm effect. A quantum conductor with one open channel (one propagating mode) is connected at point 1 to a single-mode ring. The ring is connected at point 2 to another quantum single-mode conductor.

[14] The transparency never vanishes in usual purely one-dimensional problems of scattering on finite potentials.

[15] Because the geometry of such an interferometer is not one-dimensional (four contacts exist), the transmission probabilities are no longer symmetric in the contact indices in a nonzero magnetic field.

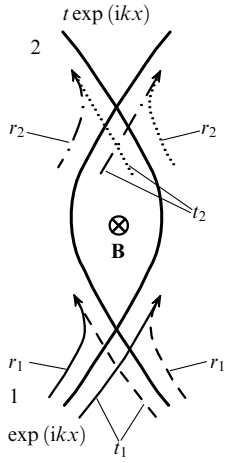

Figure 15. Reflectionless scattering in a 'four-tail' figure.

ter'). This task is quite complicated but can be fulfilled under quantum Hall effect conditions (see, e.g., [64]).

7. Double barrier: the Fabry–Perot interferometer

As mentioned in the Introduction, scattering by a real potential in meso- and nano-quasi-one-dimensional conductors can be simulated by scattering from potentials for which the problem can be solved exactly. We considered one such example in Section 4.3, where the Kemble formula for scattering by a quadratic potential was used. Another example (perhaps the one used most frequently) involves the Dirac delta function $\delta(x)$. The potential can be written in the form $U(x) = \alpha\delta(x)$ if its range is shorter than the wavelength λ of a scattering particle. In the case of metals, such a description is usually valid for boundaries between different materials. But in quasi-one-dimensional conductors, where the effective wavelength can considerably exceed 1 nm, the applicability range of such a description broadens, and this approximation can sometimes be used even for QPCs.

The scattering amplitudes in such a potential are given by the known expressions

$$t = t' = \frac{1}{1 + \mathrm{i}Z}\,, \tag{91}$$

$$r = r' = \frac{\mathrm{i}Z}{1 + \mathrm{i}Z}\,, \tag{92}$$

where

$$Z = \frac{m\alpha}{\hbar^2 k}\,. \tag{93}$$

7.1 Double delta barrier

Another very important case, which we consider several time further, is scattering from the double barrier. The double barrier is a structure with two scatterers connected in series. Such a scatterer can successfully simulate transport through a quantum dot, for example, in a carbon nanotube. In the case of coherent transport, interference occurs due to multiple scatterings and resonances appear in the transmission amplitude and the transparency of the double barrier. Each of the barriers can be typically described by a delta function. The transmission and refection amplitudes of this structure can be calculated in a standard way by matching the wave functions on different sides of the scatterers. However, we consider a more illustrative calculation method based on an analogy with the optical Fabry–Perot interferometer, which also gives an exact result. The method involves the summation of all possible semiclassical trajectories with successive reflections, along which the particle can propagate (the method can be formally substantiated by integrating over Feynman trajectories). In addition, this method accounts for the fluctuations of the phase accumulated during motion between barriers.

We assume that the left scatterer has the transmission and reflection amplitudes t_1 and r_1, and the right scatterer has the corresponding amplitudes t_2 and r_2; the distance between the barriers is L. All possible paths of the particle are shown in Fig. 16. The transmission amplitude is determined by the sum of the series

$$t = t_2 t_1 + t_2\left[r_1' r_2 \exp(2\mathrm{i}kL)\right] t_1 + t_2\left[r_1' r_2 \exp(2\mathrm{i}kL)\right]^2 t_1 + \ldots, \tag{94}$$

where the first term corresponds to the trajectory passing through the two barriers without reflection, the second term corresponds to the trajectory with two reflections forming one loop, and so on. The summation of the (geometrical) series gives

$$t = t' = \frac{t_1 t_2}{1 - r_1' r_2 \exp(2\mathrm{i}kL)}\,. \tag{95}$$

We recall that $t_1 = t_1'$, $t_2 = t_2'$, and $t' = t$ if the Hamiltonian of the system is invariant under time reversal (in the general case, $r \neq r'$ in the absence of spatial symmetry).

Similarly, we can sum over trajectories for the backward reflection amplitude:

$$r = r_1 + t_1 r_2 \exp(2\mathrm{i}kL)\, t_1 + t_1\left[r_2 \exp(2\mathrm{i}kL) r_1\right] r_2 \exp(2\mathrm{i}kL)\, t_1 + \ldots, \tag{96}$$

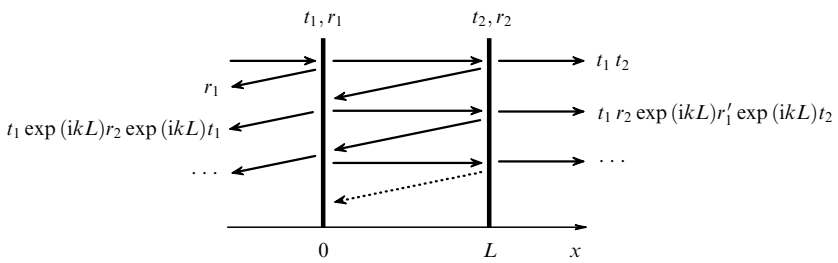

Figure 16. A double barrier (two scattering potentials in series) can be regarded as an analogue of the Fabry–Perot interferometer known in optics.

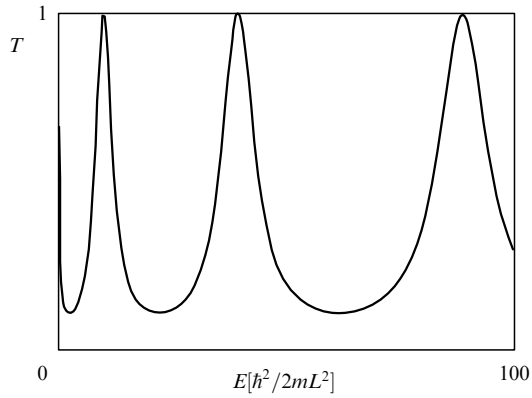

Figure 17. Transmission probability T as a function of energy; $T_1 = T_2 = 0.5$ and $\chi^r = 0$ [65].

which gives

$$r = r_1 + \frac{t_1 t_1 r_2 \exp(\mathrm{i}2kL)}{1 - r_1 r_2 \exp(2\mathrm{i}kL)} = \frac{r_1 + r_2 \exp(2\mathrm{i}kL)(t_1 t_1 - r_1^2)}{1 - r_1 r_2 \exp(2\mathrm{i}kL)} . \tag{97}$$

The transparency of the whole system is

$$T \equiv |t|^2 = \frac{T_1 T_2}{1 + R_1 R_2 - 2\sqrt{R_1 R_2}\cos\theta} , \tag{98}$$

where $\theta = 2kL + 2\chi^r$, $T_i = |t_i|^2$ and $R_i = |r_i|^2$ are the transmission and reflection probabilities for barriers, and $\chi^r = (\chi_1^{r'} + \chi_2^r)/2$ (for example, $\chi_1^{r'} \equiv \arg r_1'$). Relation (98) is illustrated in Fig. 17. The total transparency $T(E)$ attains a maximum at $\theta = 2\pi n$, $n = 1, 2, \ldots$, which corresponds to wave vectors $k_n = (\pi n - \chi^r)/L$ with the energies

$$E_n = \frac{\hbar^2}{2mL^2}(\pi n - \chi^r)^2 . \tag{99}$$

The maximum value of $T(E)$,

$$T_{\max} = \frac{T_1 T_2}{(1 - \sqrt{R_1 R_2})^2} , \tag{100}$$

is equal to unity for $T_1 = T_2$ and to $4T_1T_2/(T_1 + T_2)^2$ for $T_i \ll 1$, $i = 1, 2$.[16]

The obtained transmission probability demonstrates the important property that for a symmetric barrier with $|t_1| = |t_2|$, the resonances are ideal, $|t| = 1$. Therefore, the two-barrier structure becomes ideally transparent at resonance (neglecting the phase gain) even for very strong scattering from each of the barriers. This effect, appearing due to interference, can be an indicator of the full coherence of particle motion. If coherence is absent, the transmission probability is given by the product of probabilities $T \approx T_1 T_2$, which can be much smaller than unity. The measurement of T is used for the experimental verification of the coherence degree. We note that if $T < 1$, then it is impossible to find by this method whether the system is coherent. But the case $T = 1$ unambiguously indicates full coherence.

[16] We assume that T_1, T_2, and χ' are virtually independent of energy at scales of the order of the distance between resonances.

Outside the resonance (in the destructive interference region), we have

$$T = T_{\min} = \frac{T_1 T_2}{(1 + \sqrt{R_1 R_2})^2} . \tag{101}$$

For $T_1, T_2 \ll 1$, we obtain $T \approx T_1 T_2/4$, and therefore the destructive interference effect is stronger than the dephasing effect, which we discuss in more detail below.

We define the spacing between resonances as

$$\Delta_n = \frac{|E_{n+1} - E_{n-1}|}{2} = 2\pi \frac{\hbar^2 |\pi n - \chi^r|}{2mL^2} = \frac{\pi\hbar v_n}{L} = \pi\hbar\nu_n , \tag{102}$$

where $v_n = (\mathrm{d}E/\hbar\,\mathrm{d}k)|_{E=E_n}$ is the velocity of an electron moving between the potential walls of the double-barrier potential. We note that the resonance energies are not equidistant and the definition $\Delta_n = |\partial E_n/\partial n|$ gives the same result. The quantity

$$\nu_n = \frac{v_n}{L} \tag{103}$$

has the dimension of frequency and its physical meaning corresponds to number of electron attempts to leave the trap between potential barriers per unit time.

We analyze expression (98) near the resonance energy E_n in Eqn (99). For this, we expand the cosine in the denominator in the right-hand side of (98) to the second order in the energy deviation from the resonance $\delta E_n = E - E_n$:

$$\cos\theta \approx 1 - \frac{1}{2}\left(\frac{\mathrm{d}\theta}{\mathrm{d}E_n}\right)^2 (\delta E_n)^2 ,$$
$$\frac{\mathrm{d}\theta}{\mathrm{d}E_n} = \frac{\mathrm{d}\theta}{\mathrm{d}E}\bigg|_{E=E_n} = \frac{1}{\hbar\nu_n} . \tag{104}$$

Substituting this expression in (98), we find that the transmission probability near the nth resonance can be approximated by a Lorentzian function (the Breit–Wigner approximation [42]):

$$T(E \sim E_n) \approx T_{\mathrm{BW}} = \frac{\gamma_n^2}{\gamma_n^2 + (\delta E_n)^2} T_{\max} . \tag{105}$$

Here, we define the resonance half-width as

$$\gamma_n = \frac{1}{2}\frac{\mathrm{d}E}{\mathrm{d}\theta}\bigg|_{E=E_n} \frac{1 - \sqrt{R_1 R_2}}{\sqrt[4]{R_1 R_2}} = \frac{\hbar\nu_n(1 - \sqrt{R_1 R_2})}{2\sqrt[4]{R_1 R_2}} . \tag{106}$$

The transmission probability T can be approximated by a Lorentzian function for all energies:

$$T(E) \approx \sum_n T_{\mathrm{BW}}(\delta E_n) . \tag{107}$$

The relative error of the approximation (107) does not exceed a few percent, even for $T_1, T_2 \lesssim 0.5$. For example, in Fig. 17, if we additionally plot approximation (107) with the same parameters that determine the plot of T shown in this figure, these plots coincide so perfectly that the difference is visually indistinguishable [65].

For a strong resonance, $T_1, T_2 \ll 1$, simpler expressions are often used. We introduce the partial resonance widths

$$\Gamma_n^{(i)} = \frac{\mathrm{d}\theta}{\mathrm{d}E_n} T_i = \hbar\nu_n T_i , \qquad i = 1, 2 . \tag{108}$$

The ratio $\Gamma_n^{(i)}/\hbar$ gives the number of successful attempts of a particle to leave the trap between the walls of the double-barrier potential per unit time. Expanding the right-hand side of (105) in small probabilities of transitions through potential walls, we find that

$$T(E) \approx \frac{\Gamma_n^{(1)}\Gamma_n^{(2)}}{\Gamma_n^{(1)}+\Gamma_n^{(2)}}\, A_n(E-E_n)\,, \tag{109}$$

$$A_n(\epsilon) = \frac{\Gamma_n}{\epsilon^2 + (\Gamma_n/2)^2} \tag{110}$$

near the resonance, where $\Gamma_n = \Gamma_n^{(1)} + \Gamma_n^{(2)}$ is the total resonance width and A is the Lorentzian function. Then $\gamma_n = \hbar v_n(T_1+T_2)/4 = \Gamma_n/4$. We see that resonances become sharper as T_1 and T_2 decrease.

We next discuss the dephasing effects mentioned above. We rewrite expression (94) by adding phase factors with random phases α_i, $i = 1, 2, \ldots$, to each term:

$$t = t_2 t_1 \exp(\mathrm{i}\alpha_1) + t_2\left[r_1' r_2 \exp(2\mathrm{i}kL)\right] t_1 \exp(\mathrm{i}\alpha_2) + t_2\left[r_1' r_2 \exp(2\mathrm{i}kL)\right]^2 t_1 \exp(\mathrm{i}\alpha_3) + \ldots\,. \tag{111}$$

These phases can appear due to time fluctuations of the electrostatic potential in the quantum dot (i.e., in the region between barriers), which should be taken into account in multiple reflections in the resonance potential, which are described by the terms in the sum.[17]

We now find the transmission probability by averaging it over phase realizations α_i, assuming that the α_i are independent random quantities with dispersion greatly exceeding 2π. Such a model corresponds to the assumption that the dephasing length is smaller than the distance between barriers. Then

$$\langle T\rangle_\alpha = |t_2 t_1|^2 + \left|t_2\left[r_1' r_2 \exp(2\mathrm{i}kL)\right] t_1\right|^2 + \left|t_2\left[r_1' r_2 \exp(2\mathrm{i}kL)\right]^2 t_1\right|^2 + \ldots = \frac{T_1 T_2}{1 - R_1 R_2}\,. \tag{112}$$

It is interesting to compare incoherent tunneling described by Eqn (112) with the so-called sequential tunneling [72, 73]. Sequential tunneling is usually considered in a situation where the quasi-equilibrium distribution is established in a quantum dot. In this case, the total resistance is given by the sum of the first and second barrier resistance,

$$R_\mathrm{s} = \frac{h}{2e^2}\left(\frac{1}{T_1} + \frac{1}{T_2}\right) = \frac{h}{2e^2}\,\frac{T_1+T_2}{T_1 T_2}\,. \tag{113}$$

In the case of incoherent tunneling (i.e., for the phase-averaged transparency considered above), the resistance

$$R = \frac{h}{2e^2}\,\frac{T_1+T_2-T_1T_2}{T_1T_2} = \frac{h}{2e^2}\,\frac{T_1+T_2}{T_1T_2} - \frac{h}{2e^2} \tag{114}$$

is smaller than R_s by the contact resistance formed by the internal modes of the region between barriers.

An interesting question arises: When is the simple summation of Landauer resistances applicable? For example, if we assume that the relaxation in momentum with the same propagation direction occurs inside the quantum dot such that the independent Fermi surfaces (points) appear for each direction, then no additional voltage drop occurs and the Landauer voltage can be summed (assuming that the delta function provides energy-independent scattering). We note that the reasoning about the summation of Landauer resistances when averaging over scattering amplitudes was used in different variants in the scaling theory of localization in well-known papers [6, 25].[18]

If $T_1, T_2 \ll 1$, then

$$\langle T\rangle_\alpha \approx \frac{T_1 T_2}{T_1+T_2}\,. \tag{115}$$

We note that destructive interference [see Eqn (101)] suppresses T much more strongly than phase coherence: in the former case, $T \propto T_1T_2/4$, while in the latter case, $T \propto T_1/2$ for $T_1 \sim T_2 \ll 1$.

7.2 Transport properties of contacts with the resonance potential

We consider a quantum contact between two electron reservoirs in which a resonance potential, similar to that considered in Section 7, serves as a scattering potential (see Fig. 16). For simplicity, we assume that only one channel is open, and hence Eqn (48) reduces to

$$I = \frac{2e}{h}\int_0^\infty \mathrm{d}E\left[f_1(E) - f_2(E)\right] T(E)\,. \tag{116}$$

We also assume that $T_1, T_2 \ll 1$, and therefore the Breit–Wigner approximation in form (109) can be used. Then

$$T(E) \approx \sum_n \frac{\Gamma_n^{(1)}\Gamma_n^{(2)}}{\Gamma_n^{(1)}+\Gamma_n^{(2)}}\, A_n(E-E_n)\,, \tag{117}$$

$$A_n(\epsilon) = \frac{\Gamma_n}{\epsilon^2 + (\Gamma_n/2)^2}\,, \tag{118}$$

where $\Gamma_n^{(i)}$ are the partial widths of resonances ($i = 1, 2$) and $\Gamma_n = \Gamma_n^{(1)} + \Gamma_n^{(2)}$ is the total width of the resonance (Fig. 18a). Substituting (117) into (116), we find (for the temperature $\Theta = 0$)

$$I = \frac{2e}{h}\sum_n \frac{\Gamma_n^{(1)}\Gamma_n^{(2)}}{\Gamma_n^{(1)}+\Gamma_n^{(2)}} \int_{E_1^\perp}^{V} \mathrm{d}E\, A_n(E-E_n)\,, \tag{119}$$

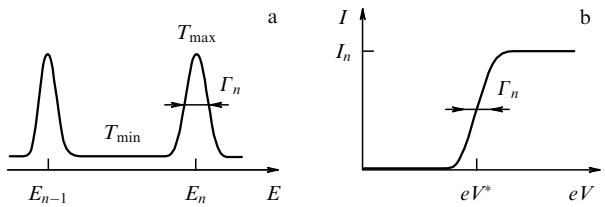

Figure 18. (a) Energy dependence of the transmission T. (b) Current as a function of the bias voltage V. In the symmetric case, each resonance gives the current increment by $I_n = (2e/\hbar)\pi\Gamma_n$.

[17] Electron transport in the presence of time-dependent fields can also be described by means of scattering matrices, which was discussed, e.g., in [66–71]. We do not consider this question because of the limited scope of our review.

[18] The transparency of a conductor containing many scatterers with random parameters was studied more accurately in [34], where a transfer matrix was used to describe the effect produced by the addition of a new scatterer. The total transparency was found to behave like a particle randomly diffusing in the parameter space.

where we introduce the superscript $\perp$ at the transverse quantization energy $E_1^{\perp}$ in the constriction to distinguish it from the resonance energy of the scattering potential.

We assume that the energy interval $E_n \in [E_1^{\perp}, V]$ contains several transmission probability resonances. Then, according to (119), the contribution from each of them to the current is

$$I_n = \frac{4e}{\hbar}\,\pi\,\frac{\Gamma_n^{(1)}\Gamma_n^{(2)}}{\Gamma_n^{(1)}+\Gamma_n^{(2)}} \tag{120}$$

(we took into account that $\int_{-\infty}^{\infty} A_n(E)\,\mathrm{d}E = 2\pi$). In the symmetric case, we obtain the simplest expression

$$I_n = \frac{2e}{\hbar}\,\pi\Gamma_n\,. \tag{121}$$

In this case, the $I-V$ characteristic has a typical step-like profile (Fig. 18b).

8. Conductance in dirty conductors

We now consider a multichannel dirty conductor in which electrons diffuse from one boundary to another (Fig. 19). Some important parameters of such a sample at low temperatures, when all inelastic processes can be neglected, surprisingly resemble those of a QPC and the double-barrier system considered in Sections 4 and 7.

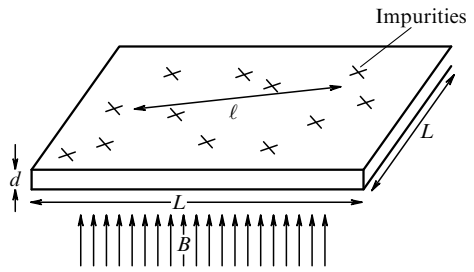

Figure 19. Two-dimensional dirty conductor. Crosses indicate the positions of impurities fluctuating from sample to sample; ℓ is the mean free path. A magnetic field can be applied perpendicularly to the sample.

8.1 Mesoscopic conductance fluctuations

The question about strong fluctuations of the resistance of such mesoscopic conductors was first considered in Azbel's work [74] (It is starting with this work that the term 'mesoscopic' was coined for such systems).

Quantitative investigations of mesoscopic quantum effects in transport were initiated in theoretical papers by Al'tshuler [75] and Lee and Stone [76], where large fluctuations of the conductance G in a two-dimensional dirty film were predicted even for large (but still coherent) samples. A standard quantity characterizing fluctuations of the conductance from sample to sample is the mean-square deviation

$$\langle \delta G^2\rangle_{\mathrm{im}} = \left\langle \left(G - \langle G\rangle_{\mathrm{im}}\right)^2\right\rangle_{\mathrm{im}}\,, \tag{122}$$

where the subscript im means averaging over all the possible variants of the location of impurities, and the mean conductance is

$$\langle G\rangle_{\mathrm{im}} = \frac{dL\sigma}{L}\,, \tag{123}$$

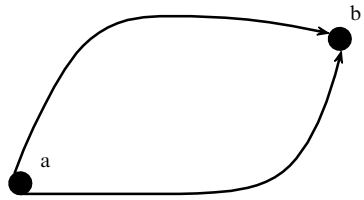

Figure 20. Interference between two trajectories contributing to the conductance. A magnetic field induces the Aharonov–Bohm phase, which changes the relative phase between the trajectories. The sensitivity to the magnetic field (i.e., a change in the magnetic field resulting in a change in the conductance by a value of the order of G_0) is specified by the condition of obtaining the magnetic flux quantum $\Phi_0 = hc/e$ per sample area L^2.

where σ is the conductivity. The authors of [75, 76] found that the standard deviation

$$\delta G = \sqrt{\langle \delta G^2\rangle_{\mathrm{im}}} \approx G_0 \tag{124}$$

is universal (i.e., is independent of the disorder details) and is approximately equal to the conductance quantum $G_0 = e^2/h$. The relative fluctuations

$$\frac{\delta G}{\langle G\rangle_{\mathrm{im}}} \approx \frac{e^2}{h}\,\frac{1}{d\sigma} \tag{125}$$

are independent of the sample size L. This is a surprising result because it was usually assumed that at large scales, the conductivity of even quantum conductors is a self-averaging quantity, and its relative fluctuations decrease upon increasing the sample size. But this is not the case for a coherent quantum conductor. In addition, Lee and Stone [76] and Al'tshuler and Khmel'nitskii [77] described mesoscopic fluctuations as a function of the applied magnetic field and other parameters. The fluctuations of the conductance appearing when changing the magnetic field can be qualitatively explained as follows: [19] the conductance is proportional to the probability $P_{\mathrm{a}\to\mathrm{b}}$ of an electron starting from one side of the conductor reaching its opposite side. Using the path integral formalism, the probability can be represented as the square of a sum of amplitudes over all possible paths:

$$P_{\mathrm{a}\to\mathrm{b}} = |A_1 + A_2|^2 = |A_1|^2 + |A_2|^2 + A_1A_2^* + A_1^*A_2\,. \tag{126}$$

For simplicity, we here consider only two semiclassical paths with amplitudes A_1 and A_2 (Fig. 20). The cross terms $A_1A_2^*$ and $A_1^*A_2$ vanish in the mean probability $\langle P_{\mathrm{a}\to\mathrm{b}}\rangle_{\mathrm{im}}$ due to averaging over the random phase (the exception is the contributions from paths or segments of paths repeating the motion backward and contributing to weakly localized corrections, which we do not consider here); the two probabilities are simply added, $\langle P_{\mathrm{a}\to\mathrm{b}}\rangle_{\mathrm{im}} = |A_1|^2 + |A_2|^2 = P_1 + P_2$, and the interference terms vanish. In the calculation of the second moment,

$$\begin{aligned}\langle P_{\mathrm{a}\to\mathrm{b}}^2\rangle_{\mathrm{im}} &\propto (P_1+P_2)^2 + 2|A_1|^2|A_2|^2\\ &= \langle P_{\mathrm{a}\to\mathrm{b}}\rangle_{\mathrm{im}}^2 + 2P_1P_2\,,\end{aligned} \tag{127}$$

the terms with $A_1A_2^*$ and $A_1^*A_2$ also vanish after averaging. But additional terms $2|A_1|^2|A_2|^2$ remain finite after averaging.

[19] The explanation by D E Khmel'nitskii.

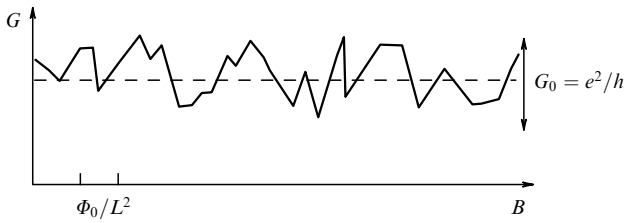

Figure 21. Conductance fluctuations as the magnetic field changes.

The root-mean-square has the form

$$\delta P_{\mathrm{a}\to\mathrm{b}} = \sqrt{\left\langle \left(P_{\mathrm{a}\to\mathrm{b}} - \langle P_{\mathrm{a}\to\mathrm{b}}\rangle_{\mathrm{im}}\right)^2\right\rangle_{\mathrm{im}}} = \sqrt{2P_1P_2}\,. \qquad (128)$$

If we now apply a weak magnetic field, the relative phases between all the paths change and the conductance changes accordingly. Thus, the conductance fluctuates upon changing the magnetic field, as when the realization of a random potential is changed. Detailed calculations show that the fluctuation value is of the order of $G_0 = 2e^2/h$ (Fig. 21). Similar fluctuations of the conductance also appear as functions of the Fermi energy (chemical potential). The characteristic energy scale at which fluctuations occur is determined by the inverse diffusion time in the sample. The phase increment on a typical path during the diffusion time is then $\delta kL \sim \pi$. Such fluctuations appear as voltage changes (Fig. 22) [78] and also in thermoelectric phenomena (see Section 9). Conductance fluctuations were observed in experiments [79, 80] (also see the results of subsequent experiments and the references in [81]).

We note that there is a possibility of some resonances existing in the transparency of dirty samples, as already discussed in the pioneering papers by Azbel [74].

8.2 The Dorokhov distribution function

We consider the problem of fluctuations from the standpoint of scattering matrices. The conductance represented with the help of 'eigenchannels', which diagonalize the transmission matrix, has the form

$$G = \frac{2e^2}{h}\sum_n T_n\,. \qquad (129)$$

For a conductor with N_{ch} channels, Eqn (129) can be written as

$$G = N_{\mathrm{ch}}\,\frac{2e^2}{h}\,\langle T\rangle\,, \qquad (130)$$

where $\langle T\rangle$ is the transparency averaged over all channels. Comparing (130) with the usual expression

$$G = \frac{S}{L}\,\sigma\,, \qquad (131)$$

where $\sigma = e^2\nu D$ is the conduction calculated from the Kubo formula [82, 83] at zero frequency, ν is the density of states on the Fermi surface, and $D = v_{\mathrm{F}}\ell/3$ is the diffusion coefficient, we obtain

$$G = \frac{2e^2}{h}\,\frac{Sk_{\mathrm{F}}^2}{\pi^2}\,\frac{\pi\ell}{3L}\,. \qquad (132)$$

The number of channels in a wire can be estimated in the semiclassical approximation as $N_{\mathrm{ch}} = Sk_{\mathrm{F}}^2/\pi^2$ [i.e., one channel per the area $\pi^2/k_{\mathrm{F}}^2 = (\lambda_{\mathrm{F}}/2)^2$]. Comparing expressions (130) and (132), we obtain the mean transparency

$$\langle T\rangle = \frac{\pi\ell}{3L}\,, \qquad (133)$$

which, being proportional to ℓ/L, tends to zero as $L\to\infty$. Does this mean that the typical transparency is approximately equal to ℓ/L? This turns out to not be the case. A surprising property of transport in diffuse conductors is that for the eigenchannels, for which the problem is diagonal (channels are not mixed), the transparency is either very small or close to unity. In reality, most of the channels are virtually closed and $T\approx 0$, and only $n = N_{\mathrm{ch}}\,\ell/L$ channels are almost completely open with $T\approx 1$, providing the total conductivity. The distribution function for T, which was first calculated by Dorokhov (Fig. 23), has the form [34, 84]

$$P(T) \propto \frac{1}{T\sqrt{1-T}}\,. \qquad (134)$$

This is the general result for a quasi-one-dimensional conductor (a thick wire) with the total length $L \ll L_{\mathrm{loc}}$, where the localization length L_{loc} can be estimated as $L_{\mathrm{loc}} \approx N_{\mathrm{ch}}\ell$, i.e., the conductance becomes comparable to the quantum $G_0 = 2e^2/h$. Using the normalization determined by the mean conductance

$$P(T) = \frac{\pi\ell}{6L}\,\frac{1}{T\sqrt{1-T}}\,, \qquad (135)$$

we obtain

$$G = \frac{2e^2}{h}\,N_{\mathrm{ch}}\int \mathrm{d}T\,P(T)\,T = \frac{2e^2}{h}\,\frac{Sk_{\mathrm{F}}^2}{\pi^2}\,\frac{\pi\ell}{3L}\,. \qquad (136)$$

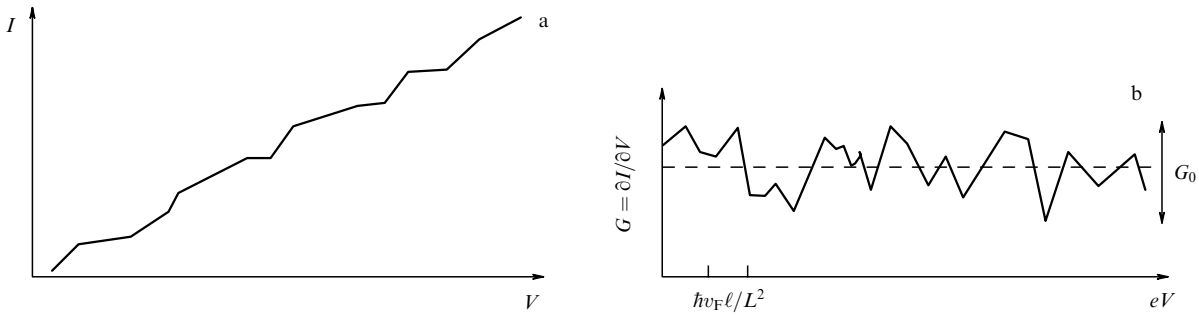

Figure 22. Conductance fluctuations as the voltage changes.

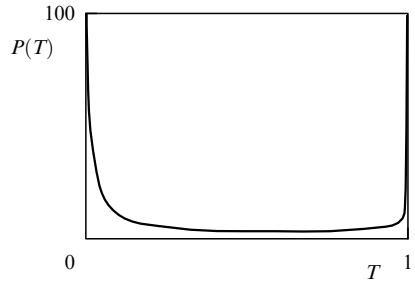

Figure 23. Bimodal Dorokhov distribution function $P(T)$ with the most probable values of T equal to 0 or 1.

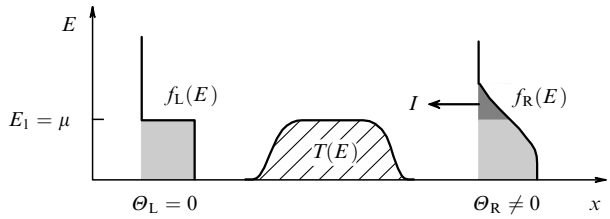

Figure 24. Appearance of the thermoelectric current. Only electrons with energies $E > \mu$ can overcome the barrier on the right, producing the thermoelectric current.

The situation resembles the case of a point contact with $n = N_{\rm ch}\,\ell/L$ open channels, but the difference is that the eigenmodes for different energies and different magnetic field strengths in a sample are different combinations of usual propagating modes. The switching between conducting and nonconducting channels provides mesoscopic fluctuations of the conductance $\delta G \approx e^2/h$ [75]. We can prove that the transparency distribution function is nontrivial by considering noises whose intensity is given by the sum $\sum_n T_n(1-T_n)$. Because of such a nonlinearity in T, the result [85]

$$\left\langle \sum_n T_n(1-T_n) \right\rangle = N_{\rm ch} \int {\rm d}T\, P(T) T(1-T) = \frac{1}{3} \left\langle \sum_n T_n \right\rangle \tag{137}$$

can give additional information on the properties of $P(T)$ (see Section 10.3).

As mentioned in Section 5.2, the quantization of the conductance in QPCs and the IQHE in the ballistic case has a similar nature, namely, a relatively sharp switching on of new modes under a variation in the external parameters. The situation with the IQHE in dirty conductors is much more complicated and is usually described by completely different methods, in particular, by using field models [86]. It is interesting that the authors of [87] proved that the descriptions of a quasi-one-dimensional (multichannel) conductor in terms of a sigma model [88, 89] and by the Dorokhov method (in particular, in the presence of a weak magnetic field) are equivalent. It seems that the analogy between a dirty conductor and a QPC described above is also valid in the presence of a strong magnetic field, and we can assume that the IQHE in dirty conductors is also provided by the presence of high-transparency eigenchannels (the number of open channels for the IQHE is obviously determined not by the ratio of the mean free path to the wire length but already by the number of occupied Landau levels [90]). The behavior of edge states in the presence of impurities was qualitatively discussed in [14].

9. Thermoelectric effects

We now show how thermoelectric effects can be described by using scattering matrices. So far, we have considered only the situation at zero temperature. The occupation numbers $f(E)$ at finite temperatures are given by Fermi distribution (47). The trivial effect of a nonzero temperature is manifested, for example, in the smearing of the steps of the conductance $G(W)$ or the peaks of $I(V)$ in the vicinity of resonances.

9.1 Thermoelectric current and thermoelectromotive force

To study nontrivial thermoelectric effects, we consider the case where the temperatures $\Theta_{\rm L}$ and $\Theta_{\rm R}$ in the reservoirs are different and their difference $\delta\Theta = \Theta_{\rm L} - \Theta_{\rm R}$ is finite. A thermoelectric current (i.e., the current caused by the difference in temperatures at a constant electrochemical potential) (Fig. 24) then appears, which is described in the one-dimensional case by the expression

$$I(V) = \frac{2e}{h} \int_{-\infty}^{\infty} {\rm d}E \left[f_{\rm L}(E) - f_{\rm R}(E) \right] T(E)\,. \tag{138}$$

It follows from this general expression that the current is absent in the case of energy-independent transparency, $\partial_E T(E) = 0$.

As an illustration, we first consider a simple example where the transparency depends on energy, namely, a QPC with ideal quantization:

$$T(E) = \begin{cases} 0\,, & E < E_1\,, \\ 1\,, & E > E_1\,, \end{cases} \tag{139}$$

where the electrochemical potentials of the reservoirs are equal to the quantization energy in the first channel, $\mu = E_1$, and hence μ is the opening threshold energy for the first channel. We assume that the temperature in the left reservoir is zero, $\Theta_{\rm L} = 0$, and particles on the left cannot overcome the contact, while electrons with energies $E > \mu$ in the right reservoir can overcome the barrier, resulting in the appearance of the current

$$\begin{aligned} I &= \frac{2e}{h} \int_{-\infty}^{\infty} {\rm d}E \left[n_{\rm L}(E) - n_{\rm R}(E) \right] T(E) \\ &= -\frac{2e}{h} \int_0^{\infty} {\rm d}\varepsilon\, \frac{1}{\exp(\varepsilon/\Theta_{\rm R}) + 1}\,, \end{aligned} \tag{140}$$

where $\varepsilon = E - \mu$. Integrating over ε, we obtain [91][20]

$$I = \frac{2e}{h} (\log 2)\, \delta\Theta\,. \tag{141}$$

If a circuit containing our quantum wire is opened, a voltage V (thermoelectromotive force) should appear to compensate the thermoelectric current produced due to the difference in temperatures. With the temperature difference

[20] We use the relation

$$\int_0^{\infty} \frac{{\rm d}\zeta}{\exp\zeta + 1} = \int_1^{\infty} \frac{{\rm d}\lambda}{\lambda(\lambda+1)} = \int_1^{\infty} \left(\frac{1}{\lambda} - \frac{1}{\lambda+1} \right) {\rm d}\lambda = \log \frac{\lambda}{\lambda+1} \bigg|_1^{\infty} = \log 2\,.$$

$\delta\Theta$ taken into account, the general expression for current (138) takes the form

$$I(\delta\Theta, V) = \frac{2e}{h}\int_{-\infty}^{\infty} \mathrm{d}E \left\{ \frac{1}{\exp\left[(E-\mu-eV)/(\Theta+\delta\Theta)\right]+1} - \frac{1}{\exp\left[(E-\mu)/\Theta\right]+1} \right\} T(E)\,. \tag{142}$$

If the temperature difference $\delta\Theta$ is small and $T(E)$ depends on the energy E relatively weakly, then the Fermi distribution function can be expanded in the vicinity of μ and the condition for the absence of the current $I(\delta\Theta, V) = 0$ gives

$$\frac{2e}{h}\,\delta\Theta \int_{-\infty}^{\infty} \mathrm{d}E\, \frac{\partial f(E)}{\partial E}\, \frac{E-\mu}{\Theta} \left[T(\mu) + (E-\mu)\, \frac{\partial T(\mu)}{\partial E} \right] + \frac{2e^2}{h}\, V \int_{-\infty}^{\infty} \mathrm{d}E\, \frac{\partial f(E)}{\partial E}\, T(\mu) = 0\,. \tag{143}$$

From (143), we obtain the Katler–Mott formula

$$\alpha = -\frac{\Theta}{e}\, \frac{\partial \log T(\mu)}{\partial E} \int_{-\infty}^{\infty} \zeta^2\, \frac{\partial n}{\partial \zeta}\, \mathrm{d}\zeta = \frac{\pi^2}{3}\, \frac{\Theta}{e}\, \frac{\partial \log T(\mu)}{\partial E}\,, \tag{144}$$

for the thermoelectric coefficient $\alpha = V/\delta\Theta$, where $\zeta = (E-\mu)/\Theta$.[21]

The generalization to the multichannel case is straightforward: a sum of transparencies appears instead of a transparency. For a dirty sample, we then have

$$\alpha \approx \frac{\Theta}{e}\, \frac{e^2}{h}\, G^{-1}\, \frac{hL^2}{D}\,. \tag{145}$$

A large thermoelectric coefficient for mesoscopic conductors was explicitly predicted in [92]. The nonlinear case, which cannot be described using only the first derivative of the transparency with respect to energy (in which case the Katler–Mott formula becomes invalid), is considered in [93].

9.2 Thermal flow: the Wiedemann–Franz law

For a nonzero difference in temperatures, $\delta\Theta \neq 0$, electric current appears only when T depends on energy in the vicinity of μ. But the thermal flow also exists when the transparency is constant:

$$I_Q = \frac{2}{h}\int_{-\infty}^{\infty} \mathrm{d}E\, \left[f_{\mathrm{L}}(E) - f_{\mathrm{R}}(E) \right] T(E)(E-\mu)\,. \tag{146}$$

Here, the factor $2/h$ gives the number of electrons transmitted per unit time, while the factor $E-\mu$ in the integrand determines the amount of energy (which can dissipate) carried by each electron. For $\alpha = 0$ $(\partial_E T(\mu) = 0)$, the thermal flow is

$$I_Q = \frac{G}{e^2}\int_{-\infty}^{\infty} \mathrm{d}E\, \left[f_{\mathrm{L}}(E) - f_{\mathrm{R}}(E) \right](E-\mu)\,, \tag{147}$$

where G is the electric conductance and $G = (2e^2/h)T$.

[21] The relation

$$\int_{-\infty}^{\infty} \zeta^2\, \frac{\partial n}{\partial \zeta}\, \mathrm{d}\zeta = -\frac{\pi^2}{3}$$

is used.

Assuming that $\delta\Theta$ is small and expanding the difference $f_{\mathrm{L}}(E) - f_{\mathrm{R}}(E)$, we find

$$I_Q = \delta\Theta\, \frac{G}{e^2}\, \Theta \int_{-\infty}^{\infty} \zeta^2\, \frac{\partial n}{\partial \zeta}\, \mathrm{d}\zeta\,, \tag{148}$$

where $\zeta = (E-\mu)/\Theta$. Integrating, we obtain the Wiedemann–Franz law [94, 95]

$$\varkappa = \frac{\pi^2}{3}\left(\frac{1}{e}\right)^2 G\,\Theta \tag{149}$$

for the heat conduction $\varkappa = I_Q/\delta\Theta$, which is also valid for usual (nonmesoscopic) conductors.

9.3 Violation of the Wiedemann–Franz law

The transparency of meso- and nanoconductors, unlike that in usual conductors, can strongly depend on energy in the vicinity of the electrochemical potential μ, resulting in the appearance of the thermoelectromotive force

$$V = \alpha\,\delta\Theta\,, \tag{150}$$

which also contributes to the thermal flow, and then Wiedemann–Frantz law (149) can be violated. Substituting (150) in expression (146) for the thermal flow, we find

$$I_Q = \frac{2}{h}\int_{-\infty}^{\infty} \mathrm{d}E \left\{ \frac{1}{\exp\left[(E-\mu+e\alpha\,\delta\Theta)/(\Theta+\delta\Theta)\right]+1} - \frac{1}{\exp\left[(E-\mu)/\Theta\right]+1} \right\} T(E)(E-\mu)\,. \tag{151}$$

Standardly expanding (151) in $\delta\Theta$, we obtain

$$I_Q = \frac{2}{h}\int_{-\infty}^{\infty} \mathrm{d}E \left[e\alpha\, \frac{\partial T(\mu)}{\partial E} - \frac{T(\mu)}{\Theta} \right](E-\mu)^2\, \frac{\partial n(E)}{\partial E}\, \delta\Theta\,. \tag{152}$$

After integration, we obtain

$$I_Q = G\Theta \left[-\alpha^2 + \frac{\pi^2}{3}\left(\frac{1}{e}\right)^2 \right] \delta\Theta\,. \tag{153}$$

Hence, the Wiedemann–Franz law is valid only if $\alpha \ll (\pi/\sqrt{3})(1/e)$. We note that in principle, the situation is possible where $\alpha > (\pi/\sqrt{3})(1/e)$, but in that case, as follows from a more careful consideration, κ also remains positive.

The possibility of the violation of the Wiedemann–Frantz law in mesoscopic samples was first pointed out by Anderson and Engquist [96], which became in important step in the understanding of specific features of quantum low-dimension conductors different from usual metals.

10. Second quantization formalism and scattering matrix approach

In the preceding sections, we discussed the mean current in coherent conductors. The method used for the calculation of the current involves the summation of contributions to the current from different energy intervals. This method cannot be directly generalized to describe current fluctuations in time. Such calculations can be conveniently performed within the secondary quantization method

(using the Landauer approach, this was first done in [21]).[22]

In this section, we describe this method, derive the Landauer formula more rigorously, and consider noises. We find the mean current and noise by averaging current operators (in the secondary quantization representation) over the nonequilibrium density matrix of the system, taking the difference in the distribution of occupation numbers in electron reservoirs into account.

The state of an electron in the secondary quantization formalism is described not by the wave function $\varphi_k(x)$ but by the creation operator $\hat{c}_k^\dagger$ acting on a vacuum state $|0\rangle$. The current density operator

$$\hat{\mathbf{j}} = \frac{\mathrm{i}e\hbar}{2m}\left[(\nabla\hat{\Psi}^\dagger)\hat{\Psi} - \hat{\Psi}^\dagger\nabla\hat{\Psi}\right] \tag{154}$$

is defined in terms of the $\hat{\Psi}$ operators

$$\hat{\Psi}(x,\mathbf{r}_\perp) = \int\frac{\mathrm{d}k}{2\pi}\sum_{\alpha=1}^{N}\hat{c}_{\alpha,k}\,\varphi_{\alpha,k}(x,\mathbf{r}_\perp)\,, \tag{155}$$

where $\mathbf{r}_\perp$ is a vector in the cross section of a conductor. One-particle wave functions $\varphi_{\alpha,k}$ (where k is the wave vector at infinity and the subscript denotes a set of discrete quantum numbers, for example, the spin or number of a channel or a reservoir) used in secondary quantization form a complete orthonormalized set,

$$\int\mathrm{d}x\,\mathrm{d}\mathbf{r}_\perp\,\varphi^*_{\alpha',k'}(\mathbf{r})\,\varphi_{\alpha,k}(\mathbf{r}) = 2\pi\delta_{\alpha\alpha'}\,\delta(k'-k)\,, \tag{156}$$

and satisfy the Schrödinger equation

$$\hat{H}\varphi_{\alpha,k} = E_\alpha(k)\varphi_{\alpha,k}\,, \tag{157}$$

from which the dispersion law $E_\alpha(k)$ is also determined. The normalization condition for the annihilation and creation operators $\hat{c}_{\alpha,k}$ and $\hat{c}^\dagger_{\alpha',k'}$ has the form

$$\{\hat{c}^\dagger_{\alpha',k'}\hat{c}_{\alpha,k}\} = \hat{c}^\dagger_{\alpha',k'}\hat{c}_{\alpha,k} + \hat{c}_{\alpha,k}\hat{c}^\dagger_{\alpha',k'} = 2\pi\delta_{\alpha'\alpha}\,\delta(k'-k)\,. \tag{158}$$

The total current operator is the integral of the current density $\hat{\mathbf{j}}$ over the cross section:

$$\hat{I} = \int\mathrm{d}\mathbf{r}_\perp\,\hat{\mathbf{j}}(x,\mathbf{r}_\perp)\,. \tag{159}$$

We express the $\hat{\Psi}$ operators in terms of the Lippmann–Schwinger scattering states, which form the complete orthonormalized set of eigenstates of the Hamiltonian $\hat{H}$ (the proof of this fact is given in Appendix A.1). We note that normalizations in (156) and (158) should be matched. For convenience, we can redefine the normalization; for example, to obtain the delta function of energy in the right-hand side of (156), we should redefine (158) correspondingly such that the same delta function is in the right-hand side. Below, we use this renormalization.[23]

[22] An alternative can be either the method of wave packets developed by Landauer and Martin [23, 97–99], which is not rigorous either, or a rigorous description in terms of wave functions [26, 100], which allows describing the full counting statistics, but is too cumbersome, for example, for the calculation of noise.

[23] Such a normalization is convenient, for example, in the case where scattering states are to be defined in a region with a smooth semiclassical potential.

We now consider the problem of two electron reservoirs connected through a constriction with one open channel. If a particle with energy E is incident on a scatterer from the side of the left (right) reservoir, we let $\psi_{E,1}(x)$ ($\psi_{E,2}(x)$) denote the corresponding state. Quantum numbers characterizing the one-particle state are then the energy E and the number of the reservoir from which the particle was emitted (for simplicity, we omit the spin subscript). The $\hat{\Psi}$ operator has the form

$$\begin{aligned}\hat{\Psi}(x) &= \int\mathrm{d}E\left\{\psi_{E,1}(x)\hat{a}_{E,1} + \psi_{E,2}(x)\hat{a}_{E,2}\right\}\\ &= \int\mathrm{d}E\sum_{\alpha=1,2}\psi_{E,\alpha}(x)\hat{a}_{E,\alpha}\,,\end{aligned} \tag{160}$$

where $\hat{a}_{E,\alpha}$ are electron annihilation operators in the state with quantum numbers $\{E,\alpha\}$ ($\alpha = 1,2$). These operators satisfy the commutation relations

$$\{\hat{a}_{E,\alpha},\hat{a}^\dagger_{E',\alpha'}\} = \delta_{\alpha\alpha'}\,\delta(E-E')\,,\quad \{\hat{a}_{E,\alpha},\hat{a}_{E',\beta}\} = 0\,, \tag{161}$$

$$\left\{\hat{\Psi}(x),\hat{\Psi}^\dagger(x')\right\} = \delta(x-x')\,. \tag{162}$$

In the left asymptotic region, we then have

$$\begin{aligned}\hat{\Psi}(x\to-\infty) &= \int\frac{\mathrm{d}E}{\sqrt{2\pi\hbar v_1}}\\ &\times\left\{\left[\exp(\mathrm{i}k_1x) + r_E\exp(-\mathrm{i}k_1x)\right]\hat{a}_{E,1} + t_E\exp(-\mathrm{i}k_1x)\hat{a}_{E,2}\right\}.\end{aligned} \tag{163}$$

Similarly, we can obtain the expression for $\hat{\Psi}$ in the right asymptotic region in the form

$$\begin{aligned}\hat{\Psi}(x\to+\infty) &= \int\frac{\mathrm{d}E}{\sqrt{2\pi\hbar v_2}}\\ &\times\left\{\hat{a}_{E,1}t_E\exp(\mathrm{i}kx) + \hat{a}_{E,2}\left[r_E\exp(\mathrm{i}kx) + \exp(-\mathrm{i}kx)\right]\right\}.\end{aligned} \tag{164}$$

Using (163) and (164), we can find the current operator in the asymptotic regions. For example, to the right of the scatterer, we have

$$\begin{aligned}\hat{I}(x) &= e\int\mathrm{d}E'\,\mathrm{d}E\,\frac{\mathrm{i}}{2\pi m\sqrt{v_1v_2'}}\\ &\times\Big\{\hat{a}^\dagger_{E',1}\hat{a}_{E,1}(-\mathrm{i}k'-\mathrm{i}k)\,t^*_{E'}t_E\exp\left[\mathrm{i}(k-k')x\right]\\ &+\hat{a}^\dagger_{E',1}\hat{a}_{E,2}\Big[(-\mathrm{i}k')\,t^*_{E'}\exp(-\mathrm{i}k'x)\\ &\times\left(\exp(-\mathrm{i}kx) + r_E\exp(\mathrm{i}kx)\right)\\ &-t^*_{E'}\exp(-\mathrm{i}k'x)\left(-\mathrm{i}k\exp(-\mathrm{i}kx) + \mathrm{i}kr_E\exp(\mathrm{i}kx)\right)\Big]\\ &+\hat{a}^\dagger_{E',2}\hat{a}_{E,1}\Big[\left(\mathrm{i}k'\exp(\mathrm{i}k'x) - \mathrm{i}k'r^*_{E'}\exp(-\mathrm{i}k'x)\right)t_E\exp(\mathrm{i}kx)\\ &-\left(\exp(\mathrm{i}k'x) + r^*_{E'}\exp(-\mathrm{i}k'x)\right)\mathrm{i}kt_E\exp(\mathrm{i}kx)\Big]\\ &+\hat{a}^\dagger_{E',2}\hat{a}_{E,2}\Big[\left(\mathrm{i}k'\exp(\mathrm{i}k'x) - \mathrm{i}k'r^*_{E'}\exp(-\mathrm{i}k'x)\right)\\ &\times\left(\exp(-\mathrm{i}kx) + r_E\exp(\mathrm{i}kx)\right)\\ &-\left(\exp(\mathrm{i}k'x) + r^*_{E'}\exp(-\mathrm{i}k'x)\right)\\ &\times\left(-\mathrm{i}k\exp(-\mathrm{i}kx) + \mathrm{i}kr_E\exp(\mathrm{i}kx)\right)\Big]\Big\}\,.\end{aligned} \tag{165}$$

For a pure state of a many-particle quantum system, which is described in the framework of second-quantized formalism by an expression like $|\psi\rangle = \hat{a}^{\dagger}_{E_1}\hat{a}^{\dagger}_{E_2}\ldots|0\rangle$ (where $|0\rangle$ is the vacuum state), the mean current is defined as

$$I = \langle\psi|\hat{I}|\psi\rangle\,. \tag{166}$$

If the state is described by the density matrix $\hat{\rho}$ (i.e., the state is an incoherent superposition of pure states), the mean current is given by

$$I = \sum_{\{\psi\},\{\psi'\}} \langle\psi'|\hat{\rho}|\psi\rangle\langle\psi|\hat{I}|\psi'\rangle \equiv \mathrm{Tr}\,\{\hat{\rho}\hat{I}\}\,, \tag{167}$$

where the current operator is multiplied by the density matrix and the trace of this product is taken. For an equilibrium system with a Hamiltonian $\hat{H}$, a finite temperature Θ, and an electrochemical potential μ, the density matrix is given by[24]

$$\hat{\rho} = \exp\left(-\frac{\hat{H}-\mu\hat{N}}{\Theta}\right). \tag{168}$$

The Landauer assumption that reservoirs are completely independent in the nonequilibrium case, which was adopted above, means that the density matrix of the total system is equal to the product of the density matrices of the left and right reservoirs, $\hat{\rho} = \hat{\rho}_1 \otimes \hat{\rho}_2$. The density matrix of the reservoir α has the form

$$\hat{\rho}_\alpha = \exp\left(-\sum_E \hat{a}^{\dagger}_{E,\alpha}\hat{a}_{E,\alpha}\,\frac{E-\mu_\alpha}{\Theta_\alpha}\right). \tag{169}$$

Then the density matrix of the total system is

$$\hat{\rho} = \exp\left(-\sum_E\left\{\hat{a}^{\dagger}_{E,1}\hat{a}_{E,1}\,\frac{E-\mu_1}{\Theta_1} - \hat{a}^{\dagger}_{E,2}\hat{a}_{E,2}\,\frac{E-\mu_2}{\Theta_2}\right\}\right). \tag{170}$$

Using this density matrix, we can find all averages,

$$\langle\hat{a}^{\dagger}_{E,\alpha\sigma}\hat{a}_{E',\alpha'\sigma'}\rangle = \delta(E-E')\,\delta_{\alpha\alpha'}\,\delta_{\sigma\sigma'}\,f_{\alpha\sigma}(E) \tag{171}$$

(as an example, we indicate the spin index σ explicitly).

Almost all calculations presented in this review are in fact rather simple. One of the important sources of this simplicity is just relation (171), which implies that the only nonzero means are those that are diagonal in the scattering states in whose basis the current operator is written.

The electron distribution function $f_\alpha(E)$ inside reservoirs is given by Fermi distribution (47).[25] In the general case, temperatures and electrochemical potentials in reservoirs are different.

We also note that the real bias voltage V (specifying $\Delta\mu$ in the contact) can differ from the voltage V_0 (electromotive force) far in the reservoirs, and hence a part of the voltage drop $V_0 - V$ occurs in the lead wires of a quantum contact. This fact is taken into account experimentally quite simply, however. In addition, it may happen that a reservoir partially reflects electrons rather than absorbs them without reflection. This reflection can also be taken into account in principle as a correction to the density matrix, such that a nonzero average value $\langle\hat{a}^{\dagger}_1\hat{a}_2\rangle$ appears. In any case, we emphasize that approximations leading to the expressions used in this section (and above) are valid according to the experimental results. It seems that this is the main reason why the interaction with a reservoir, the possible role of reflection, the values of corrections, and so on have been insufficiently studied theoretically so far.

10.1 Average current

Using expressions (165), (167), and (170), we obtain expressions for the average current,[26] coinciding in the one-dimensional case with expression (49):

$$\langle\hat{I}\rangle = \frac{2e}{h}\int \mathrm{d}E\,T(E)\{f_1(E) - f_2(E)\}\,. \tag{172}$$

In the general case, in the presence of many channels and reservoirs, we have

$$I_\beta = \frac{2e}{h}\sum_\alpha\sum_{j,l}\int \mathrm{d}E\,[f_\beta(E) - f_\alpha(E)]\,T_{\beta\alpha,lj}(E)\,, \tag{173}$$

where α and β are the numbers of the reservoirs, and j and l are the numbers of the channels.

If $\mu_1 = E_{\mathrm{F}} + eV$, $\mu_2 = E_{\mathrm{F}}$, and $\Theta_1 = \Theta_2 = \Theta$, then as $V \to 0$, the conductance in the one-dimensional case has the form

$$G = \frac{2e^2}{h}\int T(E)\left(-\frac{\partial f}{\partial E}\right)\mathrm{d}E\,. \tag{174}$$

10.2 The Landauer approach from the standpoint of the Keldysh Green's functions

Many efforts have been devoted to a rigorous derivation of the Landauer formula by more traditional methods, in particular, based on the Kubo formula [101]. We show, omitting obvious details, how the Landauer formula can be obtained with the help of a more formal (or, more precisely, better formalized) approach used in Keldysh's paper [102] to construct a diagram technique for nonequilibrium situations. The Keldysh Green's function

$$\mathrm{i}G^{-+}(\mathbf{r},\mathbf{r}') = \mathrm{Tr}\,\{\hat{\rho}\hat{\Psi}^{\dagger}(\mathbf{r}')\,\hat{\Psi}(\mathbf{r})\} = \langle\hat{\Psi}^{\dagger}(\mathbf{r}')\,\hat{\Psi}(\mathbf{r})\rangle \tag{175}$$

is an analogue of the distribution function $f(q,p,t)$ in the kinetic equation. The kinetic equation is typically solved by specifying the boundary conditions in the reservoirs, such that the distribution function be coincident with the local equilibrium function. For the Keldysh function, the boundary conditions at infinity, i.e., in the reservoirs (see, e.g., [78]), are

$$G^{-+}(\mathbf{r},\mathbf{r}')\Big|_{\mathbf{r},\mathbf{r}'\in\mathrm{L(R)}} = G^{-+}_{\mathrm{eq}}(\mathbf{r},\mathbf{r}')\,, \tag{176}$$

where $\mathbf{r},\mathbf{r}' \in \mathrm{L(R)}$ means that $\mathbf{r}$ and $\mathbf{r}'$ belong to either the left or right, but always to the same reservoir. The current is

[24] In this case, we use the standard theoretical 'ensemble averaging'. However, experimental averaging occurs in time. The fact that these two averaging methods give the same result is the subject of the ergodic hypothesis. Thus, we calculate one quantity, but another is measured. However, the ergodic hypothesis gives grounds to assume that they should coincide. For some particular systems, the ergodic hypothesis can be proved.

[25] At distances from the contact greatly exceeding the characteristic energy relaxation length l_E associated with inelastic scattering of electrons on phonons or electron–electron scattering.

[26] It is important that the terms in (165) responsible for the mixing of the reservoirs, which contain creation and annihilation operators with different subscripts α, vanish due to (171).

expressed in terms of the Keldysh Green's function as

$$\mathbf{j} = \frac{e\hbar}{2m}\left[\frac{\partial}{\partial \mathbf{r}} - \frac{\partial}{\partial \mathbf{r}'}\right] G^{-+}(\mathbf{r},\mathbf{r}')\Big|_{\mathbf{r}=\mathbf{r}'} . \tag{177}$$

We consider a quasi-one-dimensional QPC with several open channels. Most of the electrons located far in the reservoirs belong to closed channels, which do not penetrate through the contact, and only a small fraction of electrons comes from the opposite reservoir. Therefore, because the ratio of open and closed channels in the reservoir is small,

$$\delta f \sim \frac{N_{\text{wire}}}{N_{\text{reservoir}}} , \tag{178}$$

the distribution function in the reservoirs can be treated as the equilibrium function with the specified μ_α and temperature, the boundary conditions for the Keldysh function calculated with density matrix (170) are satisfied, and hence the derivation of the Landauer formula is completely confirmed.

We qualitatively describe the transport picture once more. Particle fluxes emerging from the left and right reservoirs have distribution functions characterized by their temperatures and electrochemical potentials. In the contact region, particles experience only elastic scattering, and the distribution function is strongly nonequilibrium. Along with the states associated with the conducting channels in the contact, both reservoirs contain many other states not connected via the contact, which do not contribute to the current, although play a dominant role in the formation of distribution functions (far away in the reservoirs), which turn out to be close to equilibrium functions with good accuracy.

10.3 Noise description

We consider current fluctuations in time. To describe current fluctuations (noise), we need the time-dependent current operator in the Heisenberg picture. For the time-independent Hamiltonian H_0 of the system, this operator is written as

$$\hat{I}(x,\tau) = \exp\left(\frac{\mathrm{i}\hat{H}_0\tau}{\hbar}\right)\hat{I}(x)\exp\left(-\frac{\mathrm{i}\hat{H}_0\tau}{\hbar}\right), \tag{179}$$

$$\begin{aligned}
\hat{I}(x,\tau) = e\int \mathrm{d}E'\,\mathrm{d}E\,&\frac{\mathrm{i}\exp\left[-\mathrm{i}(E-E')\tau/\hbar\right]}{2\pi m\sqrt{v_1 v_2'}} \\
&\times\Big\{\hat{a}^\dagger_{E',1}\hat{a}_{E,1}(-\mathrm{i}k'-\mathrm{i}k)\,t^*_{E'}t_E\exp\left[\mathrm{i}(k-k')x\right] \\
&+\hat{a}^\dagger_{E',1}\hat{a}_{E,2}\Big[(-\mathrm{i}k')\,t^*_{E'}\exp(-\mathrm{i}k'x) \\
&\times\big(\exp(-\mathrm{i}kx)+r_E\exp(\mathrm{i}kx)\big) \\
&-t^*_{E'}\exp(-\mathrm{i}k'x)\big(-\mathrm{i}k\exp(-\mathrm{i}kx)+\mathrm{i}kr_E\exp(\mathrm{i}kx)\big)\Big] \\
&+\hat{a}^\dagger_{E',2}\hat{a}_{E,1}\Big[\big(\mathrm{i}k'\exp(\mathrm{i}k'x) \\
&-\mathrm{i}k'r^*_{E'}\exp(-\mathrm{i}k'x)\big)\,t_E\exp(\mathrm{i}kx) \\
&-\big(\exp(\mathrm{i}k'x)+r^*_{E'}\exp(-\mathrm{i}k'x)\big)\,\mathrm{i}kt_E\exp(\mathrm{i}kx)\Big] \\
&+\hat{a}^\dagger_{E',2}\hat{a}_{E,2}\Big[\big(\mathrm{i}k'\exp(\mathrm{i}k'x)-\mathrm{i}k'r^*_{E'}\exp(-\mathrm{i}k'x)\big) \\
&\times\big(\exp(-\mathrm{i}kx)+r_E\exp(\mathrm{i}kx)\big) \\
&-\big(\exp(\mathrm{i}k'x)+r^*_{E'}\exp(-\mathrm{i}k'x)\big) \\
&\times\big(-\mathrm{i}k\exp(-\mathrm{i}kx)+\mathrm{i}kr_E\exp(\mathrm{i}kx)\big)\Big]\Big\} .
\end{aligned} \tag{180}$$

Fluctuations are described using the average $\langle\Delta\hat{I}(x,\tau)\,\Delta\hat{I}(x',\tau')\rangle$, where the operator $\Delta\hat{I} = \hat{I} - \langle\hat{I}\rangle$ determines a deviation from the mean current. This average is called the *irreducible correlator*, is denoted by $\langle\langle\hat{I}(x,\tau)\,\hat{I}(x',\tau')\rangle\rangle$, and is given by

$$\begin{aligned}
&\big\langle\big\langle\hat{I}(x,\tau)\,\hat{I}(x',\tau')\big\rangle\big\rangle \\
&\quad\equiv\big\langle\hat{I}(x,\tau)\,\hat{I}(x',\tau')\big\rangle - \big\langle\hat{I}(x,\tau)\big\rangle\big\langle\hat{I}(x',\tau')\big\rangle \\
&\quad=\big\langle\Delta\hat{I}(x,\tau)\,\Delta\hat{I}(x',\tau')\big\rangle .
\end{aligned} \tag{181}$$

Current operators evaluated at different instants do not commute, and therefore the operator $\Delta\hat{I}(x,\tau)\,\Delta\hat{I}(x',\tau')$ is not Hermitian and quantity (181) is typically complex. This means that this quantity cannot be directly measured in experiments. In Landau and Lifshitz's book [103], the symmetrized correlator

$$\frac{1}{2}\Big(\big\langle\big\langle\hat{I}(x,\tau)\,\hat{I}(x',\tau')\big\rangle\big\rangle + \big\langle\big\langle\hat{I}(x',\tau')\,\hat{I}(x,\tau)\big\rangle\big\rangle\Big) \tag{182}$$

is considered to be a measurable quantity. Another standard quantity characterizing noise is the Fourier transform of current correlators: the *spectral noise density*. In [103], it was proposed to take the Fourier transform of symmetrized correlator (182). However, as follows from the analysis of the measurement process, the measurable quantity is typically the Fourier transform of the nonsymmetrized correlator[27] [104–106]

$$S(\omega) = \int \mathrm{d}\tau\,\exp(\mathrm{i}\omega\tau)\big\langle\big\langle\hat{I}(x,0)\,\hat{I}(x,\tau)\big\rangle\big\rangle . \tag{183}$$

This fact was confirmed in recent experiments [107] (see also previous experiments [108–110] in which only the excessive noise was measured, and, as a result, it was impossible to rigorously distinguish the symmetrized correlator from the nonsymmetrized one [111]).

In (183), we used the fact that in the absence of time-dependent external fields, the correlation function must depend only on the time difference. Therefore, the Fourier transform with respect to two times has the form

$$\big\langle\big\langle\hat{I}(x,\omega)\,\hat{I}(x,\omega')\big\rangle\big\rangle = S(\omega)2\pi\delta(\omega+\omega') . \tag{184}$$

The quantity studied most often is the spectral noise density at the zero frequency:

$$\begin{aligned}
S(0) = \frac{2e^2}{h}\int_0^{+\infty}\mathrm{d}E\Big\{&f_1(E)\big[1-f_1(E)\big]\,T^2(E) \\
&+f_2(E)\big[1-f_2(E)\big]\,T^2(E)+T(E)\big[1-T(E)\big] \\
&\times\big[f_1(E)\big(1-f_2(E)\big)+f_2(E)\big(1-f_1(E)\big)\big]\Big\} .
\end{aligned} \tag{185}$$

This quantity is independent of coordinates (which is the general property following from the stationarity of the random process of charge transfer).

Expression (185) was first obtained by one of us [21]. Its generalization to the multichannel case [21] looks surprisingly simple in the representation of eigenchannels in [23], for

[27] Which, unlike the nonsymmetrized current correlator at different times, is always a real quantity.

which the transparency is diagonalized,

$$S(0) = \frac{2e^2}{h}\sum_n \int_0^{+\infty} \mathrm{d}E \Big\{ f_1(E)\big(1-f_1(E)\big)T_n^2(E) + f_2(E)\big(1-f_2(E)\big)T_n^2(E) + T_n(E)\big(1-T_n(E)\big) \times \big[f_1(E)\big(1-f_2(E)\big) + f_2(E)\big(1-f_1(E)\big)\big]\Big\}, \quad (186)$$

and coincides in form with the expression for a QPC in which the channels are not mixed [21].

We consider the value of $S(0)$ in the limit case where the reservoirs are in equilibrium with each other ($f_1 = f_2 = f$). Then the relation $f(1-f) = -\Theta\,\partial_E f$ holds, and we obtain

$$S(0) = \frac{4e^2\Theta}{h}\int \mathrm{d}E \left(-\frac{\partial f}{\partial E}\right) T(E) = 2\Theta G\,. \quad (187)$$

This is the equilibrium noise (the Johnson–Nyquist noise) appearing due to *temperature* fluctuations of the electron occupation numbers in the reservoirs.

We now consider noise in the limit (quantum) case where the temperature of the reservoirs is zero. Then $f_\alpha(E) = \theta(E-\mu_\alpha)$ and

$$S(0) = \frac{2e^2}{h}\int \mathrm{d}E\,\big[1-T(E)\big]\,T(E)\big[f_2(E)-f_1(E)\big] \approx \frac{2e^3|V|}{h}\,(1-T)T = e\langle\hat{I}\rangle(1-T)\,, \quad (188)$$

where we set $\mu_1 = \mu + eV$ and $\mu_2 = \mu$.

The approximate equality in (188) is valid if the transmission probability $T(E)$ weakly depends on energy. In this case, expression (188) (the Khlus–Lesovik formula) was obtained in [112] and then independently in [21], as a particular case of general expression (185).[28]

It follows from (188) that the quantum shot noise intensity is determined by scattering from a potential barrier. If a scatterer is absent, $T = 1$, the noise is also absent. Noise also disappears if $T = 0$ because the electron transfer is then completely absent. In the intermediate situation, the wave packets describing electrons split into transmitted and reflected fractions during tunneling through the barrier. During measurements, electrons can be detected both in the left reservoir ('reflected electrons') and in the right reservoir ('transmitted electrons'), and this occurs absolutely unpredictably and randomly. This principal quantum mechanical unpredictability is the main source of the quantum shot noise. It is important that in the quantum case, the electrons obeying the Fermi–Dirac statistics leave the reservoir in an almost ordered way, and therefore, in the absence of the uncertainty caused by scattering from the barrier ($T = 1$), the low-frequency shot noise is suppressed. Expression (188) was confirmed in the excellent experiments of two groups [113, 114] studying noise in QPCs. At a plateau, where $T_n = 1$ or $T_n = 0$ for all channels, the noise was suppressed, while in the region of steps, it was finite, according to (188), and correctly depended on transparency.

Expressions obtained for the dependence of noise on the transparency make the theory closed in some sense. In describing the conductance for a QPC, we compared theoretical results based on the calculations of T with experimental data. But having theoretical results for the average current and noise, it is possible not to calculate the transparency T but to determine it *experimentally from current measurements, and then to compare these measurements with independent experimental data on noise*.

The measurements of noise in dirty samples allow proving that the transparency distribution function (the Dorokhov function) is actually nontrivial and the simple estimates of transparencies discussed in Section 8.2 are incorrect. If all the transparencies are small, it follows from the general expression that

$$S(0) \approx e\langle\hat{I}\rangle\,, \quad (189)$$

and the Fano factor F, defined as the ratio $F = S(0)/eI$, is unity, $F = 1$, as for the classical shot noise (see the end of this section). By averaging the sum $\sum_n T_n(1-T_n)$ entering the expression for noise with the Dorokhov distribution function, it is possible to obtain the relation $\langle\sum_n T_n(1-T_n)\rangle = (1/3)\langle\sum_n T_n\rangle$ and the Fano factor $F = 1/3$ [85]. Experiments [115, 116] confirmed these calculations.

The energy dependence of transparency gives rise to some additional effects. In the case of ideal resonance at a voltage exceeding the width of the resonance, i.e., in the plateau of the current–voltage characteristic (Fig. 18b), the Fano factor F is $1/2$. This result is obtained because the energy dependence of the transparency distribution function is nontrivial (see also Section 15.2, where noise in the hybrid INIS junction is considered). We also note that for a certain energy dependence of the transparency, noise can begin to decrease at a nonzero voltage: in other words, the 'excess noise' can become negative [117].

Finally, we see that expression (188) for noise contains the electron charge, and therefore the discreteness of the charge carried by quantum particles is also significantly manifested in the shot noise. Schottky was the first to point out this circumstance in 1918 and to derive the famous formula

$$S(0) = e\langle I\rangle \quad (190)$$

for the classical shot noise, assuming that the random electron transfer process is Poissonian (i.e., all electrons escape independently of each other) with the escape probability for m electrons $P_m = (\bar{N}^m/m!)\exp(-\bar{N})$, where $\bar{N} = It/e$. The mean-square deviation for the transferred charge in this process is $\langle(\delta Q)^2\rangle = e^2\langle(\delta N)^2\rangle = e^2\langle N\rangle$. Using the relation

$$\lim_{t\to\infty}\frac{\big\langle\big(\delta Q(t)\big)^2\big\rangle}{t} = S(0)\,, \quad (191)$$

Schottky obtained formula (190).

The ratio $S(0)/I$ of the noise intensity to the mean current is used for experimental measurements of the charge of an elementary current carrier, which is not always an isolated electron. Important measurements of a fractional charge in the fractional quantum Hall effect were performed by two groups [118–121]. A more complete bibliography on noises is presented in reviews [122, 123].

11. Full counting statistics

Typical quantities that were studied until recently in the quantum transport are the time-averaged current and noise, i.e., a pair current correlator. However, it is known from the theory of random processes that to characterize a random

[28] To extract expression (188) from paper [112], some care is required.

process completely, it is also necessary to study higher-order correlators and the distribution function for the transferred charge (which requires the knowledge of current correlators of all orders at low frequencies). This knowledge provides the maximally complete information on a system, taking into account that the process is nondeterministic. One of the sources of uncertainty, as pointed out in Section 10.3, is related to the probabilistic nature of quantum mechanics, and another to the inaccurate knowledge of the reservoir states. Hence, along with the mean current $\langle I\rangle$, transferred charge $\langle Q(t)\rangle = \langle I\rangle t$, or mean-square deviation $\langle(\delta Q)^2\rangle$ [and, correspondingly, noise $S(0)$], it is also interesting to study the higher-order moments

$$\langle Q^n\rangle = \int_0^t \mathrm{d}t_1 \ldots \mathrm{d}t_n \left\langle I(t_1)\ldots I(t_n)\right\rangle \tag{192}$$

and the characteristic function, as was first done in [24, 124]. The characteristic function for the distribution function of the transferred charge (we define it for the dimensionless number Q/e of transferred particles),

$$\chi(\lambda) = \sum_n \frac{\langle (Q/e)^n\rangle}{n!}(\mathrm{i}\lambda)^n = \left\langle \exp\frac{\mathrm{i}\lambda Q}{e}\right\rangle, \tag{193}$$

contains information on all moments because it is a generating function, and all the moments are determined by differentiating this function:

$$\left\langle \left(\frac{Q}{e}\right)^n\right\rangle = \frac{\mathrm{d}^n}{\mathrm{d}(\mathrm{i}\lambda)^n}\,\chi(\lambda)\bigg|_{\lambda=0}. \tag{194}$$

A random process can be more conveniently characterized by cumulants instead of moments. The cumulant is defined by the expression

$$\left\langle\left\langle \left(\frac{Q}{e}\right)^n\right\rangle\right\rangle = \frac{\mathrm{d}^n}{\mathrm{d}(\mathrm{i}\lambda)^n}\log\chi(\lambda)\bigg|_{\lambda=0}. \tag{195}$$

Cumulants have the following important properties: (i) those with $n > 1$ do not change when a random variable is shifted by c, $\langle\langle (Q+c)^n\rangle\rangle = \langle\langle Q^n\rangle\rangle$, (ii) they are homogeneous of degree n, $\langle\langle (cQ)^n\rangle\rangle = c^n\langle\langle Q^n\rangle\rangle$, and (iii) they are additive, $\langle\langle (Q+\tilde{Q})^n\rangle\rangle = \langle\langle Q^n\rangle\rangle + \langle\langle \tilde{Q}^n\rangle\rangle$, if Q and $\tilde{Q}$ are independent variables. It follows from the last property that $\langle\langle Q^n\rangle\rangle \propto t$ for large times t exceeding correlation times in the system. The argument is as follows: the whole process at large times can be divided into independent subprocesses contributing to the net result. Because the number of subprocesses increases linearly with increasing t, the total cumulant behaves similarly.

Knowing all the cumulants, for example, we can describe the Josephson generation frequency shift [125] and accurately describe the influence of noise in a wire on near quantum systems (for example, qubits) without assuming that the noise distribution is Gaussian, as is usually accepted [126–128]. In addition, it becomes possible to accurately describe the properties of a QPC as a detector related to a quantum bit [129]. A third-order correlator can indicate asymmetry in a two-level system, affecting conduction electrons [125, 126], and the presence of other effects.[29]

[29] We do not present here the list of all possible effects in which the non-Gaussian distribution of fluctuations is manifested, because this question is outside the scope of our review.

We now determine the number n of electrons transferred in time t, which are related to the charge as $Q = en$. The random process is defined by the probabilities P_n that exactly n particles are transferred in time t, i.e.,

$$\chi(\lambda) = \left\langle \exp\frac{\mathrm{i}\lambda Q}{e}\right\rangle = \sum_n P_n \exp(\mathrm{i}\lambda n). \tag{196}$$

We note that the assumption that n is an integer leads to the periodicity of $\chi(\lambda)$ with the period 2π.

The probabilities P_n can be obtained from the characteristic function via the Fourier transform

$$P_n = \int_0^{2\pi}\frac{\mathrm{d}\lambda}{2\pi}\exp(-\mathrm{i}\lambda n)\,\chi(\lambda). \tag{197}$$

In the quantum case, the relation between current correlators and moment observables (192) and charge cumulants is not as simple as in the classical case. Different definitions are found to lead to different results, and to obtain unambiguous results, it is necessary to describe not only a wire but also a detector and a measurement scheme. In the calculation of the characteristic function defined similarly to the classical expression as $\chi(\lambda) = \langle\exp[\mathrm{i}\lambda\int_0^t \hat{I}(t')\,\mathrm{d}t']\rangle$, the problem of time ordering of current operators appears. If we follow this definition literally, current operators in the expressions for moments and cumulants should be symmetrized. This definition was used in 1992 in the first paper [124] on the full counting statistics. The result obtained for a one-channel conductor with a transparency T at a finite voltage V and zero temperature has the form

$$\begin{aligned}\chi(\lambda) &= \left\langle \exp\left[\mathrm{i}\lambda\int_0^t \mathrm{d}t'\,\frac{\hat{I}(t')}{e}\right]\right\rangle \\ &= \left[\cos(\lambda\sqrt{T}) + \mathrm{i}\sqrt{T}\sin(\lambda\sqrt{T})\right]^N,\end{aligned} \tag{198}$$

where $N = 2eVt/h \gg 1$ is the 'number of attempts'. This expression is periodic with the period $2\pi/\sqrt{T}$, which can be interpreted by saying that the distribution function exists for a fractional charge $e^* = e\sqrt{T}$, which appears in some way in a system, but is manifested neither in the mean current nor in the noise. Although result (198) is formally correct and follows from the definition of the characteristic function, a further analysis has shown that such a distribution function was not directly realized in all the measurement schemes considered.

To solve the problem of determining the characteristic function in the quantum case, it was necessary to analyze the measurement scheme, and the authors of [69, 130] proposed the analog of a classical galvanometer measuring (counting) a charge — a quantum galvanometer represented by a spin 1/2 located near the wire and precessing in a magnetic field induced by the current. The precession angle allows measuring the charge $Q = \int_0^t I(t')\,\mathrm{d}t'$ that has flown. The interaction between the spin and an electron in the wire is described by the Hamiltonian

$$\hat{H}_{\mathrm{int}} = -\frac{1}{c}\int \mathrm{d}x\,\hat{I}(x)\,A(x), \tag{199}$$

where $A(x)$ is the component of the vector potential induced by the spin 1/2 in the quantum conductor (along the wire). In the general case, such an interaction is long-range, but to simplify calculations, it can be replaced with a local interac-

tion by representing $A(x)$ in the form[30]

$$A(x) = A_0\,\delta(x - x_0)\sigma_z\,, \tag{200}$$

where σ_z is the Pauli matrix, x_0 is the position of the measuring spin, and A_0 specifies the strength of interaction with electrons in the wire. Correspondingly, the interaction Hamiltonian takes the form $\hat{H}_{\rm int} = \hat{H}_{{\rm int},+}|\uparrow\rangle\langle\uparrow| + \hat{H}_{{\rm int},-}|\downarrow\rangle\langle\downarrow|$, where

$$\hat{H}_{{\rm int},\pm} = \mp\lambda\,\frac{\hbar I(x_0)}{2e}\,, \tag{201}$$

$\lambda = 2eA_0/\hbar c$, and $|\uparrow\rangle$ and $|\downarrow\rangle$ are spin states.

We assume that the initial state of the measuring spin is specified by the density matrix $\hat{\rho}^{\,\rm s}(0)$ at the instant $t = 0$. The transfer statistics can be 'rewritten' in terms of the angle of spin rotation for time t, which can be obtained from nondiagonal elements of the spin density matrix. The time evolution of nondiagonal elements of the spin density matrix [assuming that it is independent at the instant $t = 0$ of the density matrix $\hat{\rho}^{\,\rm e}(0)$ of the electron system] is described by

$$\begin{aligned}\hat{\rho}^{\rm s}_{\uparrow\downarrow}(t) &= {\rm Tr_e}\left\{\exp\left(-\frac{{\rm i}(\hat{H}_{\rm e} + \hat{H}_{{\rm int},+})t}{\hbar}\right)\hat{\rho}_{\rm e}(0)\right.\\ &\quad\left.\times\exp\left(\frac{{\rm i}(\hat{H}_{\rm e} + \hat{H}_{{\rm int},-})t}{\hbar}\right)\right\}\hat{\rho}^{\rm s}_{\uparrow\downarrow}(0)\\ &= {\rm Tr_e}\left\{\mathcal{T}\left[\exp\left({\rm i}\lambda\int_0^t {\rm d}t'\,\frac{I(x_0,t')}{2e}\right)\right]\hat{\rho}^{\,\rm e}(0)\right.\\ &\quad\left.\times\tilde{\mathcal{T}}\left[\exp\left({\rm i}\lambda\int_0^t {\rm d}t'\,\frac{I(x_0,t')}{2e}\right)\right]\right\}\hat{\rho}^{\rm s}_{\uparrow\downarrow}(0)\,,\end{aligned} \tag{202}$$

where the trace (${\rm Tr_e}$) is taken over the electron degrees of freedom and $\hat{H}_{\rm e}$ is the Hamiltonian of the electron subsystem. The expression after the second equality sign in (202) is written in the interaction picture in which the free energy operator $\hat{H}_{\rm e}$ determines the time dependence of the current operator $I(x_0, t)$, while $\mathcal{T}$ and $\tilde{\mathcal{T}}$ respectively denote time ordering and antiordering.[31] Defining $\chi(\lambda)$ as $\hat{\rho}^{\rm s}_{\uparrow\downarrow}(t)/\hat{\rho}^{\rm s}_{\uparrow\downarrow}(0)$,[32] we obtain the characteristic function of the transfer statistics:

$$\chi(\lambda) = \left\langle\tilde{\mathcal{T}}\left(\exp\left[{\rm i}\lambda\int_0^t\frac{{\rm d}t'\hat{I}(t')}{2e}\right]\right)\mathcal{T}\left(\exp\left[{\rm i}\lambda\int_0^t\frac{{\rm d}t'\,I(t')}{2e}\right]\right)\right\rangle. \tag{203}$$

We see that this definition differs from (198) by the presence of time ordering of current operators.

Characteristic function (203) at zero temperature and a finite voltage has the form [24]

$$\chi(\lambda) = \left[1 - T + T\exp({\rm i}\lambda)\right]^N \tag{204}$$

and has the period 2π as a function of λ, which leads to the charge quantization in units of e. However, although the characteristic function determined by the measuring spin 1/2 is 2π-periodic in this particular case, there are no grounds to believe that this result is general for arbitrary $\hat{H}_{\rm e}$ and $\hat{\rho}_{\rm e}(0)$. Moreover, an explicit example is presented in [132] where the initial state is a superposition of the left and right scattering states and the characteristic function has the period 4π (which means the charge quantization in units of $e/2$). Nevertheless, although the chosen definition (203) does not always give an integer charge quantization, the quantity $\chi(\lambda)$ is measurable and, in particular, describes the decoherence of a qubit (spin) coupled to a quantum wire. Indeed, according to the accepted definition, $\chi(\lambda)$ is a nondiagonal (normalized) element of the spin density matrix, and the absolute value $|\chi(\lambda)|$ specifies the decoherence degree. From relation (204), we obtain

$$\left|\chi(\lambda)\right| = \left|1 - T + T\exp({\rm i}\lambda)\right|^N = \left[1 - 4T(1-T)\sin^2\frac{\lambda}{2}\right]^{N/2}. \tag{205}$$

Since the value of λ is determined by the interaction strength, the decoherence rate is a nonmonotonic function of the coupling between the conductor and the measuring spin. In reality, a phase or a charge qubit can play the role of a spin (see the discussion in [133]).

Shelankov and Rammer [132] proposed an alternative definition of $\chi(\lambda)$, which always gives the period 2π and positive probabilities P_n. This definition corresponds to the approach in which P_n is measured directly, as proposed in [134]. The same definition was used in [100, 135] (also see the discussion in [131]). By performing the measurement corresponding to the operator $\mathcal{Q} = \int_{x_0}^{\infty}{\rm d}x\,|x\rangle\langle x|$, which determines a charge to the right of the detector at $t = 0$, and comparing the measurement result with a charge at time t, we can obtain the number of electrons that have passed in the time t. The formulation of the problem in this way leads to the characteristic function

$$\chi(\lambda) = \left\langle\exp\left(\frac{{\rm i}\lambda U^{\dagger}\mathcal{Q}U}{e}\right)\exp\left(-\frac{{\rm i}\lambda\mathcal{Q}}{e}\right)\right\rangle, \tag{206}$$

where $U = \exp(-{\rm i}\hat{H}_{\rm e}t)$ is the unitary evolution operator; the angular brackets denote averaging over the eigenstate of $\mathcal{Q}$ in which particles are initially certainly located either on the left or on the right of the scatterer (in particular, such a definition allows avoiding the states leading to periodicity with the period 4π).

11.1 Analysis of statistics in the one-electron example

To understand better how the transport statistics are described by means of the formalism presented (or rather outlined) above, which is based on the use of a measuring spin, we consider a simple problem for one electron. We assume that a wave packet with the wave function $f(k)$ in the k space concentrated near some $k_0 > 0$,

$$\Psi_{\rm in}(x,t) \equiv \Psi_f(x,t) = \int\frac{{\rm d}k}{2\pi}\,f(k)\exp\left[{\rm i}(kx - \omega_k t)\right], \tag{207}$$

located on the left for $t \to -\infty$, moves to the right and incidentes on a scatterer having the transmission amplitude t_k and reflection amplitude r_k. The function $f(k)$ is normalized by the condition $\int({\rm d}k/2\pi)|f(k)|^2 = 1$; $\omega_k = \hbar k^2/2m$. We locate a measuring spin near the scatterer. Then the

[30] Strictly speaking, a potential of this form can give rise to certain difficulties caused by the fact that the interaction Hamiltonian should take not only linear terms but also terms quadratic in $A(x)$ into account. This leads to some peculiarities in the description of statistics in the many-particle perturbation theory, which we do not consider here.

[31] If the measuring spin is located near the scatterer, the more complicated, so-called Matthew time ordering is required [131].

[32] During the flow of a classical current near the measuring spin, this quantity exponentially depends on the charge that has flowed (in units of the charge e), $\exp({\rm i}\lambda N)$.

transmitted part of the wave packet acquires an additional phase due to the interaction with the spin: in the case of magnetic interaction, the additional phase at the point x has the form $\delta\phi_A(x) = 2\pi\int_{-\infty}^{x} \mathrm{d}x'\, A_x(x')/\Phi_0$ and does not depend on k; as $x \to \infty$, we obtain the full phase $\lambda/2 = 2\pi\int_{-\infty}^{\infty} \mathrm{d}x\, A_x(x)/\Phi_0$. We note that ϕ_A has opposite signs for particles moving in opposite directions ($k \to -k$). Scattered waves, which have the form (for $t \to \infty$)

$$\Psi^{\pm}_{\mathrm{out}}(x,t) = \int \frac{\mathrm{d}k}{2\pi} f(k) \exp(-\mathrm{i}\omega_k t)\left[r_k \exp(-\mathrm{i}kx)\,\Theta(-x) + \exp\left(\pm\frac{\mathrm{i}\lambda}{2}\right) t_k \exp(\mathrm{i}kx)\,\Theta(x)\right], \tag{208}$$

acquire an additional phase, depending on the spin state $|\pm\rangle$ (or, in reality, a qubit state). The characteristic function for the full counting statistics is described by the expression

$$\begin{aligned}\chi(\lambda,t) &= \int \mathrm{d}x\, \Psi^{-*}_{\mathrm{out}}(x,t)\, \Psi^{+}_{\mathrm{out}}(x,t)\\ &= \int \frac{\mathrm{d}k}{2\pi}\left[R_k + \exp(\mathrm{i}\lambda)\, T_k\right]\left|f(k)\right|^2\\ &= \langle R\rangle_f + \exp(\mathrm{i}\lambda)\langle T\rangle_f,\end{aligned} \tag{209}$$

where $R_k = |r_k|^2$ and $T_k = |t_k|^2$. We neglected the nondiagonal term $\int \mathrm{d}k\, f^*(-k) f(k)$, which is typically exponentially small. The Fourier transform of the characteristic function gives the probabilities $P_0 = \langle R\rangle_f$ and $P_1 = \langle T\rangle_f$, coinciding, as expected, with the reflection and transmission probabilities for particles. We see from this simple example that the definition (with the measuring spin) works correctly. Of course, this method offers no advantages over standard probability calculations in this simple case, the advantages being manifested only for a large or infinite number of particles.

11.2 Analysis of the full counting statistics for two electrons

Following [136] and using the wave-packet formalism, we calculate the characteristic function for the full counting statistics for two particles — the simplest case where the Fermi statistics of particles is already manifested. Incident particles are described by the wave packets

$$\psi_{\mathrm{in},m}(x;t) = \int_0^{\infty} \frac{\mathrm{d}k}{2\pi} f_m(k) \exp\left[\mathrm{i}k(x - v_{\mathrm{F}}t)\right], \tag{210}$$

with wave functions $f_1(k)$ and $f_2(k)$ in the momentum space satisfying the normalization condition $\int(\mathrm{d}k/2\pi)|f_m(k)|^2 = 1$. Because we eventually consider electrons at low temperatures in the vicinity of the Fermi energy, it is convenient to linearize the spectrum $\epsilon = v_{\mathrm{F}}|k|$, where v_{F} is the Fermi velocity, $\hbar k$ is the momentum, and $\hbar\epsilon$ is the energy. After propagation through the scatterer, wave packet (210) is split into reflected and transmitted parts:

$$\begin{aligned}\psi^{\sigma}_{\mathrm{out},m}(x,t) = \int_0^{\infty} \frac{\mathrm{d}k}{2\pi} f_m(k) \exp(-\mathrm{i}kv_{\mathrm{F}}t)\\ \times\left[r_k \exp(-\mathrm{i}kx)\,\Theta(x_{\mathrm{s}} - x)\right.\\ \left. + \exp\left(\frac{\mathrm{i}\sigma\lambda}{2}\right) t_k \exp(\mathrm{i}kx)\,\Theta(x - x_{\mathrm{s}})\right],\end{aligned} \tag{211}$$

where we introduce the phase $\exp(\mathrm{i}\sigma\lambda/2)$ in the transmitted part of the wave packet; the sign $\sigma = \pm 1$ corresponds to the spin state, as in Section 11.1. The two-particle wave function symmetrized (antisymmetrized) in the proper way has the form

$$\Psi_{\alpha,\pm}(x_1,x_2;t) \propto \psi_{\alpha,1}(x_1;t)\psi_{\alpha,2}(x_2;t) \pm (x_1 \leftrightarrow x_2), \quad \alpha = \mathrm{in}, \mathrm{out};$$

here, we use the sign $\pm$ to distinguish the triplet and singlet states of two electrons. The characteristic function has the form

$$\chi_{\pm}(\lambda) = \int \mathrm{d}x_1\, \mathrm{d}x_2\, \Psi^{-1\,*}_{\mathrm{out},\pm}\, \Psi^{+1}_{\mathrm{out},\pm}.$$

From this, we obtain

$$\begin{aligned}\chi_{\pm}(\lambda) &= \frac{\left[1 + \left(\exp(\mathrm{i}\lambda) - 1\right)\langle 1|T|1\rangle\right]\left[1 + \left(\exp(\mathrm{i}\lambda) - 1\right)\langle 2|T|2\rangle\right]}{1 \pm |S|^2}\\ &\pm \frac{\left[S + \left(\exp(\mathrm{i}\lambda) - 1\right)\langle 1|T|2\rangle\right]\left[S^* + \left(\exp(\mathrm{i}\lambda) - 1\right)\langle 2|T|1\rangle\right]}{1 \pm |S|^2}\end{aligned} \tag{212}$$

with the matrix element

$$\langle n|T|m\rangle = \int \frac{\mathrm{d}k}{2\pi} f_n^*(k) T_k f_m(k),$$

where $T_k = |t_k|^2$; the overlap integral is

$$S = \int \frac{\mathrm{d}k}{2\pi} f_1^*(k) f_2(k).$$

The transmission probability for n particles is determined by the Fourier transform of the characteristic function

$$P_n = \int \frac{\mathrm{d}\lambda}{2\pi} \chi(\lambda) \exp(-\mathrm{i}\lambda n).$$

For the amplitude $t_k \equiv t$ independent of energy, the denominator in (212) cancels with the factor in the numerator that depends on the exchange term, and, as a result, the transfer statistics is independent of the exchange symmetry of the two-particle wave function. This property is typical for the one-dimensional case, whereas such a cancelation does not occur, generally speaking, in the multichannel case, and the interference (exchange) term is not zero even if the transmission amplitude is independent of energy.

If the transmission amplitude depends on energy, the exchange terms lead to significant effects in the transfer statistics. For simplicity, we consider two packets of the same form separated by a distance δx. The Fourier components of the packets satisfy the relation $f_2(k) = f_1(k)\exp(-\mathrm{i}k\,\delta x)$, whence

$$\langle 1|T|1\rangle = \langle 2|T|2\rangle \equiv \langle T\rangle = \int \frac{\mathrm{d}k}{2\pi} T_k \left|f_1(k)\right|^2.$$

The overlap integral $S = \int \mathrm{d}k/(2\pi)\left|f_1(k)\right|^2 \exp(\mathrm{i}k\delta x)$ is the Fourier transform of the packet distribution function in the

momentum space. The transmission probabilities $P_{n,\pm}$, which have the form

$$P_{0,\pm} = \frac{\left(1-\langle T\rangle\right)^2 \pm \left|S - \langle 1|T|2\rangle\right|^2}{1 \pm |S|^2}\,,$$
$$P_{1,\pm} = 2\,\frac{\langle T\rangle\left(1-\langle T\rangle\right) \pm \left[\mathrm{Re}\left(\langle 1|T|2\rangle S^*\right) - \left|\langle 1|T|2\rangle\right|^2\right]}{1 \pm |S|^2}\,,$$
$$P_{2,\pm} = \frac{\langle T\rangle^2 \pm \left|\langle 1|T|2\rangle\right|^2}{1 \pm |S|^2} \tag{213}$$

(with $\sum_n P_{n,\pm} = 1$), depend on the exchange symmetry if $\langle 1|T|2\rangle \neq S\langle T\rangle$.

Probabilities (213) can be easily transformed into the cumulants of the transmitted charge $Q = \int \mathrm{d}t\, I(t)$. The first two cumulants for two particles incident on the scatterer have the form

$$\begin{aligned} \langle n\rangle_\pm &= P_{1,\pm} + 2P_{2,\pm}\,, \\ \langle\langle n^2\rangle\rangle_\pm &= P_{1,\pm}(1-P_{1,\pm}) + 4P_{2,\pm}P_{0,\pm} \end{aligned} \tag{214}$$

(with $n = Q/e$), and they both depend on the exchange symmetry. Strangely enough, the effect caused by the exchange symmetry in the mean charge $\langle Q\rangle$ was discovered [136] considerably later than in the noise and charge fluctuations $\langle\langle Q^2\rangle\rangle$ [137–139].

To analyze the effect quantitatively, it is necessary to specify the form of the wave packet f_1 and the dependence of T_k on the momentum. We do not resort to the standard approximation of the Gaussian wave packet, but consider a more realistic example.

Recently, a method has been developed for sending isolated electrons on demand in quantum wires [140, 141]. In this case, electrons move not very high over the Fermi surface. Otherwise, the electron transport becomes incoherent due to the emission of phonons and photons (plasmons) by electrons. The presence of the Fermi sea bocks these inelastic processes, and the coherence length can reach a few micrometers, exceeding the size of a conductor, for example, a QPC.

Strictly one-particle excitations over the Fermi surface can be produced by applying a Lorentzian voltage pulse [69, 142][33] $V_{t_1}(t) = -(2v_\mathrm{F}\xi\Phi_0/c)/[v_\mathrm{F}^2(t-t_1)^2 + \xi^2]$, where the pulse duration ξ/v_F is expressed in terms of the length parameter ξ, and $\Phi_0 = hc/e$. Such a voltage pulse gives rise to a wave packet with the amplitude

$$f_1(k) = \sqrt{4\pi\xi}\,\exp\left[-\xi(k-k_\mathrm{F}) - \mathrm{i}kx_1\right]\Theta(k-k_\mathrm{F}) \tag{215}$$

($x_1 = v_\mathrm{F}t_1$) and the Lorentzian profile in the usual space,

$$|\psi_1|^2 = \frac{\xi/\pi}{(x-x_1-v_\mathrm{F}t)^2 + \xi^2}\,. \tag{216}$$

The overlap integral for the wave packets separated by a distance δx has the form

$$S = \frac{\exp\left(-\mathrm{i}k_\mathrm{F}\delta x\right)}{1 + \mathrm{i}\delta x/2\xi}\,.$$

[33] Generally speaking, a pulse with an arbitrary profile excites an infinite number of electron–hole pairs, which is a phenomenon quite similar to the so-called Anderson catastrophe (see the discussion in [69]).

We consider scatterers of two types:

(i) *with a transparency resonance*, which we write in the form

$$T_k^\mathrm{res} = \frac{\alpha}{1 + \beta^2(k-k_\mathrm{F}-k_0)^2}\,,$$

where $\alpha \leqslant 1$ is the amplitude of the resonance and $k_0 > 0$ is its position relative to the Fermi wave vector k_F. The resonance width β^{-1} should be much smaller than the wave-packet width ξ^{-1} in the k-space, $\beta^{-1} \ll \xi^{-1}$. The transparency $\langle T^\mathrm{res}\rangle$ for one packet with the amplitude $f_1(k)$ for $\beta^{-1} \ll k_0$ takes the form

$$\langle T^\mathrm{res}\rangle \approx \frac{2\pi\alpha\xi}{\beta}\exp\left(-2\xi k_0\right),$$

which is a resonance away from the Fermi level. Although the small parameter $k_0\xi$ provides a strong total signal, it leads to the suppression of exchange effects because the transparency is already maximal; we therefore consider intermediate and large values of $k_0\xi$;

(ii) *with a sharp transparency step* ($\beta^{-1} \ll \xi^{-1}$), for example, in a QPC. In this case, we use the Kemble formula considered above, which can now be conveniently written in the form

$$T_k^\mathrm{QPC} = \frac{\alpha}{1 + \exp\left[-\beta(k-k_\mathrm{F}-k_0)\right]}\,.$$

The mean transparency here is $\langle T^\mathrm{QPC}\rangle \approx \alpha\exp\left(-2\xi k_0\right)$; a small factor ξ/β is absent in this case.

For a pronounced (narrow) resonance, the exchange term takes the simple form

$$\left\langle 1|T^\mathrm{res}|2\right\rangle \approx \exp\left[-\mathrm{i}(k_\mathrm{F}+k_0)\delta x\right]\langle T^\mathrm{res}\rangle\,,$$

and its product with the overlap integral S^* is proportional to $\exp\left(-\mathrm{i}k_0\delta x\right)$ and independent of k_F. The mean number of particles oscillates as a function of the distance δx:

$$\begin{aligned} \langle n\rangle_\pm^\mathrm{res} = 2\langle T^\mathrm{res}\rangle\Bigg\{1 + \left(\frac{\delta x}{2\xi}\right)^2 \\ \pm\left[\cos\left(k_0\delta x\right) + \frac{\delta x}{2\xi}\sin\left(k_0\delta x\right)\right]\Bigg\}\left[1 + \left(\frac{\delta x}{2\xi}\right)^2 \pm 1\right]^{-1}. \end{aligned} \tag{217}$$

For wave packets with a large delay, $\delta x \gg \xi$, the exchange term decays as $(\delta x)^{-2}$, while the number of transmitted particles is $\langle n\rangle^\mathrm{res} = 2\langle T^\mathrm{res}\rangle$, irrespective of the exchange term sign. On the other hand, for strongly overlapped wave packets, $\delta x \to 0$, the result $\langle n\rangle_+^\mathrm{res} = 2\langle T^\mathrm{res}\rangle$ obtained for independent particles in the singlet case is reproduced. In the asymmetric case (a triplet), the number of particles

$$\langle n\rangle_-^\mathrm{res} = 2\langle T^\mathrm{res}\rangle(1 - 2\xi k_0 + 2\xi^2 k_0^2) \tag{218}$$

decreases for narrow wave packets with $\xi k_0 < 1$ and increases for packets with $\xi k_0 > 1$. The decrease can reach 50% for $\xi k_0 = 1/2$,[34] while the (relative) increase for $\xi k_0 > 1$ is unlimited. We note that this increase occurs because $P_{1,-}$ and $P_{2,-}$ almost vanish.

[34] It follows from the exponential decrease of $\langle T^\mathrm{res}\rangle \propto \exp\left(-2k_0\xi\right)$ that $\langle -Q/e\rangle^\mathrm{res} \ll 2$ for $\xi k_0 > 1$.

In the case of a QPC, the result is similar: the nondiagonal matrix elements take the form

$$\langle 1|T^{\mathrm{QPC}}|2\rangle \approx \exp\left(-\mathrm{i}k_0\delta x\right) S\langle T^{\mathrm{QPC}}\rangle\,,$$

and the interference term in P_2 vanishes. The number of transmitted particles

$$\langle n\rangle_{\pm}^{\mathrm{QPC}} = 2\langle T^{\mathrm{QPC}}\rangle\,\frac{1+(\delta x/2\xi)^2 \pm \cos\left(k_0\delta x\right)}{1+(\delta x/2\xi)^2 \pm 1} \tag{219}$$

oscillates with $k_0\delta x$. Different limits discussed above are also reproduced, except for the case of antisymmetric exchange and strongly overlapping packets [see (218)], in which the mean number of transmitted particles is

$$\langle n\rangle_{-}^{\mathrm{QPC}} = 2\langle T^{\mathrm{QPC}}\rangle(1+2\xi^2k_0^2)\,. \tag{220}$$

Equations (218) and (220) contain the most surprising results: for a large parameter ξk_0, the mean number of particles can increase very strongly compared to that of two independent packets. This is the case when all characteristic lengths are smaller than the dephasing length L_φ. Finally, we present the expression for the characteristic function in the case of the transfer statistics for two particles:

$$\begin{aligned}\chi_{\pm}^{\mathrm{res}} &= 1+\langle n\rangle_{\pm}^{\mathrm{res}}\left[\exp\left(\mathrm{i}\lambda\right)-1\right]\\ &\quad+\langle T^{\mathrm{res}}\rangle^2\,\frac{(1\pm 1)\left[(\delta x/2\xi)^2+1\right]}{(\delta x/2\xi)^2+1\pm 1}\left[\exp\left(\mathrm{i}\lambda\right)-1\right]^2,\end{aligned} \tag{221}$$

$$\chi_{\pm}^{\mathrm{QPC}} = 1+\langle n\rangle_{\pm}^{\mathrm{QPC}}\left[\exp\left(\mathrm{i}\lambda\right)-1\right]+\langle T^{\mathrm{QPC}}\rangle^2\left[\exp\left(\mathrm{i}\lambda\right)-1\right]^2. \tag{222}$$

The increase in $\langle n\rangle_-$ is completely caused by the increasing P_1. This effect is determined by the Pauli principle and the energy dependence of the transparency. The energy dependence of the transparency leads to the wave packet broadening, which, in conjunction with the Pauli principle, causes a decrease in P_0 and P_2, and therefore an increase in P_1. Nevertheless, situations are possible where P_2 also increases.

For example, a high probability $P_{2,-}$ [see (212)] is obtained for wave packets with the amplitudes shifted in the k-space, $f_2(k)=f_1(k+\delta k)$, and the large overlap integral S of the transmission amplitude is suppressed for k belonging to the overlap region. A large increase in the transmission probability P_2 for two electrons was also observed in [143].

We note that exchange effects in the transfer statistics at constant voltages are considered in [24], where, in particular, a simple example with a 'Y-joint' containing three channels is discussed and the characteristic function is found (pair correlators in this geometry are studied in [23, 137]).

11.3 Statistics for N particles

Following [136], we extend the previous analysis to the case of N particles with the (incident) wave function $\Psi(\mathbf{k})$ defined in the momentum space; the vector $\mathbf{k}=(k_1,\ldots,k_N)$ determines N momenta of particles. We consider independent noninteracting particles scattered from a barrier. The scattered wave function in the asymptotic region (for $t\to\infty$) takes the form

$$\begin{aligned}\psi_{\mathrm{out}}^{\pm}(\mathbf{x};t) = \Bigg\{\prod_{m=1}^{N}\int\frac{\mathrm{d}k_m}{2\pi}\Bigg[&r_{k_m}\exp\left[-\mathrm{i}k_m(x_m+v_{\mathrm{F}}t)\right]\Theta(-x_m)\\ &+t_{k_m}\exp\left[\mathrm{i}k_m(x_m-v_{\mathrm{F}}t)\right]\exp\left(\pm\frac{\mathrm{i}\lambda}{2}\right)\Theta(x_m)\Bigg]\Bigg\}\Psi(\mathbf{k})\,,\end{aligned} \tag{223}$$

which means that the evolution of the total wave function reduces to the individual evolutions of one-particle wave functions, and we obtain the product of asymptotic states (208). The characteristic function $\chi_N(\lambda)=\int\mathrm{d}\mathbf{x}\,\psi_{\mathrm{out}}^{-*}(\mathbf{x};t)\,\psi_{\mathrm{out}}^{+}(\mathbf{x};t)$ is expressed as

$$\chi_N(\lambda) = \left\{\prod_{m=1}^{N}\int\frac{\mathrm{d}k_m}{2\pi}\left[1-T_{k_m}+T_{k_m}\exp\left(\mathrm{i}\lambda\right)\right]\right\}\left|\Psi(\mathbf{k})\right|^2. \tag{224}$$

So far we have not specified the exact form of the incident wave function. If we restrict ourselves to the Slater determinant composed of orthonormalized one-particle functions ϕ_m,

$$\Psi(k_1,\ldots,k_N) = \frac{1}{\sqrt{N!}}\det\phi_m(k_n)\,, \tag{225}$$

then expression (224) can be represented as the determinant

$$\begin{aligned}\chi_N(\lambda) &= \det\int\frac{\mathrm{d}k}{2\pi}\,\phi_m^*(k)\left[1-T_k+T_k\exp\left(\mathrm{i}\lambda\right)\right]\phi_n(k)\\ &= \det\left\langle\phi_m\middle|1-T+T\exp\left(\mathrm{i}\lambda\right)\middle|\phi_n\right\rangle,\end{aligned} \tag{226}$$

containing one-particle matrix elements $\langle\phi_m|\mathcal{O}|\phi_n\rangle$ of the operator $\mathcal{O}=1-T+T\exp\left(\mathrm{i}\lambda\right)$.

The nonorthogonal basis. Real situations are typically described using the occupation of orthogonal states in the Slater determinant, as demonstrated above. But, for example, in the case presented in Fig. 25, electrons fill the states f_1 and f_2 that have a finite overlap, i.e., are not nonorthogonal. However, the N-particle Slater determinant can also be composed of nonorthogonal states $|f_m\rangle$ if they are linearly independent, i.e., $\det\langle f_m|f_n\rangle\neq 0$. The correctly antisymmetrized and normalized wave function (225) takes the form

$$\Psi^f(k_1,\ldots,k_N) = \frac{1}{\sqrt{N!\det\langle f_m|f_n\rangle}}\det f_m(k_n)\,. \tag{227}$$

Substituting this expression in (224) and repeating the calculations leading to (226), we obtain the characteristic

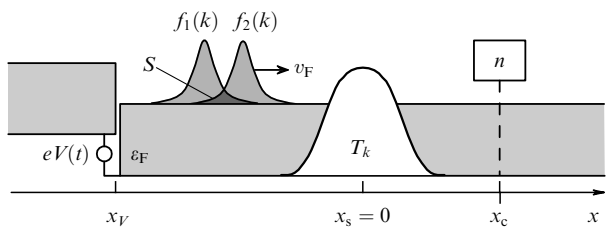

Figure 25. Quantum wire with a scattering center at x_{s} providing the momentum-dependent transparency T_k. The time-dependent potential $eV(t)$ applied at the point x_V (to the left of the scatterer) gives rise to the incident wave packets f_1 and f_2 with the overlaps $S=\langle f_2|f_1\rangle$. A detector located at the point x_{c} (to the right of the scatterer) measures the statistics of the number n of particles propagated to the right. We considered incident packets with $k>0$ outside the Fermi sea. As a result, the Fermi sea remains unperturbed in the asymptotic regime. The presence of the Fermi sea at finite times produces additional noise, which we neglect.

function as the ratio of determinants of two $N \times N$ matrices

$$\chi_N(\lambda) = \frac{\det \langle f_m | 1 - T + T \exp(\mathrm{i}\lambda) | f_n \rangle}{\det \langle f_m | f_n \rangle} = \frac{\det \left(S^f - T^f + T^f \exp(\mathrm{i}\lambda) \right)}{\det S^f}, \tag{228}$$

where the matrices S^f and T^f are defined by

$$S^f_{mn} = \langle f_m | f_n \rangle, \qquad T^f_{mn} = \langle f_m | T | f_n \rangle. \tag{229}$$

11.4 Invariance of the Slater determinant under linear transformations

Expression (228) for the characteristic function can be considerably simplified and represented in the form describing a generalized binomial distribution [26, 144, 145]. A significant feature of such a representation of the characteristic function is the fact that the Hilbert space H_N of dimension N spanned by the set of one-particle states with the wave functions $f_n(k)$ determines the only correctly antisymmetrized wave function (unentangled state) or, in other words, only one Slater determinant exists (up to a phase) for N particles (with states from H_N). The antisymmetrized N-particle (unentangled) state is thus determined by the Hilbert space H_N, i.e., by all states in the set, and is independent of the particular choice of an orthonormalized basis [146].

To clarify this, we consider a simple case of the two-particle Slater determinant in the secondary quantization representation $|\Psi\rangle = a_2^\dagger a_1^\dagger |0\rangle$ with the vacuum state $|0\rangle$ and fermion operators $a_{1,2}$. Defining the new operators $a_\pm = (a_1 \pm a_2)/\sqrt{2}$, we see that the two-particle state

$$a_+^\dagger a_-^\dagger |0\rangle = \frac{1}{2}(a_1^\dagger + a_2^\dagger)(a_1^\dagger - a_2^\dagger)|0\rangle = a_2^\dagger a_1^\dagger |0\rangle = |\Psi\rangle \tag{230}$$

remains invariant.

We now consider the N-particle Slater determinant in form (227). After the passage from basis states $f_m(k)$ to new states $g_m(k)$ via a complex linear transformation

$$g_m(k) = \sum_n A_{mn} f_n(k), \qquad \det A \neq 0, \tag{231}$$

the antisymmetric combination

$$\det g_m(k_n) = (\det A) \det f_m(k_n) \tag{232}$$

remains invariant up to the factor $\det A$; here, we took into account that the determinant of the product of matrices is equal to the product of their determinants. In addition, the normalized N-particle determinant states Ψ^f and Ψ^g satisfy the relation

$$\Psi^g(k_1, \ldots, k_N) = \operatorname{sign}(\det A)\, \Psi^f(k_1, \ldots, k_N), \tag{233}$$

where $\operatorname{sign} x = x/|x|$. The only effect of using the new basis is the appearance of the overall factor $\operatorname{sign}(\det A)$, which does not enter expression (224) for the characteristic function. The full counting statistics in bases f and g is therefore the same.

Diagonalization. The invariance of the determinant can be used to simplify the full counting statistics. In addition, even without specifying the scatterer type, it is possible to understand the full counting statistics qualitatively. In particular, we can assert that the statistics for states of the Slater determinant type always reduces to a generalized binomial form (which is valid for a single-lead conductor (two-contact wire), but not, generally speaking, for multilead conductors [147]).

We first consider how the invariance of determinant (232) is manifested in (228). We note that any one-particle matrix B of form (229) is transformed by A as

$$B^g = A^\dagger B^f A, \qquad B = S, T. \tag{234}$$

Because $\det(AB) = \det A \det B$, it follows that χ_N is invariant under the change of basis

$$\chi_N = \frac{\det X^f}{\det S^f} = \frac{|\det A|^2 \det X^f}{|\det A|^2 \det S^f} = \frac{\det X^g}{\det S^g}, \tag{235}$$

where $X^f \equiv S^f - T^f + T^f \exp(\mathrm{i}\lambda)$. This invariance can be used to pass to a new orthogonal set $g_m(k)$ with the overlap matrix $S^g_{mn} = \delta_{mn}$ and the transparency matrix taking the diagonal form $T^g_{mn} = \tau_m \delta_{mn}$. The possibility to diagonalize the matrices T^g_{mn} and S^g_{mn} simultaneously follows from transformation law (234) for bilinear forms (in contrast to a linear transformation L, which acts as $L^g = A^{-1} L^f A$), taking the positive definiteness of S^g_{mn} into account. The corresponding basis g_m and the eigenvalues τ_m of the T^g_{mn} matrix are found from the generalized eigenvalue problem

$$(T^f - \tau_m S^f) a_m = 0 \tag{236}$$

with the normalization $a_m^\dagger S^f a_m = 1$.[35] The eigenvectors a_m compose the columns of the transformation matrix $A = (a_1, \ldots, a_N)$. The eigenvalues are determined by the roots of the characteristic polynomial $\det(T^f - \tau S^f) = 0$. Expression (228) for χ_N, written in the basis $g_m(k)$ becomes a generalized binomial function,

$$\chi_N(\lambda) = \prod_{m=1}^{N} \left[1 - \tau_m + \tau_m \exp(\mathrm{i}\lambda) \right], \tag{237}$$

where the determinant is calculated explicitly, and the result depends only on the eigenvalues τ_m.

The generalized eigenvalue problem can be reduced to the usual one by passing to the orthonormalized basis $\phi_m(k)$ with $S^\phi = \mathbb{1}_N$, which can be obtained using the Gram–Schmidt diagonalization procedure, with $\phi_m(k) = \sum_n [(S^f)^{-1/2}]_{nm} f_n(k)$.

We see from the foregoing that eigenvalue problem (236) is independent of the basis, while the eigenvalues and eigenvectors are specified by the transparency operator T acting in the Hilbert space H_N endowed with the scalar product $\langle f | g \rangle$. Using the language of quadratic forms, these conclusions mean that the eigenvalues and eigenvectors can be found by using the positive definite quadratic form $T(g) = \langle g | T | g \rangle$ and $S(g) = \langle g | g \rangle$, $g \in H_N$. Representing the bilinear form $T(g)$ with $S(g) = 1$ as a polar plot with the radius $T(g)$, where g determines the direction in H_N, we obtain an ellipsoid in the N-dimensional space. The lengths of the major axes of this ellipsoid are given by the eigenvalues, while the corresponding directions are the eigenvectors of our problem (236) [148]. The eigenvalues τ_m are restricted to the

[35] This is used, for example, in the Bogoliubov transformation, where a quadratic Hamiltonian is diagonalized under the condition that the form of commutation relations be preserved (see Section 12).

interval $[0, 1]$ and $0 \leqslant T(g) \leqslant S(g)$ by virtue of the unitarity property. Such a description can be used to analyze the general properties of the generalized binomial distribution function [136].

11.5 Description of statistics at a constant voltage

The measurement of scattering characteristics of individual electrons in meso- and nanoconductors, as it is performed, for example, for particles in accelerators, is complicated.[36] It is much simpler to study the mean current or current correlators measured at a constant voltage (in this case, a large number of electrons are involved in transport). At the same time, this case of the full counting statistics is much more complicated than the cases with a fixed number of particles considered in Section 11.3 and described by wave packets with the known shape. The problem is that a fermion reservoir emits the number of particles that is unknown beforehand, and we can assume that this number experiences quantum fluctuations. However, these fluctuations are small enough and the transfer statistics (at zero temperature) is almost binomial, as in the case of a fixed number of particles considered in Section 11.3. Since the pair correlator at constant voltage in the quantum case exactly coincides with the pair correlator for the Bernoulli process, the hypothesis that the distribution function for the number of transmitted electrons is binomial appeared soon after the result for noise was obtained in [21].

But the confirmation of this hypothesis proved not to be simple [24, 69]. We do not derive the binomial statistics rigorously here, although almost all the elements required for this derivation have already been presented above, and only briefly outline the corresponding stages of the derivation in the spirit of [26], which we followed above (and then present the results). Describing a constant voltage requires not the localized packets with N particles used in Section 11.3, which are all scattered from a barrier after a long time, to describe a constant voltage, but type (2) packets, which are displaced for the observation time over a distance much smaller than their width. To obtain the characteristic function, matrices (229) still have to found. The determinant of a Toeplitz matrix obtained as a result can be calculated using the Szego theorem [26] or, as in [100], with the help of the relation $\log[\det(1+M)] = \mathrm{Tr}[\log(1+M)]$.

We present the result obtained in [24, 69] using the second quantization representations (and also other elements used in the subsequent versions of the derivation). Calculations for $t_0\Theta \gg \hbar$ and $t_0 eV \gg \hbar$ give the characteristic functions

$$\log\chi(\lambda) = \frac{2t_0}{h}\sum_n \int_{-\infty}^{\infty} \mathrm{d}E \log\Big\{1 + T_n(E)\big[\exp(\mathrm{i}\lambda) - 1\big] \times f_{\mathrm{L}}(1-f_{\mathrm{R}}) + T_n(E)\big[\exp(-\mathrm{i}\lambda) - 1\big] f_{\mathrm{R}}(1-f_{\mathrm{L}})\Big\}. \quad (238)$$

For the distribution function

$$f_{\mathrm{L,R}} = \frac{1}{\exp\big[(E \pm eV/2)/\Theta\big] + 1}$$

and the energy-independent transparency, the integral in (238) is $-\Theta \log x_1 \log x_2$, where $x_{1,2}^2 - u x_{1,2} + w = 0$, $w = \exp(eV/\Theta)$, $u = G(\lambda)\exp(eV/\Theta) + G(-\lambda)$, and $G(\lambda) = 1 + T[\exp(\mathrm{i}\lambda) - 1]$. In the limit $\Theta \ll eV$, the result is simplified, and we obtain for the shot noise statistics

$$\chi(\lambda) = \Big\{1 + T\big[\exp(\mathrm{i}\lambda) - 1\big]\Big\}^{2eVt_0/h}. \quad (239)$$

To find the probability P_m of the transfer of m electrons, it is necessary to perform the Fourier transform of $\chi(\lambda)$ to obtain the binomial distribution $P_{mN} = p^m q^{N-m} C_N^m$ with $p = T$, $q = 1 - T$, and $N = 2eVt_0/h$.

In the two limit cases $t \to 0$ and $T \to 1$, the binomial distribution reduces to the Poisson distribution. The first case corresponds to the classical shot noise, and the second one to transport in a system almost without reflections. We note that in the second case, the distribution of reflected particles, rather than the transmitted ones, is Poissonian.

For $\Theta = 0$ and $eV \neq 0$, the distribution is close to the binomial Bernoulli distribution with the 'success' probability $p = T$, the 'failure' probability $q = 1 - T$, and the number of events $N = 2eVt_0/h$ linearly increasing in time. This is caused by the almost regular sequence of 'tunneling attempts' occurring at the frequency $\nu_0 = eV/h$. While the result for the probability of tunneling events is quite clear intuitively, the smallness of fluctuations of the number of events during the measurement time is somewhat unexpected, suggesting the existence of an almost periodic process in the system with the frequency weakly fluctuating about $\omega_0 = eV/\hbar$.[37]

It is clear that the regularity of tunneling attempts is caused in one way or another by the Pauli principle. But the literal interpretation of the electron transfer process in the spirit of the consideration presented in Section 11.3, where a particle incidents the barrier once during the time interval $\tau_V = h/eV$, encounters difficulties. The wave packets of such particles should have a size of the order of $\delta k = eV/\hbar v_{\mathrm{F}}$ in the k-space, which means, as we have seen, that the tunneling probability is the mean of the transparency over the energy interval $\delta E \approx eV$. This picture does not correspond to expression (238), in which the characteristic function is the product of components for each energy and the charge transfer processes at different energies are independent.[38] The characteristic frequency $\omega_0 = eV/\hbar$ specified by voltage can be directly manifested only over short times, for example, if we study the corresponding charge fluctuations. We present the general relation useful in this case:

$$\frac{\mathrm{d}^2\langle\langle Q_{x_0}^2(t)\rangle\rangle}{\mathrm{d}t^2} = \langle\langle j_{x_0}(t) j_{x_0}(0)\rangle\rangle + \langle\langle j_{x_0}(0) j_{x_0}(t)\rangle\rangle, \quad (240)$$

where x_0 is the detector coordinate. For the excess current correlator (for the difference between current coordinates $\Delta x \ll v_{\mathrm{F}}/\omega_0$ and the energy-independent transparency), we have [68]

$$\langle\langle j(0) j(t)\rangle\rangle = \frac{2e^2}{\pi^2} T(1-T) \frac{\sin^2(\omega_0 t/2)}{t^2}. \quad (241)$$

[36] As mentioned in Section 11.2, methods for sending isolated electrons [140, 141] at specified instants ('on request') in quantum conductors were developed only recently.

[37] Such fluctuations are related to fluctuations, logarithmic in time, in the number of tunneling attempts (see the details in [24] and the discussion of logarithmic corrections to cumulants in [26, 100]).

[38] We note that such a factorization is in fact valid only for energy intervals specified by the inverse observation time $\delta E = \hbar/t$ and, according to Levitov–Lesovik formula (238), is correct only if transparencies are independent of energy at such scales.

Interference between different Fermi surfaces occurs at short times, resulting in current and transferred charge oscillations. Similar oscillations also occur in higher-order correlators. A time-unordered third-order correlator was calculated in [149] (this result was used in [131]). The third-order correlator depends on coordinates in a more complicated way because of specific interference in the scatterer region. We present the results for two different cases here. In the first case, where current is measured far from the scattering region, $|x_i| \gg v_F \tau_V$, $|t_i - t_j| \sim \tau_V$, the correlator with coinciding coordinates and at zero temperature has the form

$$\left\langle\left\langle \hat{I}(t_1, x)\, \hat{I}(t_2, x)\, \hat{I}(t_3, x)\right\rangle\right\rangle = -\frac{e^3}{4\pi^3}\, T(1-T)(1-2T) \times \frac{\sin\omega_0(t_1-t_2) + \sin\omega_0(t_3-t_1) + \sin\omega_0(t_2-t_3)}{(t_1-t_2)(t_3-t_1)(t_2-t_3)}\,. \quad (242)$$

The second case is possible near the scattering region. Formally precisely at the scattering point $x = 0$ at zero temperature, the dependence of the correlator on the transparency differs from that measured away from the scattering region,

$$\left\langle\left\langle \hat{I}(t_1, x)\, \hat{I}(t_2, x)\, \hat{I}(t_3, x)\right\rangle\right\rangle_{x=0} = \frac{e^3}{2\pi^3}\, T^2(1-T) \times \frac{\sin\omega_0(t_1-t_2) + \sin\omega_0(t_3-t_1) + \sin\omega_0(t_2-t_3)}{(t_1-t_2)(t_3-t_1)(t_2-t_3)}\,. \quad (243)$$

We note that the dependence of this correlator on the transparency $T^2(1-T)$ coincides with that for the third-order charge cumulant determined from expression (198). The layout of a thought experiment for measuring a symmetrized third-order correlator is considered in [150].

Transfer statistics at short times have been poorly investigated to date, although they are no less interesting than those at long times. We know only two papers [26, 100] in which the short-time statistics were considered.

For the long-time statistics, the third-order charge correlators were measured in [151, 152]. Third-order current correlators were measured in [153] by detecting variations in the dynamics of a Josephson contact; the voltage correlators were also measured earlier in [154].

At the same time, more complicated measurements of the total statistics or the characteristic function have been performed so far only for incoherent transport: the authors of [155] have managed to literally count individual electrons. We note, however, that this situation is not desperate, and qubits available at laboratories today can be used as measuring spins. For example, charge qubits based on double-well potentials with one electron [156] can be used for measuring statistics at relatively short times, which, however, can be longer than comparable to $\hbar/\Theta$ and $\hbar/eV$.

As we mentioned above, the presence of a wire near a qubit leads to the qubit decoherence. It is interesting that because the characteristic function is periodic in λ, the decoherence should also be periodic, or at least its dependence on the coupling constant should be nonmonotonic. From (205), in particular, we can obtain the phase breaking time for a qubit as

$$\tau^{-1} = \left|\frac{eV}{h}\log\left[1 - 4T(1-T)\sin^2\frac{\lambda}{2}\right]\right|. \quad (244)$$

We see that the phase breaking is especially large at $T = 1/2$, when noise is maximal. Then

$$\tau^{-1} = \left|\frac{eV}{h}\log\left[\cos^2\frac{\lambda}{2}\right]\right| \quad (245)$$

and the phase breaking is completely absent if $\lambda = 2n\pi$, while for $\lambda = (2n+1)\pi$, the time formally tends to zero. In this case, it is more correct to return to the definitions of the characteristic function presented above, from which it follows that the spin (qubit) phase rotates after the passage of one electron through exactly π, which can be treated as the complete phase breaking, because the obtained spin (qubit) state is orthogonal to the initial state. In this case, the maximal entanglement of the qubit state with the flying-electron state occurs (if the state of the latter is characterized only by one discrete variable taking 'transmitted' or 'reflected' values; see [157]).

The appearance of singularities of the characteristic function for $T = 1/2$ on the formal level was pointed out in [158] and interpreted as a 'phase transition' between thermodynamic phases in the time space. We have described the physical nature of this phenomenon.

11.6 Complete description of the full counting statistics for the known transparency statistics

As we discussed in Section 11.5, if the probability of transmission of electrons through a quantum conductor is known, then the full counting statistics at large times can be described completely. In turn, the transparency, which can be treated as a random quantity (meaning an irregular dependence on the scattering potential parameters), can also be described for some conductors by its own distribution function. Therefore, we can introduce the 'total' charge distribution function, taking both dynamic fluctuations and transparency fluctuations from sample to sample into account.

We begin with the simple example of a ballistic conductor with a cavity, for which the transparency distribution function in the quasi-one-dimensional case is trivial [159]. In the presence of a weak magnetic field, but such that more than one flux quantum passes through a two-dimensional asymmetric cavity connected with reservoirs by two one-channel leads, the probability T of transmission through this system is uniformly distributed over the segment $[0, 1]$, i.e.,

$$P(T) = 1\,. \quad (246)$$

The probability of transferring the charge en in time t, when the transparency is unknown beforehand but the distribution function $P_T(T)$ is known, reduces to the integral of the charge distribution function $P_Q(Q)$ over transparencies with the weight $P_T(T)$:

$$\langle P(Q)\rangle = \int_0^1 \mathrm{d}T\, P_T(T)\, P(Q)\,. \quad (247)$$

The characteristic function is averaged similarly.

The characteristic function of the binomial distribution averaged with (246) has the form

$$\langle \chi_b(\lambda)\rangle = \int_0^1 \mathrm{d}T\left[1 + T\big(\exp(\mathrm{i}\lambda) - 1\big)\right]^N = \frac{\exp\big[\mathrm{i}\lambda(N+1)\big] - 1}{\big(\exp(\mathrm{i}\lambda) - 1\big)(N+1)}\,. \quad (248)$$

For an integer N, characteristic function (248) can be easily integrated, and we obtain a interesting result for the distribution function

$$P(k) = \sum_{n=0}^{N} \frac{1}{1+N}\,\delta(k+n)\,, \tag{249}$$

which means that the transfer of any number of electrons, beginning from zero and ending with the maximum value $N = 2eVt/h$, is equiprobable. This is caused, in particular, by the boundedness of the binomial distribution function.

The more important case is the dirty conductor considered in Section 8.2, for which the transparency distribution is described by the Dorokhov function. The second cumulant was calculated in [85], while the results for the characteristic function, allowing the calculation of all the moments, were obtained in [160].

For a dirty conductor in which transparencies are described by the Dorokhov distribution function, noise is three times lower than the Poisson noise, or, in terms of the Fano factor, $F = 1/3$, as was shown in [85]. This is a consequence of the bimodal nature of the transparency distribution function. Higher moments (cumulants) can also be obtained quite simply by integration; moreover, the generating function for all cumulants, i.e., the mean of the logarithm of the characteristic function, can be obtained as in [160],

$$\overline{\log\chi(\lambda)} = \frac{GVt}{e}\,\mathrm{arsinh}^2\sqrt{\exp(\mathrm{i}\lambda)-1}\,. \tag{250}$$

In [160], the first 10 cumulants are also presented explicitly. We present the first four cumulants:

$$\overline{\langle\langle N(t)\rangle\rangle} = N_0\,, \tag{251}$$

$$\overline{\langle\langle N^2(t)\rangle\rangle} = \frac{N_0}{3}\,, \tag{252}$$

$$\overline{\langle\langle N^3(t)\rangle\rangle} = \frac{N_0}{15}\,, \tag{253}$$

$$\overline{\langle\langle N^4(t)\rangle\rangle} = -\frac{N_0}{105}\,\ldots\,. \tag{254}$$

The first cumulant simply gives the first transferred charge, the second gives the result for noise specifying the dispersion, which we already know, the third characterizes the asymmetry (skewness) of the distribution function (with respect to its top), and the fourth determines the deviation of the distribution function from being Gaussian. The higher cumulants are described by the expressions

$$\overline{\langle\langle N^k(t)\rangle\rangle} \sim \frac{N_0}{(2\pi)^{k-1}}\,\frac{(k-1)!}{\sqrt{k}}\begin{cases}(-1)^{(k+2)/2} & \text{for even } k\,,\\ (-1)^{(k+1)/2} & \text{for odd } k\,.\end{cases} \tag{255}$$

For comparison, in the case of the Poisson distribution, we have $\overline{\langle\langle N^k(t)\rangle\rangle} = N_0$ for $k > 0$, while for the Gaussian distribution function, as is known, all the cumulants higher than the second are zero.

11.7 Description of the full counting statistics in graphene

It is surprising that the transparency distribution in *pure* graphene (in the case of many conducting channels and a zero doping level) is the same as that for a dirty conductor. This property of the transport 'pseudodiffuseness' is confirmed by the measurements of noise [161], for which the Fano factor turned out to be $1/3$, as had been predicted in [162]. Scattering in pure graphene occurs at its boundaries, in the absence of doping, the transport being completely provided by decaying modes, which we always neglected above. We do not consider the difference between scattering properties for the Dirac and Schrödinger equations here, but we return to this question in Section 14. The Landauer approach to the description of transport in graphene was used in [163].

11.8 Description of the full counting statistics in the presence of interaction

The problem of the scattering statistics for two electrons can also be solved in the presence of the electron–electron interaction when it is concentrated in the quantum dot region. In this case, the scattering matrix can be found either exactly [164] or by using the perturbation theory [165]. This allows describing the result of scattering of two particles in detail, notably, the entanglement appearing in this process [164] and transport in two conductors indirectly interacting via quantum dots [165]. It is interesting that in the problem with a constant voltage, the interaction (in the low-voltage limit) does not change the form of characteristic function (238), although transparencies turn out to be renormalized in a complicated way [166]. (But we note that it is not quite clear at the moment how universal this result can be.)

The description with the help of scattering matrices can be extended to the case of electrons interacting with other degrees of freedom. It has been found that, by developing the theory of emission of photons (or other electromagnetic modes, for example, plasmons) by coherent conductors, it is possible to express photon emission rates [104] or correlators of the number of photons at different points [167, 168] in terms of scattering matrices in the conductor. This possibility appears because the wavelengths of emitted photons greatly exceed the characteristic length of a scatterer. Under these conditions, the interaction Hamiltonian

$$\hat{H}_{\mathrm{int}} = -\frac{1}{c}\int \mathrm{d}\mathbf{r}\,\hat{\mathbf{j}}(\mathbf{r})\,\hat{\mathbf{A}}(\mathbf{r})\,, \tag{256}$$

containing integrals over the coordinates of exact wave functions (scattering states), reduces to integrals of the coefficients of the scattering matrices and second-quantized operators. In intermediate calculations, all the quantities for photon correlators are reduced to the convolutions of current correlators at low frequencies, which are independent of coordinates and are expressed in terms of scattering matrices. The same approach (which can be called the perturbation theory in the interaction based on exact scattering wave functions) can be used to describe the electron–phonon interaction if the characteristic wavelengths of phonons are much longer than the characteristic length of the scatterer.

An important case where the interaction can be described by scattering matrices is the contact of a superconductor with a normal quantum conductor or a Josephson contact of two superconductors through a normal interlayer, which can be a barrier, a two-barrier system, a dirty (coherent) conductor, or a graphene film. We consider these cases in detail in Sections 13 and 14.

12. The Bogoliubov–de Gennes equations

We turn to the description of quantum transport in superconducting systems. In this section, we describe a superconducting (in the general case, spatially inhomogeneous) system using the Bogoliubov transformations [169–171].

We first consider the many-particle effective Bardeen–Cooper–Schrieffer (BCS) Hamiltonian

$$\hat{H} = \sum_{\sigma} \int \mathrm{d}\mathbf{x}\, \hat{\psi}^{\dagger}_{\sigma}(\mathbf{x}) \left[\frac{\hat{\mathbf{P}}^2}{2m} - \bar{\mu}(\mathbf{x}) \right] \hat{\psi}_{\sigma}(\mathbf{x}) + \int \mathrm{d}\mathbf{x}\, \left[\mathbf{\Delta}(\mathbf{x})\, \hat{\psi}^{\dagger}_{\uparrow}(\mathbf{x})\, \hat{\psi}^{\dagger}_{\downarrow}(\mathbf{x}) + \mathrm{h.c.} \right], \tag{257}$$

where integrals are taken over the entire volume of the system and $\mathbf{x} = (x, y, z)$. The first term in the right-hand side of (257) is kinetic, containing the operator $\hat{\mathbf{P}}^2/2m$ determining the quadratic dispersion of the system; here, $\hat{\mathbf{P}} = -\mathrm{i}\hbar\nabla - (e/c)\mathbf{A}$. Summation is performed over spins $\sigma = \uparrow, \downarrow$, $\bar{\mu}(\mathbf{x}) = \mu - eV(\mathbf{x})$ is the chemical potential (in a superconductor or a normal conductor), and μ is still the electrochemical potential (which is assumed to be a constant defined in a superconductor).[39] The second term in the right-hand side of (257) is responsible for superconductivity; it is associated with the complex order parameter in the superconductor; $\Delta(\mathbf{x}) \equiv |\mathbf{\Delta}(\mathbf{x})|$ is the superconducting gap. In the general case, the superconducting parameter $\mathbf{\Delta}(\mathbf{x})$, which is found by averaging over phonon degrees of freedom responsible for superconductivity, depends on the state of the electron system. Below, we use the self-consistent field approximation.

We replace the wave functions by a linear combination of new wave functions $u_\nu(\mathbf{x})$ and $v_\nu(\mathbf{x})$:

$$\begin{aligned} \hat{\psi}_{\sigma}(\mathbf{x}) &= \sum_{\nu} \left\{ u_\nu(\mathbf{x}) \hat{a}_{\nu,\sigma} + \operatorname{sign}\sigma\, v^*_\nu(\mathbf{x})\, \hat{a}^{\dagger}_{\nu,-\sigma} \right\}, \\ \hat{\psi}^{\dagger}_{\sigma}(\mathbf{x}) &= \sum_{\nu} \left\{ u^*_\nu(\mathbf{x}) \hat{a}^{\dagger}_{\nu,\sigma} + \operatorname{sign}\sigma\, v_\nu(\mathbf{x})\, \hat{a}_{\nu,-\sigma} \right\}. \end{aligned} \tag{258}$$

The summation over states ν means summation over the discrete spectrum and integration over the continuous spectrum. Such a substitution in the Hamiltonian is called the Bogoliubov transformation.

The operators of free electrons satisfy the standard commutation relations for Fermi particles:

$$\left[\hat{\psi}^{\dagger}_{\sigma}(\mathbf{x}), \hat{\psi}_{\sigma'}(\mathbf{x}') \right] = \delta_{\sigma,\sigma'}\, \delta(\mathbf{x} - \mathbf{x}'), \tag{259}$$

$$\left[\hat{\psi}_{\sigma}(\mathbf{x}), \hat{\psi}_{\sigma'}(\mathbf{x}') \right] = 0. \tag{260}$$

We require that new operators also satisfy commutation relations for Fermi particles, which reflects the canonical character of transformation (258) [171]:

$$\left[\hat{a}^{\dagger}_{\nu,\sigma}, \hat{a}_{\nu',\sigma'} \right] = \delta_{\sigma,\sigma'} \delta_{\nu,\nu'}, \tag{261}$$

$$\left[\hat{a}_{\nu,\sigma}, \hat{a}_{\nu',\sigma'} \right] = 0. \tag{262}$$

[39] The quantities relevant in Sections 2–11 were electrochemical potentials μ and their differences determining the deviation of the system from the equilibrium, but here we additionally consider the chemical potential $\bar{\mu}$ related to the local density of the charge involved in the formation of superconductivity.

Then $\langle \hat{a}^{\dagger}_{\nu,\sigma}\, \hat{a}_{\nu',\sigma'} \rangle = \delta_{\sigma,\sigma'} \delta_{\nu,\nu'} f(\varepsilon_\nu)$, where, as above, $f(\varepsilon)$ is the Fermi distribution function. It can be shown that conditions (259)–(262) lead to relations for the coefficients $u(\mathbf{x})$ and $v(\mathbf{x})$ in (258):

$$\sum_{\nu} \left\{ u^*_\nu(\mathbf{x})\, u_\nu(\mathbf{x}') + v_\nu(\mathbf{x})\, v^*_\nu(\mathbf{x}') \right\} = \delta(\mathbf{x} - \mathbf{x}'), \tag{263}$$

$$\sum_{\nu} \left\{ u^*_\nu(\mathbf{x})\, v_\nu(\mathbf{x}') - v_\nu(\mathbf{x})\, u^*_\nu(\mathbf{x}') \right\} = 0, \tag{264}$$

$$\int \mathrm{d}\mathbf{x}\, \left[u_\nu(\mathbf{x})\, u^*_{\nu'}(\mathbf{x}) + v_\nu(\mathbf{x})\, v^*_{\nu'}(\mathbf{x}) \right] = \delta_{\nu,\nu'}, \tag{265}$$

$$\int \mathrm{d}\mathbf{x}\, \left[u_\nu(\mathbf{x})\, v_{\nu'}(\mathbf{x}) - v_\nu(\mathbf{x})\, u_{\nu'}(\mathbf{x}) \right] = 0. \tag{266}$$

Transformation (258) diagonalizes Hamiltonian (257), reducing it to the form

$$\hat{H} = U_0 + \sum_{\sigma,\nu} \varepsilon_\nu \hat{a}^{\dagger}_{\nu,\sigma}\, \hat{a}_{\nu,\sigma} \tag{267}$$

if the coefficients $u_\nu(\mathbf{x})$ and $v_\nu(\mathbf{x})$ satisfy the second-order differential equations

$$\begin{aligned} &\left[\frac{\hat{\mathbf{P}}^2}{2m} - \bar{\mu}(\mathbf{x}) \right] u_\nu(\mathbf{x}) - \mathbf{\Delta}(\mathbf{x}) v_\nu(\mathbf{x}) = \varepsilon_\nu u_\nu(\mathbf{x}), \\ &\left[\frac{\hat{\mathbf{P}}^2_{\mathrm{c}}}{2m} - \bar{\mu}(\mathbf{x}) \right] v_\nu(\mathbf{x}) + \mathbf{\Delta}^*(\mathbf{x}) u_\nu(\mathbf{x}) = -\varepsilon_\nu v_\nu(\mathbf{x}), \end{aligned} \tag{268}$$

where $\hat{\mathbf{P}}_{\mathrm{c}} = \hat{\mathbf{P}}\big|_{e \to -e}$. The energy U_0 plays the role of the ground-state energy of the system,

$$U_0 = \int \mathrm{d}\mathbf{x} \sum_{\nu} \left\{ v_\nu(\mathbf{x}) \left[\frac{\hat{\mathbf{P}}^2}{2m} - \bar{\mu}(\mathbf{x}) \right] v^*_\nu(\mathbf{x}) + u^*_\nu(\mathbf{x}) \left[\frac{\hat{\mathbf{P}}^2}{2m} - \bar{\mu}(\mathbf{x}) \right] u_\nu(\mathbf{x}) \right\} - \sum_{\nu} \varepsilon_\nu. \tag{269}$$

Equations (268), which are called the Bogoliubov–de Gennes (BdG) equations, can be interpreted as the wave equation for the two-component wave function

$$\hat{\Psi}_\nu(\mathbf{x}) = \begin{bmatrix} u_\nu(\mathbf{x}) \\ v_\nu(\mathbf{x}) \end{bmatrix}$$

of a quasiparticle with dispersion ε_ν. The first component $u_\nu(\mathbf{x})$ can be treated as the electron-like part of the wave function, and the second component $v_\nu(\mathbf{x})$ as the hole-like component. This interpretation can be useful, for example, in the consideration of Andreev scattering [172–174].

In the western literature, Eqns (268) are usually written in the matrix form

$$\begin{bmatrix} \hat{H}_0(\mathbf{x}) & \mathbf{\Delta}(\mathbf{x}) \\ \mathbf{\Delta}^*(\mathbf{x}) & -\hat{H}_0(\mathbf{x}) \end{bmatrix} \hat{\Psi}_\nu(\mathbf{x}) = \varepsilon_\nu \hat{\Psi}_\nu(\mathbf{x}), \tag{270}$$

where $\hat{H}_0(\mathbf{x}) = -\hbar^2 \partial^2_x / 2m - \bar{\mu}(\mathbf{x})$ is the Hamiltonian of the system in the normal state with the chemical potential $\bar{\mu}(\mathbf{x})$.

The BdG equations are invariant under the transformations $\varepsilon_\nu \to -\varepsilon_\nu$, $u_\nu \to -v^*_\nu$, $v_\nu \to u^*_\nu$, and therefore the set of

solutions of Eqns (268) is redundant. This can be simply explained by the example where the superconducting parameter is zero. It is clear that in this case, the same initial electron state in terms of Bogoliubov quasiparticles can be described either by the creation of an electron-like state or by the annihilation of a hole-like state with the opposite energy. In practice, one of the following variants is usually chosen: (i) $\varepsilon > 0$: in this case, summation over spins is performed (taking both the electron-like and hole-like states into account), which is convenient, for example, for the description of Josephson contacts and most natural for the description of excitations above the Fermi sea; (ii) $\varepsilon \in \mathsf{R}$: in this case, only electron-like states are taken into account, which can be convenient for describing contacts of a normal conductor with a superconductor. We note that other variants are also possible in principle. These approaches are equivalent and are chosen in accordance with their practicality.

In the general case, the superconducting parameter $\mathbf{\Delta}(\mathbf{x})$ is not free and depends on the state of the electron system and hence on the solutions of the BdG equations. To solve the BdG equations, the parameter $\mathbf{\Delta}(\mathbf{x})$ must therefore be known, but at the same time these equations determine $\mathbf{\Delta}(\mathbf{x})$. The corresponding self-consistent solution can be obtained, for example, by the iteration method, choosing an initial function $\mathbf{\Delta}_0(\mathbf{x})$ as the initial approximation. We here present the expression for the superconducting gap in terms of u_ν, v_ν, and ε_ν without derivation:[40]

$$\mathbf{\Delta}(\mathbf{x}) = -|g| \sum_\nu u_\nu(\mathbf{x})\, v_\nu^*(\mathbf{x}) \tanh \frac{\varepsilon_\nu}{2\Theta}\,, \tag{271}$$

where Θ is the system temperature and $|g|$ is the electron–phonon coupling constant, $g < 0$. The thermodynamic potential of the system (also given without derivation) has the form

$$\begin{aligned}\Omega = {} & \frac{1}{|g|}\int \mathrm{d}\mathbf{x}\, \left|\mathbf{\Delta}(\mathbf{x})\right|^2 - 2\Theta \sum_\nu \log\left(2\cosh\frac{\varepsilon_\nu}{2\Theta}\right) \\ & + \int \mathrm{d}\mathbf{x} \sum_\nu \left\{ v_\nu(\mathbf{x}) \left[\frac{\hat{\mathbf{P}}^2}{2m} - \bar{\mu}(\mathbf{x})\right] v_\nu^*(\mathbf{x}) \right. \\ & \left. + u_\nu^*(\mathbf{x}) \left[\frac{\hat{\mathbf{P}}^2}{2m} - \bar{\mu}(\mathbf{x})\right] u_\nu(\mathbf{x}) \right\}. \end{aligned} \tag{272}$$

The superconducting gap can sometimes be specified 'manually' and the problem can be solved quite accurately without resorting to self-consistency[41] [in other words, we can select a very good initial function $\mathbf{\Delta}_0(\mathbf{x})$], for example, in the case of a small normal contact (island) connected to a massive superconductor (or superconductors) via tunneling junctions. Such an island forms a small number of states that cannot considerably affect superconductivity in massive reservoirs with a huge number of states. The same takes place for a contact between a normal (massive) conductor and a superconductor via a quasi-one-dimensional conductor. We note that this situation is quite similar to that discussed in Section 2 in the problem of two massive conductors connected via a quasi-one-dimensional conductor, with the distribution function (density matrix) in a reservoir also changing negligibly due to the presence of the second reservoir.

The current density operator is given by

$$\begin{aligned}\hat{\mathbf{j}}(\mathbf{x}) = {} & \frac{\mathrm{i}e\hbar}{2m} \sum_\sigma \left\{ \left[\nabla \hat{\psi}_\sigma^\dagger(\mathbf{x})\right] \hat{\psi}_\sigma(\mathbf{x}) - \hat{\psi}_\sigma^\dagger(\mathbf{x})\, \nabla \hat{\psi}_\sigma(\mathbf{x}) \right\} \\ & - \frac{e^2}{m}\, \mathbf{A}(\mathbf{x}) \sum_\sigma \hat{\psi}_\sigma^\dagger(\mathbf{x})\, \hat{\psi}_\sigma(\mathbf{x})\,. \end{aligned} \tag{273}$$

We rewrite (273) in terms of the coefficients $u_\nu(\mathbf{x})$ and $v_\nu(\mathbf{x})$ in the Bogoliubov transformation and average with the density matrix of the system:

$$\begin{aligned}\left\langle \hat{\mathbf{j}}(\mathbf{x}) \right\rangle = {} & \frac{\mathrm{i}e\hbar}{m} \sum_\nu \left\{ \left[v_\nu^*(\mathbf{x})\, \nabla v_\nu(\mathbf{x}) - v_\nu(\mathbf{x})\, \nabla v_\nu^*(\mathbf{x})\right] \right. \\ & \left. \times \left[1 - f(\varepsilon_\nu)\right] - \left[u_\nu^*(\mathbf{x})\, \nabla u_\nu(\mathbf{x}) - u_\nu(\mathbf{x})\, \nabla u_\nu^*(\mathbf{x})\right] f(\varepsilon_\nu) \right\} \\ & - \frac{2e^2}{m}\, \mathbf{A}(\mathbf{x}) \sum_\nu \left\{ \left|v_\nu(\mathbf{x})\right|^2 \left(1 - f(\varepsilon_\nu)\right) + \left|u_\nu(\mathbf{x})\right|^2 f(\varepsilon_\nu) \right\}. \end{aligned} \tag{274}$$

13. Electron transport in normal metal–superconductor (NS) junctions

The electron dephasing time at low temperatures in sufficiently pure structures can exceed the travel time through the normal part of a normal metal–superconductor system and wave functions can be assumed coherent not only in the superconductor but also outside it. In this case, the scattering matrix approach is especially convenient.

In the standard theory of the proximity effect, the influence of a superconductor on a normal metal can be described as the penetration of the condensate wave function from the superconductor to the normal metal over the coherence length. This phenomenon can also be interpreted as the appearance of a coherent coupling between electrons and holes in a normal metal caused by the Andreev reflection [172] from the boundary of an NS junction, and can be described by BdG equations (268). The Andreev reflection causes the transformation of a quasi-particle current to the superconducting current at the NS interface [172, 175].[42]

The scattering-matrix approach involves the concept of Bogoliubov quasiparticles with the wave functions containing both electron and hole components [25, 180, 181]. Bogoliubov free quasiparticles here play the same role as free electrons in the theory of normal conductors, and all the aspects of the theory developed for normal conductors can be extended to hybrid systems. In addition, other effects exist, for example, the Josephson effect, which can also be successfully described by the scattering matrix method.

Normal scattering near an NS junction, in particular, the quality of the boundary, determines the proximity effect

[40] See the detailed derivation, for example, in [171].

[41] We consider just these cases.

[42] Recently, another standpoint has appeared according to which the proximity effect is caused by Cooper electron pairs flying into the normal conductor. The electron wave functions in these pairs are mutually entangled in a complicated way. The entanglement is inherent both in spin variables (similarly to the entanglement in a Bohm singlet) and in orbital variables (similarly to the Einstein–Podolsky–Rosen entanglement). The entanglement of Cooper pairs penetrating into a normal conductor was studied in [176–179].

strength, affecting the shape of the current–voltage ($I-V$) characteristic. In NIS junctions, which differ from NS junctions by the presence of a normal scatterer I reflecting electrons to electrons and holes to holes, the $I-V$ characteristic was already studied in [175] (see the references to earlier papers therein), where linear transport was considered based on the BdG equations in the quasi-one-dimensional model in the presence of one barrier at the boundary.

The scattering matrix approach allows taking an arbitrary scatterer into account in a system with a superconductor. This description was first used by Takane and Ebisawa [15, 16] and Lambert [17, 18], while Beenakker [180] derived the formula for the linear conductance of NS junction using the scattering matrix in normal metal.[43] Unlike Green's function methods [183–186], which were used, notably, to describe the experiments in [187, 188], the scattering matrix approach cannot take all inelastic processes into account. However, this approach is more illustrative in the case of simple scattering potentials; for complex potentials, it allows representing the result in the general form.

Following [189], we consider the conduction of an NXS junction in which region X is a scatterer in the normal part at arbitrary temperatures and voltages. We also introduce general relations, consider the example of dirty contacts, and analyze systems with one or two scatterers in region X in detail.

13.1 Current–voltage relation and the spectral conductance

We consider a quasi-one-dimensional multichannel NXS junction (Fig. 26). The structure of the scattering matrix of quasiparticles for this contact is much more complicated than that for the normal NXN junction. Here, in addition to usual scattering occurring in the normal part, Andreev scattering takes place from the NS boundary, where the gap is assumed to jump from zero to the bulk value, and electrons can be reflected to holes and vice versa. To clarify the structure of scattering processes, we first describe scattering matrices in both parts of the contact individually and then consider the full matrix.

Coherent scattering in the normal part is described by the $4N \times 4N$ scattering matrix (we neglect decaying modes in ballistic segments)

$$\mathsf{S}_\mathrm{N} = \begin{bmatrix} r_{11}(\varepsilon) & 0 & t_{12}(\varepsilon) & 0 \\ 0 & r_{11}^*(-\varepsilon) & 0 & t_{12}^*(-\varepsilon) \\ t_{21}(\varepsilon) & 0 & r_{22}(\varepsilon) & 0 \\ 0 & t_{21}^*(-\varepsilon) & 0 & r_{22}^*(-\varepsilon) \end{bmatrix}. \tag{275}$$

The S_N matrix connects N input electron (hole) channels I_i^e (I_i^h), $i = 1, 2$, on each side to the output channels at the same energy O_i^e (O_i^h) (see Fig. 26):[44]

$$\begin{bmatrix} O_1^\mathrm{e} \\ O_1^\mathrm{h} \\ O_2^\mathrm{e} \\ O_2^\mathrm{h} \end{bmatrix} = \mathsf{S}_\mathrm{N} \begin{bmatrix} I_1^\mathrm{e} \\ I_1^\mathrm{h} \\ I_2^\mathrm{e} \\ I_2^\mathrm{h} \end{bmatrix}. \tag{276}$$

Here, $t_{ij}(\varepsilon)$ and $r_{ii}(\varepsilon)$ are the $N \times N$ matrices of transmission and reflection amplitudes in electron channels. The number of channels N is determined by the number of transverse modes; we neglect a change in the number of modes with changing voltage.[45] Matrix (275) can also be written in the block form

$$\mathsf{S}_\mathrm{N} = \begin{bmatrix} \hat{r}_{11}(\varepsilon) & \hat{t}_{12}(\varepsilon) \\ \hat{t}_{21}(\varepsilon) & \hat{r}_{22}(\varepsilon) \end{bmatrix}, \tag{277}$$

where $\hat{r}_{ii}$ and $\hat{t}_{ij}$ are extended $2N \times 2N$ matrices containing complex conjugate amplitudes for holes. Following the usual procedure, we include the propagation of particles in the ballistic segment between the scatterer X and the NS boundary into the scattering matrix (see Fig. 26).

The scattering matrix can often be conveniently represented in the electron–hole parameterization

$$\bar{\mathsf{S}}_\mathrm{N} = \begin{bmatrix} \mathsf{S}_\mathrm{e} & 0 \\ 0 & \mathsf{S}_\mathrm{h} \end{bmatrix}, \tag{278}$$

where the S_e and S_h submatrices describe the scattering of electrons with energy ε and holes with energy $-\varepsilon$. These submatrices are composed of the corresponding components of matrix (275), with the states in (276) somewhat modified:

$$\begin{bmatrix} O_1^\mathrm{e} \\ O_2^\mathrm{e} \\ O_1^\mathrm{h} \\ O_2^\mathrm{h} \end{bmatrix} = \bar{\mathsf{S}}_\mathrm{N} \begin{bmatrix} I_1^\mathrm{e} \\ I_2^\mathrm{e} \\ I_1^\mathrm{h} \\ I_2^\mathrm{h} \end{bmatrix}. \tag{279}$$

Scattering described by the S_e and S_h submatrices is shown schematically in Fig. 26.

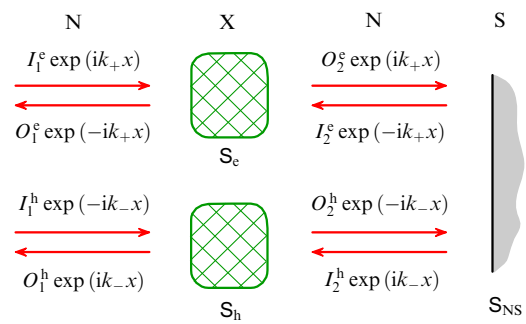

Figure 26. NS junction diagram. The left normal reservoir has the electrochemical potential $\mu + eV$, while the right, superconducting reservoir has the potential μ; X is an arbitrary normal scatterer, k_+ and k_- are the wave vectors of an electron and a hole, respectively.

[43] We also recall Anderson's paper [182], in which the independence of the critical temperature of a weak disorder (the Anderson theorem) was formally proved using exact wave functions.

[44] Hereafter, it is more convenient to measure all energies in the arguments of functions relative to the electrochemical potential μ in a massive superconductor, for example, $t_{12}^*(-\varepsilon)$ means $t_{12}^*(\mu - \varepsilon)$. The complex conjugate amplitudes for holes appear because the propagation direction of holes is opposite to the wave vector. The corresponding amplitudes are obtained from the electron amplitudes by complex conjugation, resulting in the appearance of quantities $t^*(-\varepsilon)$ rather than $t(-\varepsilon)$.

[45] In principle, the scattering matrix can depend on the applied voltage. This can be used, for example, to take a change in the scattering states into account in the case of a voltage-dependent shape of the Schottky barrier.

The scattering matrix on the NS interface can be defined in general as

$$\mathsf{S}_{\mathrm{NS}} = \begin{bmatrix} r_{\mathrm{ee}}(\varepsilon) & r_{\mathrm{eh}}(\varepsilon) & t'_{\mathrm{ee}}(\varepsilon) & t'_{\mathrm{eh}}(\varepsilon) \\ r_{\mathrm{he}}(\varepsilon) & r_{\mathrm{hh}}(\varepsilon) & t'_{\mathrm{he}}(\varepsilon) & t'_{\mathrm{hh}}(\varepsilon) \\ t_{\mathrm{ee}}(\varepsilon) & t_{\mathrm{eh}}(\varepsilon) & r'_{\mathrm{ee}}(\varepsilon) & r'_{\mathrm{eh}}(\varepsilon) \\ t_{\mathrm{he}}(\varepsilon) & t_{\mathrm{hh}}(\varepsilon) & r'_{\mathrm{he}}(\varepsilon) & r'_{\mathrm{hh}}(\varepsilon) \end{bmatrix}. \tag{280}$$

The S_{NS} matrix relates the wave functions in the normal part and the superconductor,[46]

$$\begin{bmatrix} I_2^{\mathrm{e}} \\ I_2^{\mathrm{h}} \\ O_{\mathrm{S}}^{\mathrm{e}} \\ O_{\mathrm{S}}^{\mathrm{h}} \end{bmatrix} = \mathsf{S}_{\mathrm{NS}} \begin{bmatrix} O_2^{\mathrm{e}} \\ O_2^{\mathrm{h}} \\ I_{\mathrm{S}}^{\mathrm{e}} \\ I_{\mathrm{S}}^{\mathrm{h}} \end{bmatrix}. \tag{281}$$

The input and output channels are labeled in accordance with Fig. 26. This matrix can be written in the block form

$$\mathsf{S}_{\mathrm{NS}} = \begin{bmatrix} \hat{r}_{\mathrm{NS}}(\varepsilon) & \hat{t}'_{\mathrm{NS}}(\varepsilon) \\ \hat{t}_{\mathrm{NS}}(\varepsilon) & \hat{r}'_{\mathrm{NS}}(\varepsilon) \end{bmatrix}, \tag{282}$$

where r, r', t, and t' are the $N \times N$ matrices describing reflection and transmission for the states normalized to the unit flux in normal and superconducting segments and are grouped into the $2N \times 2N$ matrices $\hat{r}_{\mathrm{NS}}$, $\hat{r}'_{\mathrm{NS}}$, $\hat{t}_{\mathrm{NS}}$, and $\hat{t}'_{\mathrm{NS}}$.

We calculate the current by considering matrix (275) in the general form and refining it, if necessary, for specific models. We find matrix (280) explicitly with the help of BdG equation (268). We temporarily assume that both these matrices are arbitrary. The complete result for all types of scattering can be described by the $\mathsf{S}_{\mathrm{NXS}}$ matrix like (280), which is also unitary. We restrict ourselves to its $2N \times 2N$ submatrix

$$\mathsf{R}_{\mathrm{NXS}} = \begin{bmatrix} R_{\mathrm{ee}} & R_{\mathrm{eh}} \\ R_{\mathrm{he}} & R_{\mathrm{hh}} \end{bmatrix}, \tag{283}$$

describing reflection to the normal region,

$$\begin{bmatrix} O_1^{\mathrm{e}} \\ O_1^{\mathrm{h}} \end{bmatrix} = \mathsf{R}_{\mathrm{NXS}} \begin{bmatrix} I_1^{\mathrm{e}} \\ I_1^{\mathrm{h}} \end{bmatrix}. \tag{284}$$

Here, R_{ee}, R_{eh}, R_{he}, and R_{hh} are $N \times N$ reflection matrices. Below, we calculate the matrix $\mathsf{R}_{\mathrm{NXS}} = \mathsf{R}_{\mathrm{NXS}}(\varepsilon, V)$ for the scattering matrices given in (275) and (280).

We now derive an expression for the current using total scattering matrix (280). The contribution to the current from the state coming from the normal conductor with a given energy ε is

$$I_n(\varepsilon, V) = \frac{e\hbar k_n}{m} \left\{ 1 - \sum_m \left| R_{\mathrm{ee},mn}(\varepsilon, V) \right|^2 + \sum_m \left| R_{\mathrm{he},mn}(\varepsilon, V) \right|^2 \right\}. \tag{285}$$

This contribution depends on the voltage because a change in the electrostatic potential causes a change in the scattering state. But the deformation of the scattering state caused by the applied voltage does not itself lead to the appearance of a nonzero total current.[47]

It is important that the applied voltage produces a difference of electrochemical potentials in the normal part and the superconductor, resulting in the finite total current

$$I = -\int \mathrm{d}\varepsilon \, \frac{G_{\mathrm{s}}(\varepsilon, V)}{e} \left[f(\varepsilon) - f(\varepsilon - eV) \right], \tag{286}$$

where the spectral conductance

$$G_{\mathrm{s}}(\varepsilon, V) = \frac{2e^2}{h} \, \mathrm{Tr} \left\{ 1 - R_{\mathrm{ee}}^{\dagger}(\varepsilon, V) \, R_{\mathrm{ee}}(\varepsilon, V) + R_{\mathrm{he}}^{\dagger}(\varepsilon, V) \, R_{\mathrm{he}}(\varepsilon, V) \right\} \tag{287}$$

describes the contribution to the current from the input states with the energy ε for a specified voltage V (the energy is measured from the electrochemical potential in the superconductor). The factor 2 in the right-hand side of (287) takes the spin degeneracy into account.

Expressions (286) and (287) determine the differential conductivity

$$\left. \frac{\mathrm{d}I}{\mathrm{d}V} \right|_V = -\int \mathrm{d}\varepsilon \, f'(\varepsilon - eV) \, G_{\mathrm{s}}(\varepsilon, V) - \int \mathrm{d}\varepsilon \, \frac{1}{e} \frac{\partial G_{\mathrm{s}}(\varepsilon, V)}{\partial V} \left[f(\varepsilon) - f(\varepsilon - eV) \right]. \tag{288}$$

At zero temperature, Eqn (288) can be conveniently represented as a series

$$\left. \frac{\mathrm{d}I}{\mathrm{d}V} \right|_V = G_{\mathrm{s}}(eV, 0) + 2V \left. \frac{\partial G_{\mathrm{s}}(\varepsilon, V)}{\partial V} \right|_{\varepsilon = eV,\, V=0} + \ldots . \tag{289}$$

Unlike the definition of the differential conductance $\mathrm{d}I/\mathrm{d}V = G_{\mathrm{s}}(eV, 0)$ in [175], expression (289) takes the change in transparency into account.

To complete the general derivation, the matrix $\mathsf{R}_{\mathrm{NXS}}$ in (283) must be expressed in terms of scattering matrices (275) and (280):

$$\mathsf{R}_{\mathrm{NXS}}(\varepsilon, V) = \hat{r}_{11}(\varepsilon) + \hat{t}_{12}(\varepsilon) \left[1 - \hat{r}_{\mathrm{NS}}(\varepsilon) \, \hat{r}_{22}(\varepsilon) \right]^{-1} \hat{r}_{\mathrm{NS}}(\varepsilon) \hat{t}_{21}(\varepsilon). \tag{290}$$

The simplest process contributing to the resistance, apart from direct scattering in the normal part, is the propagation through the normal part ($\hat{t}_{21}$), reflection from the NS interface ($\hat{r}_{\mathrm{NS}}$), and propagation back through the normal segment ($\hat{t}_{12}$). All subsequent processes can be treated as multiple reflections from the normal scatterer and the NS interface. Expressions (286), (287), and (290) determine the general form of the $I-V$ characteristic without any assumptions about the scattering type; for example, the shape of $\Delta(x)$ on the NS interface can be arbitrary.

We now calculate spectral conductance (287) using the Andreev approximation and assuming that $\Delta(x)$ is a step function.

We briefly consider the $I-V$ characteristic symmetry under the change of the sign of V. We take into account that for $|eV| < \Delta$, the incoming quasiparticles cannot penetrate into a massive superconductor. The probability flux in states with $|\varepsilon| < \Delta$ is completely reflected, and therefore the total scattering matrix $\mathsf{R}_{\mathrm{NXS}}(\varepsilon, V)$ in Eqn (283) is unitary. The unitarity property leads to the relations $R_{\mathrm{ee}}^{\dagger} R_{\mathrm{ee}} + R_{\mathrm{he}}^{\dagger} R_{\mathrm{he}} = 1$ and $R_{\mathrm{ee}} R_{\mathrm{ee}}^{\dagger} + R_{\mathrm{eh}} R_{\mathrm{eh}}^{\dagger} = 1$. The symmetry of the solutions of the electron and hole BdG

[46] In Fig. 26, the states in the superconductor are not indicated because we mainly consider scattering amplitudes for those states coming to the superconductor from the normal part.

[47] This can be shown by using the total scattering matrix that takes Andreev scattering into account.

equations guarantees that $R_{\rm eh}(\varepsilon, V) = -R^*_{\rm he}(-\varepsilon, V)$. Hence, the conduction for $|eV| < \Delta$ can be written as

$$G_{\rm s}(\varepsilon, V) = \frac{4e^2}{h}\,{\rm Tr}\left\{R^\dagger_{\rm he}(\varepsilon, V)\,R_{\rm he}(\varepsilon, V)\right\} = \frac{4e^2}{h}\,{\rm Tr}\left\{R^\dagger_{\rm eh}(\varepsilon, V)\,R_{\rm eh}(\varepsilon, V)\right\} = \frac{4e^2}{h}\,{\rm Tr}\left\{R^\dagger_{\rm he}(-\varepsilon, V)\,R_{\rm he}(-\varepsilon, V)\right\} = G_{\rm s}(-\varepsilon, V)\,. \tag{291}$$

However, this symmetry does not lead to the $I-V$ characteristic symmetry under the change of the bias-voltage sign [190]. Such an $I-V$ characteristic symmetry would mean the fulfillment of the condition $G_{\rm s}(\varepsilon, V) = G_{\rm s}(-\varepsilon, -V)$, which requires that $G_{\rm s}(\varepsilon, V)$ be independent of the voltage. In this case, we would obtain $G_{\rm s}(\varepsilon)\big|_{\varepsilon=eV} = {\rm d}I/{\rm d}V\big|_V$, and the differential conductivity would therefore be symmetric with respect to voltage.

In reality, however, experiments with SNS junctions [191, 192] revealed an $I-V$ characteristic asymmetry for $|eV| > \Delta$, which can be explained in the context of the previous discussion, taking the voltage dependence of the Schottky barrier into account (on the SN boundaries). The asymmetry degree is determined by a quantity of the order of eV/μ or eV/U, where U characterizes the height of the scattering potential. To take the voltage dependence of $G_{\rm s}$ into account explicitly, it is necessary to calculate the scattering matrix $\mathsf{S}_{\rm N}$ taking the applied electrostatic potential into account. In principle, this problem requires a self-consistent solution of the scattering problem and the Poisson equation [193]. In many practically interesting cases, it is possible to take the voltage dependence of the scattering matrix into account only approximately.

13.2 Conductance in the Andreev approximation

We use expression (287) and evaluate it under boundary conditions for a pure NS interface in the Andreev approximation. Stationary states in the ballistic segment are plane-wave solutions of the BdG equations [170, 171]. We assume that $\mathbf{\Delta}(x) = \Delta\exp({\rm i}\varphi)$ for $x > 0$ and $\mathbf{\Delta}(x) = 0$ for $x < 0$, which means that the gap suppression in the contact region in the superconductor is neglected.

The NS boundary couples holes and electrons from one spatial channel with the scattering amplitude depending on the excitation energy and the effective chemical potential. Taking transverse quantization into account, the effective chemical potential has he form $\bar\mu_n = \bar\mu - \hbar^2\mathbf{k}^2_{\perp,n}/2m$. In the limit $\varepsilon, \Delta \ll \bar\mu_n$, the BdG equations are reduced to linear equations by linearizing the dispersion law $k^{(0)}_n = \sqrt{2m\bar\mu_n}/\hbar$.

The matrix of scattering from the ideal NS boundary has the form (Fig. 27)

$$\hat r_{\rm NS} = \begin{bmatrix} 0 & r_{\rm eh} \\ r_{\rm he} & 0 \end{bmatrix} = \begin{bmatrix} 0 & \exp({\rm i}\varphi)\Lambda(\varepsilon) \\ \exp(-{\rm i}\varphi)\Lambda(\varepsilon) & 0 \end{bmatrix}, \tag{292}$$

where

$$\Lambda(\varepsilon) = \begin{cases} \dfrac{\varepsilon - {\rm sign}\,(\varepsilon)\sqrt{\varepsilon^2 - \Delta^2}}{\Delta} \sim \dfrac{\Delta}{2|\varepsilon|}\,, & |\varepsilon| > \Delta\,, \\ \dfrac{\varepsilon - {\rm i}\sqrt{\Delta^2 - \varepsilon^2}}{\Delta} = \exp\left(-{\rm i}\arccos\dfrac{\varepsilon}{\Delta}\right), & |\varepsilon| < \Delta\,. \end{cases} \tag{293}$$

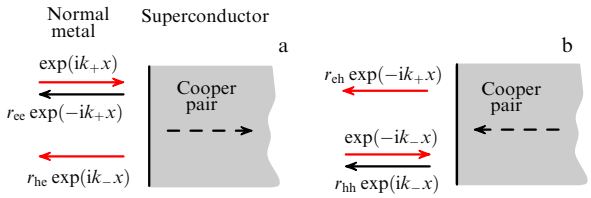

Figure 27. Scattering on the NS interface. (a) Scattering of an electron to a hole. (b) Scattering of a hole to an electron. The light (red at www.ufn.ru) arrows indicate nonzero amplitudes in the case of the ideal NS boundary.

The total $N \times N$ reflection matrices $R_{\rm ee}$ and $R_{\rm he}$ can be determined from Eqn (290). Using (287), we obtain the expression for the spectral conductance for all energies:

$$G_{\rm s}(\varepsilon, V) = \frac{2e^2}{h}\left(1 + |\Lambda(\varepsilon)|^2\right) \times {\rm Tr}\left\{t^\dagger_{21}(\varepsilon)\left[1 - \left[\Lambda^*(\varepsilon)\right]^2 r^\top_{22}(-\varepsilon)\,r^\dagger_{22}(\varepsilon)\right]^{-1} \times \left[1 - |\Lambda(\varepsilon)|^2 r^\top_{22}(-\varepsilon)\,r^*_{22}(-\varepsilon)\right] \times \left[1 - \Lambda^2(\varepsilon)\,r_{22}(\varepsilon)\,r^*_{22}(-\varepsilon)\right]^{-1} t_{21}(\varepsilon)\right\}. \tag{294}$$

Here, the superscript $\top$ denotes transposition.

Equations (286) and (294) specify the $I-V$ characteristic in the Andreev approximation. The spectral conductance depends on the electron scattering matrix at energies $\pm\varepsilon$, indicating the presence of Andreev reflection. The dependence of conductance (294) on the phases of transmission and reflection amplitudes is extremely important for determining resonance peaks in the conductance. Elementary processes contributing to these phases are the propagations of electrons and holes between the NS interface and the normal scatterer.

If the channels do not mix and the matrices t_{ij} and r_{ij} are diagonal, the conductance reduces to the quasi-one-dimensional conductance

$$G_{\rm s}(\varepsilon, V) = \sum_{n=1}^{N} G_n(\varepsilon, V)\,, \tag{295}$$

where

$$G_n(\varepsilon, V) = \frac{2e^2}{h}\left[1 + |\Lambda(\varepsilon)|^2\right] T_n(\varepsilon, V) \times \left[1 - |\Lambda(\varepsilon)|^2 R_n(-\varepsilon, V)\right]\left\{1 + |\Lambda(\varepsilon)|^4 R_n(\varepsilon, V) \times R_n(-\varepsilon, V) - 2\,{\rm Re}\left[\Lambda^2(\varepsilon)\,r_n(\varepsilon, V)\,r^*_n(-\varepsilon, V)\right]\right\}^{-1}, \tag{296}$$

$r_n \equiv (r_{22})_{nn}$ are the amplitudes of normal reflection on the superconductor side, and $R_n = |r_n|^2$ and $T_n = 1 - R_n$ are the reflection and transmission probabilities in the nth channel. The last term in curly brackets in the right-hand side of (296) describes the important scattering process involving the propagation through a sector between the superconductor and the normal scatterer twice: once by an electron and once by a hole.

For high energies, $|\varepsilon| \gg \Delta$ (ad $|\varepsilon| \ll \bar\mu$), the Andreev scattering is strongly suppressed, decaying as $\Lambda(\varepsilon) \sim \Delta/2|\varepsilon| \to 0$. In this case, spectral conductance (294) tends to

the normal limit (the usual Landauer formula),

$$G_s(\varepsilon, V) = \frac{2e^2}{h}\,\mathrm{Tr}\left\{t_{21}^{\dagger}(\varepsilon, V)\,t_{21}(\varepsilon, V)\right\}. \tag{297}$$

We note that conductance (297) is not necessarily symmetric under the change of the voltage sign.

For voltages smaller than the gap width, $|\varepsilon| < \Delta$, reflections of an electron to a hole and conversely occur with probability one, $|\Lambda(\varepsilon)| = 1$, and then expression (296) takes the form [189]

$$G_n(\varepsilon, V) = \frac{4e^2}{h}\,T_n(\varepsilon, V)\,T_n(-\varepsilon, V)\left\{1 + R_n(\varepsilon, V) \times R_n(-\varepsilon, V) - 2\,\mathrm{Re}\left[\Lambda^2(\varepsilon)\,r_n(\varepsilon, V)\,r_n^*(-\varepsilon, V)\right]\right\}^{-1}. \tag{298}$$

The reflection and transmission amplitudes at energies $\pm\varepsilon$ enter (298) symmetrically, providing the $I-V$ characteristic symmetry (with the voltage dependence of the scattering potential neglected).

By contrast, for voltages exceeding the gap, spectral conductance (295) becomes asymmetric in general. An important difference between the conductance of the NS junction (298) and normal conductance (297) is dependence (298) on the scattering amplitude phases in the normal part.

In the linear response limit ($\varepsilon, eV \to 0$), which can be obtained by setting $\Lambda^2(0) = 1$ in (298), the conductance takes the remarkably simple form [180]

$$G(0) = \frac{4e^2}{h}\sum_n \frac{T_n^2(0)}{\left[2 - T_n(0)\right]^2}. \tag{299}$$

This expression is also valid for mixed channels: in this case, $T_n(0)$ are the eigenvalues of the transparency [see (51)].

13.3 Linear conductance in particular cases

We analyze expression (299) in limit cases. The best-known limit is the weak tunneling limit for $T \ll 1$, in which

$$G(0) = \frac{e^2}{h}\sum_n T_n^2(0). \tag{300}$$

In this case, the subgap conductivity is strongly suppressed and a current appears either at high voltages, as in the experiments in [194–196], or at finite temperatures and voltages comparable to the gap. Until recently, only such NS junctions could be studied experimentally.

In the opposite limit, when the NS boundary is ideal, we obtain

$$G(0) = \sum_n \frac{4e^2}{h}. \tag{301}$$

We see that in this last case, the conduction per channel is twice the normal conduction. This result is sometimes interpreted by saying that due to electron pairing into Cooper pairs and spin degeneracy, the factor 2 in the expression for the conductance is lost, but the factor 4 appears since the charge of the elementary carrier doubles. Such an interpretation has the right to exist; but we believe that the situation here is most likely as follows: the spin degeneracy does not disappear at all (which can be seen, for example, from the analysis of injections of single electrons from the normal region to the superconductor); in this case, a pair in the superconductor can be found for each electron with any spin direction (in other words, a hole is reflected). But in contrast to a normal contact, no electrons with energies in the interval from $\mu - |eV|$ to μ escape from the superconductor. This can be explained by the fact that electrons escaping from the normal reservoir below the Fermi level are paired with electrons above the Fermi level and are absorbed in the superconductor, resulting in the appearance of an uncompensated current in the energy interval $2|eV|$, which leads to the doubled total current.

We finally consider the contact between a dirty normal conductor and a superconductor. In this case, we know the transparency distribution function [34, 38], and, as for other quantities, we can obtain the mean conductance of the NS junction. If the transparency of the normal part is described by the Dorokhov function, then the conductance accidentally coincides with the normal conductance [197]

$$G_{\mathrm{NS}} = \frac{4e^2}{h}\sum_n \left\langle \frac{T_n^2(0)}{\left[2 - T_n(0)\right]^2} \right\rangle = G_{\mathrm{N}} = \frac{2e^2}{h}\left\langle \sum_n T_n \right\rangle. \tag{302}$$

This result was already obtained by the Green's function method in [198].

13.4 NINIS junction conductance

In the 1990s, several very interesting experiments [187, 188, 199] were performed in which the dependences of the NS junction conductance on temperature, voltage, and magnetic fluxes were studied. It is interesting that the ratio of scattering intensities at the contact boundary and in the normal part determines the $I-V$ characteristic profile. This ratio determines whether a peak in the conduction appears at the zero temperature or at small but finite voltages [186, 200, 201]. Such peaks, which are called the zero anomaly and the finite-voltage anomaly, were studied in a number of interesting experiments [191, 192, 202–205].

We consider a model NINIS junction, whose analysis is useful for understanding $I-V$ characteristic anomalies in dirty NS junctions. In addition, this system is of interest as an example of rather complicated scattering in the normal part and can be used as a model for studying the interaction of smeared normal levels in an $\mathrm{I_1NI_2}$ interferometer and Andreev levels in an INS Fabry–Perot interferometer. We describe mechanisms giving rise to zero and finite-voltage anomalies [189] under certain conditions imposed on the scattering intensity in barriers, which allows a qualitative understanding of the nature of these anomalies.

We first discuss the conductance structure in a single-channel $\mathrm{NI_1NI_2S}$ junction and then present numerical results for a multichannel case in which the resonance structure does not disappear after averaging over channels, unlike that in INI junctions [189].

As before, we assume that channels are separated[48] and the result in (295) can be used for the conductance G_s, which depends on the phases $\chi_\pm^r$ of reflection amplitudes $r(\pm\varepsilon)$ and the complex amplitude $\Lambda(\varepsilon)$ of Andreev reflection. We use the notation $r(\pm\varepsilon) = \sqrt{R_\pm}\,\exp(\mathrm{i}\chi_\pm^r)$ for the reflection amplitude, where the phase factors $\chi_\pm^r$ are determined by barriers $\mathrm{I_1}$ and $\mathrm{I_2}$ and propagation between them (for simplicity, the voltage dependence of scattering is neglected).

[48] In considering a single channel, we omit the subscript n.

We represent the Andreev reflection amplitudes as $\Lambda(\varepsilon) = |\Lambda| \exp[-\mathrm{i}\vartheta(\varepsilon)]$ with the phase $\vartheta(\varepsilon) = \arccos(\varepsilon/\Delta)$ for $\varepsilon < \Delta$ and $\vartheta(\varepsilon) = 0$ for $\varepsilon > \Delta$. The expression for the conductance then reduces to the form

$$G_{\mathrm{s}}(\varepsilon) = \frac{2e^2}{h}\left(1 + |\Lambda|^2\right) T_+ \left(1 - |\Lambda|^2 R_-\right) \Big\{ 1 + |\Lambda|^4 R_+ R_- - 2|\Lambda|^2 \sqrt{R_+ R_-} \cos\left[\chi_+^r - \chi_-^r - 2\vartheta(\varepsilon)\right] \Big\}^{-1} . \quad (303)$$

It follows from (303) that the conductance is always less than or equal to $4e^2/h$. We note that for $\varepsilon > \Delta$, Andreev scattering is suppressed, $|\Lambda| < 1$. For $\varepsilon < \Delta$, the phase $\vartheta(\varepsilon)$ is defined for resonances. Conductance (303) takes the maximum value $4e^2/h$, which is twice the normal value, when the reflection probabilities R_+ and R_- are equal and the phases $\chi_\pm^r$ satisfy the resonance condition

$$\cos\left[\chi_+^r - \chi_-^r - 2\vartheta(\varepsilon)\right] = 1 . \quad (304)$$

A similar condition is known for the normal two-barrier system $\mathrm{NI_1NI_2N}$, in which the transmission probability $T = 1$ and the maximum conductance $2e^2/h$ can be achieved if the probabilities of reflection from barriers at the resonance energy are equal.

Using expression (303) for the conductance, we consider a single-channel NINS junction consisting of a ballistic NS junction containing one barrier at a distance d from the ideal NS boundary. In the high-barrier limit, R_+ and R_- are approximately equal. The reflection amplitudes $r(\pm\varepsilon)$ describing the propagation of electrons and holes have almost constant absolute values, while the phases are $\chi_\pm^r = \pi + 2k_\pm d$. Substituting the wave number $k_\pm = mv_{\mathrm{F}} \pm \varepsilon/v_{\mathrm{F}}$ (where v_{F} is the Fermi velocity in the channel) in (304), we obtain the positions of Anderson resonances:

$$\varepsilon_n = \frac{v_{\mathrm{F}}}{2d}\left(n\pi + \arccos\frac{\varepsilon_n}{\Delta}\right) . \quad (305)$$

Expression (305) predicts resonances in the conductance with a typical width proportional to the barrier transparency T [similar Rowell–Macmillan resonances with a width of the order of $T/\Lambda(\varepsilon)$ are located at $\varepsilon_n = n\pi v_{\mathrm{F}}/2d$ at voltages exceeding the gap width]. The phase $\vartheta(\varepsilon)$, changing from $\pi/2$ to 0 as ε changes from 0 to Δ, ensures the existence of at least one Andreev resonance for an arbitrarily small d. In the limit $d \to 0$, the resonance position coincides with the gap voltage, which is in accordance with the result obtained for the NIS junction in [175]. Hence the peak that was assigned in [175] to a singularity in the density of states near the gap can be interpreted in the picture considered here as an Andreev resonance shifted to the gap at $d \to 0$.

We now introduce an additional barrier at the NS boundary and analyze a two-barrier $\mathrm{NI_1NI_2S}$ junction obtained in this way, still using expression (303).

According to the adopted definitions, $\chi_\pm^r$ are the reflection phases of an electron incident on a two-barrier potential from the superconductor side. The corresponding reflection amplitudes are given by

$$r(\pm\varepsilon) = r_2 + \frac{t_2^2 r_1 \exp(2\mathrm{i}k_\pm d)}{1 - r_1 r_2 \exp(2\mathrm{i}k_\pm d)} , \quad (306)$$

where r_i and t_i are the amplitudes of the left ($i = 1$) and right ($i = 2$) (on the NS interface) barriers [also see expression (97)]. The phases of these reflection amplitudes play an important role in the formation of the conductance structure because they control the existence of resonances according to (304). We fix the barrier $\mathrm{I_1}$ and gradually increase $\mathrm{I_2}$, keeping the inequality $R_1 > R_2$. In this case, the INI interferometer produces noticeable Andreev resonances. For $r_1 \gg r_2$, the phases $\chi_\pm^r$ of reflection amplitudes $r(\pm\varepsilon) \approx t_2^2 r_1 \exp(2\mathrm{i}k_\pm d)$ linearly depend on energy and change by 2π on the scale hv_{F}/d, giving rise to equidistant resonances, in accordance with (305).

The positions of resonances can be found from the known phase function $\chi^r(\varepsilon)$: they are determined by the energies $\pm\varepsilon$ for which the phase difference is $\delta\chi^r(\varepsilon) = \chi_+^r - \chi_-^r = \pi + 2n\pi$. The doubled period of $\delta\chi^r(\varepsilon)$ compared with the period of $\chi_\pm^r(\varepsilon)$ takes the pairing of resonances into account.

When barrier strengths are equal, $R_1 \approx R_2$, due to a large phase gradient near the normal resonance with energy ε, the Andreev resonances tend to be pinned by normal resonances and are located at the energies $+\varepsilon$ or $-\varepsilon$. This rule is violated when the normal resonance coincides with the electrochemical potential. In this case, the Andreev resonances are separated from the electrochemical potential by a finite value.

As the strength of the second barrier increases further, $R_2 > R_1$, Andreev resonances become weaker and finally disappear. Although normal resonances are still present in this regime in the normal INI interferometer, only weak Andreev resonances are manifested in the conductance. The phase function becomes almost constant for $R_2 \gg R_1$ [see (306)] and condition (304) for resonance phases cannot be satisfied.

We now compare transport in two-barrier systems $\mathrm{NI_1NI_2S}$ and $\mathrm{NI_2NI_1S}$, i.e., in systems with the reversed sequence of barriers $\mathrm{I_1}$ and $\mathrm{I_2}$. We note that the transparency $T(\varepsilon)$ is the same in both cases. Hence, unlike the nonlinear conductance of the NINIS junction, the nonlinear conductance (297) of the normal NININ junction, as the linear conductance (299) of the superconducting NINIS junction, is independent of the sequence of barriers $\mathrm{I_1}$ and $\mathrm{I_2}$. We assume that $R_1 \gg R_2$. For the direct barrier sequence ($\mathrm{NI_1NI_2S}$), the energy dependence of the phase $\chi^r(\varepsilon)$ is strong, resulting in the appearance of Andreev resonances at a finite voltage. Electrons entering the INI interferometer on the normal side have enough time to form Andreev resonances and escape, typically to the superconductor. For the reversed barrier sequence ($\mathrm{NI_2NI_1S}$), the barrier $\mathrm{I_1}$ on the NS boundary becomes the main one. The weak energy dependence of the scattering phase $\chi^r(\varepsilon)$ prevents the formation of narrow resonances. This reflects the fact that electrons entering the INI interferometer escape through $\mathrm{I_2}$ to the normal part without forming Andreev resonances.

We now analyze a multichannel NINIS junction numerically with the help of expression (295). This expression allows the analysis to be performed for finite voltages and temperatures beyond the scope of a linear response studied in [206]. We consider an $\mathrm{NI_1NI_2S}$ junction with two delta barriers with scattering probabilities R_i from 0.2 to 1 ($i = 1, 2$). We change the relative strength of the barriers to cover the interval between the two limits $R_1 > R_2$ and $R_1 < R_2$, which were discussed in Section 13.4. The distance L between the barriers was chosen to be of the order of the coherence length $L \approx \xi = v_{\mathrm{F}}\hbar/\Delta$ in the superconductor, such that one or several Andreev resonances can be formed in the first channel (with the maximal longitudinal velocity). The number of resonances increases upon increasing the angle of incidence (counted from the normal to the NS interface) or,

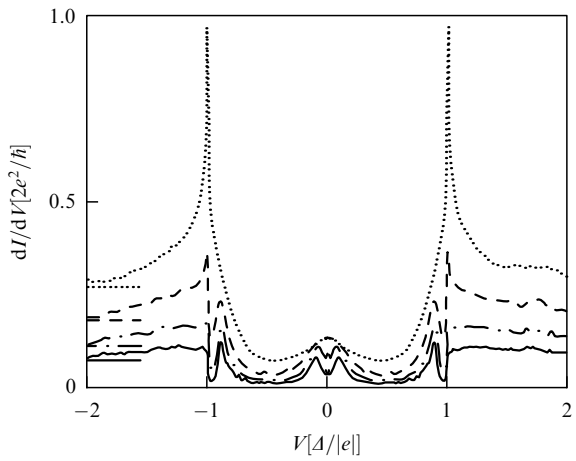

Figure 28. Differential conductance (averaged per channel) in a multichannel NINIS junction of the width $d = 2v_F/\Delta = 2\pi\xi$ as a function of the applied voltage at the temperature $\Theta = 0$. The curves (from top down) correspond to the probabilities of reflection from the first barrier $R_1 = 0.2$, 0.5, 0.7, and 0.8 for the constant reflection probability $R_2 = 0.5$ for the second barrier. The corresponding conductances in the normal state, indicated by horizontal segments in the left part of the figure, are virtually independent of voltage in the limits indicated. As the strength I_1 of the first barrier increases, an anomaly appears at zero voltage, because a new Andreev resonance arises at $R_1 > R_2$ [189].

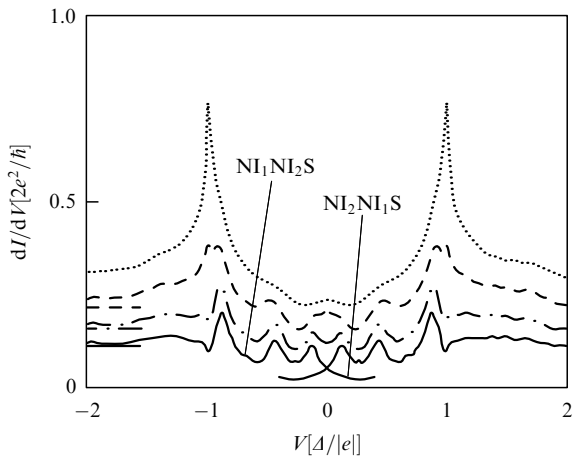

Figure 29. Differential conductance (averaged per channel) in a multichannel NINIS junction of the width $d = 4v_F/\Delta = 4\pi\xi$ as a function of the applied voltage at the temperature $\Theta = 0$. The curves (from top down) correspond to the probabilities of reflection from the first barrier $R_1 = 0.04$, 0.2, 0.4, and 0.54 for the constant reflection probability $R_2 = 0.2$ from the second barrier. The corresponding conductances in the normal state are indicated by horizontal segments in the left part of the figure. As the strength of the first barrier increases, the zero-voltage anomaly transforms into a finite-voltage anomaly and several Andreev resonances appear. For $R_1 = 0.54$ and $R_2 = 0.2$, we interchanged scatterers I_1 and I_2 in the INI part ($R_1 = 0.2$ and $R_2 = 0.54$) (the lower short curve); in this case, the conduction at zero voltage remains the same, but the local minimum transforms into a local maximum [189].

equivalently, upon increasing the channel number. The contact cross section was set equal to $(100/k_F)^2$, while the ratio of the gap width to the chemical potential was $\Delta/\bar{\mu} = 0.002$.

Each channel yields the typical structure of paired Andreev resonances discussed at the beginning of this section. Their position and width depend on the strength ratio of barriers I_1 and I_2 and the longitudinal kinetic energy in each channel. We note that the total conductance obtained by summation over channels still has the structure produced by Andreev resonances. In contrast, the total conductance of the corresponding normal NI_1NI_2N junction is almost constant, i.e., normal resonances are averaged out almost completely.

The numerical study of three-dimensional NINS junctions shows that the position and number of resonances in the total conductivity coincide with those in the first channel [207].[49] In NINIS junctions, such a direct dependence has not been found.

We now consider expression (298) for the conductivity, which is valid for voltages lower than the gap, and the properties of the $I-V$ characteristic near zero voltage. For $R_1 > R_2$, the denominator in (298) changes rapidly because of a strong energy dependence of the phase of the reflection amplitude $r_n(\varepsilon)$, which is responsible for the appearance of a peak in the $I-V$ characteristic at nonzero voltage. The $I-V$ characteristic structure after summation is shown in Figs 28 and 29 (solid curves). The repulsion of Andreev levels from zero energy gives a minimum of dI/dV for zero voltage. For $R_1 < R_2$, the phase of the reflection amplitude $r_n(\varepsilon)$ is almost independent of the energy, and the conductance structure is determined by the numerator in expression (298). The expansion of the product $T_n(\varepsilon)\,T_n(-\varepsilon) = T_n^2 - w_n^2\varepsilon^2$ near zero energy indicates the presence of a maximum at zero (zero anomaly).[50]

The manifestation of the zero-voltage anomaly is shown in Figs 28 and 29 (dashed curves). These figures illustrate crossovers from the zero to finite anomaly for two different distances d between barriers upon increasing the barrier strength I_1 for a constant barrier strength I_2. If d exceeds the coherence length in the superconductor, several resonances appear (see Fig. 29). In the case of the reversed barrier sequence, the local minimum of the conductance at zero voltage transforms into a local maximum, but the conductance value at zero does not change. This is shown in Fig. 29 by two solid curves near the zero voltage: the upper curve corresponds to the direct barrier sequence (NI_1NI_2S) and the short lower curve is the reversed sequence (NI_2NI_1S). To understand what determines the width of the peaks and the position of the finite anomaly, we compare them with the Thouless energy. The Thouless energy E_{Th} [208, 209] in a disordered system can be defined as the dimensionless conductance g times the distance δE between levels (in a closed system), $E_{Th} = g\,\delta E$. In a system with weakly transparent barriers, good correspondence exists between this energy, the width, and the position of the finite bias anomaly. The width of the peak at zero voltage coincides with the characteristic correlation energy $\langle G(E+\varepsilon)\,G(E)\rangle_E$ in the conductance correlator and with the Thouless energy.[51] In this case, the transparency distribution function of the two-barrier system is bimodal and resembles that of a dirty system [206]. But as the total transparency approaches unity, the width of the resonances no longer coincides with the energy E_{Th}. In this limit, the two-barrier system poorly

[49] This occurs due to a decrease in the transparency with an increase in the angle of incidence and the nonuniform distribution of the angle of incidence over channels [207].

[50] The dominator cannot affect this property as long as the total transparency of a two-barrier system is not too large, $T_n < 0.55$.

[51] Angular brackets $\langle\cdot\rangle_E$ denote averaging over energies.

simulates the bimodal distribution for a dirty system and the Thouless energy is no longer the characteristic energy of the problem. At finite temperatures, the anomaly at a finite bias is smeared to form the zero bias anomaly.

The behavior of the zero bias and finite bias anomalies in disordered NS junctions has been studied in many experiments [191, 202–205]. The theoretical consideration of dirty NS systems showed that this behavior is determined by the relation between scattering rates on the NS interface and in the normal part [186, 200, 201, 210]. In the case of a small disorder, the zero bias anomaly appears, while in the case of a strong disorder, a peak appears in the normal part at a finite bias [201] of the order of the Thouless energy E_{Th}, which has been confirmed experimentally [192]. Such a behavior of the anomaly is similar to the behavior in a ballistic two-barrier NINIS junction, described in [189]. The 'ballistic' model of a dirty NS junction considered above therefore assumes the interpretation of the peak at a finite bias as a superposition of the smeared Andreev levels appearing between the superconductor and the strongly reflecting normal part.

14. Electron transport in SNS junctions

In this section, we consider nondissipative transport in superconductor–normal metal–superconductor junctions (SNS), i.e., the Josephson effect [211]. Recently, it has become possible to manufacture such contacts at meso- and nanoscales, for example, based on a two-dimensional electron gas in heterostructures [36, 37, 212–215], with the help of an electron tunneling microscope [216] and lithography [217, 218], based on atomic contacts [219–221], carbon nanotubes [222–225], single molecules [226, 227], and graphene [228–230]. It is very interesting to use these contacts in applications [231].

The specific features of these systems are mainly manifested in the regime when the conduction is determined by several conducting channels (or even a single channel). As the number of conducting channels changes, quantization of the superconducting critical current [20, 213, 220, 232–235] and charge [236–238] can be observed. The current is quantized in units of $e\Delta/\hbar$ [232, 233, 239] and the charge in units of $2e$ [236]. As a rule, the potential of the gate serves as a control parameter in experiments. The effective chemical potential in two-dimensional gases is varied by changing this potential; by varying the gate potential in structures with resonances, it is possible to shift resonances with respect to the electrochemical potential, thereby opening and closing conducting channels. Interesting phenomena also occur in the intermediate state, when the channel is opened only partially. In this case, the current and charge strongly depend on the phase and are in a state intermediate between their quantized values.

The interest in such structures is additionally stimulated by the possibility of their practical application in superconducting quantum interference devices (SQUIDs) [240–244], in which Josephson contacts inserted into a superconducting ring act as sensitive elements converting magnetic flux into current. SQUIDs are fabricated based on well-known multichannel macroscopic Josephson contacts [245, 246]. The study of Josephson nanocontacts can help decrease the size and increase the sensitivity of such devices. Other applications are also possible, such as a Josephson transistor [235, 247–251].

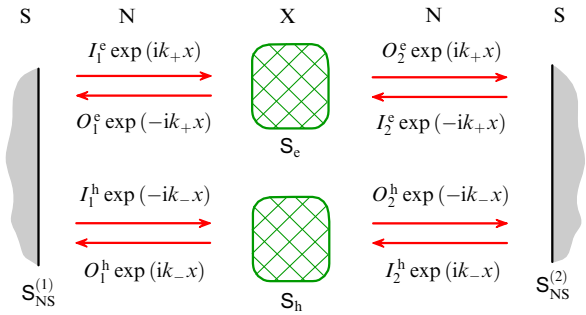

Figure 30. States of Bogoliubov particles in an SXS junction. Calculations are performed by using the model SÑXÑS system with the Ñ region length tending to zero. Andreev reflection, occurring on the NS boundaries, is described by the respective scattering matrices $\mathsf{S}_{\mathrm{NS}}^{(1)}$ and $\mathsf{S}_{\mathrm{NS}}^{(2)}$ on the left and right boundaries. The normal part X is characterized by a scattering matrix S_{N}, which is separated for clarity into two parts, the electron matrix S_{e} and the hole matrix S_{h}.

Below, we consider the SXS junction with the nonsuperconducting part X of an arbitrary structure and derive the equation for energy levels (carrying almost all the current) expressed in terms of the scattering matrix of this part, and analyze this equation in the most interesting cases.

14.1 Energy levels and current in an SXS junction

We consider the problem of two superconductors separated by a distance L (Fig. 30). We assume that a normal scatterer X with the scattering matrix S_{N} given by expression (277) in general is located between NS interfaces. Since we are going to look for the quantization conditions, we consider only one conducting channel.[52] We write the scattering matrix S_{N} in the convenient form

$$\mathsf{S}_{\mathrm{N}} = \begin{bmatrix} \sqrt{R_+}\exp(\mathrm{i}\chi_+^r) & 0 & \sqrt{T_+}\exp(\mathrm{i}\chi_+^t) & 0 \\ 0 & \sqrt{R_-}\exp(\mathrm{i}\chi_-^r) & 0 & \sqrt{T_-}\exp(\mathrm{i}\chi_-^t) \\ \sqrt{T_+}\exp(\mathrm{i}\chi_+^t) & 0 & \sqrt{R_+}\exp(\mathrm{i}\chi_+^r) & 0 \\ 0 & \sqrt{T_-}\exp(\mathrm{i}\chi_-^t) & 0 & \sqrt{R_-}\exp(\mathrm{i}\chi_-^r) \end{bmatrix}, \tag{307}$$

where T and R are the transmission and reflection probabilities for the scatterer X, and χ^t and χ^r are the corresponding gained phases. The subscripts $\pm$ correspond to the energies $\pm\varepsilon$. For the convenience of calculations, we assume that normal metal regions with an infinitely small length are located between the normal scatterer and the NS interfaces.

We now define matrices similar to (282), describing scattering on the left and right NS boundaries in the Andreev approximation. On the left and right NS interfaces, expression (292) takes the respective forms

$$\hat{r}_{\mathrm{NS}}^{(1)} = \begin{bmatrix} 0 & r_{\mathrm{eh}}^{(1)} \\ r_{\mathrm{he}}^{(1)} & 0 \end{bmatrix} = \begin{bmatrix} 0 & \exp(\mathrm{i}\varphi_1) \\ \exp(-\mathrm{i}\varphi_1) & 0 \end{bmatrix} \Lambda(\varepsilon)\,, \tag{308}$$

$$\hat{r}_{\mathrm{NS}}^{(2)} = \begin{bmatrix} 0 & r_{\mathrm{eh}}^{(2)} \\ r_{\mathrm{he}}^{(2)} & 0 \end{bmatrix} = \begin{bmatrix} 0 & \exp(\mathrm{i}\varphi_2) \\ \exp(-\mathrm{i}\varphi_2) & 0 \end{bmatrix} \Lambda(\varepsilon)\,. \tag{309}$$

[52] Assuming that a normal metal is connected to a superconductor adiabatically, we believe that transverse modes are well defined, and we solve the one-dimensional BdG equations for each channel.

The states below the gap, $|\varepsilon| < \Delta$, form a discrete spectrum, while the states above the gap, $|\varepsilon| > \Delta$, form a continuous spectrum. We consider the first case and write the quantization condition for discrete Andreev levels:

$$\det\left[1 - \mathsf{S}_{\mathrm{e}}\hat{r}_{\mathrm{eh}}^{(1)}\mathsf{S}_{\mathrm{h}}\hat{r}_{\mathrm{he}}^{(2)}\right] = 0\,, \tag{310}$$

where we again use the electron–hole parameterization in (278) and (279). Processes described by this equation are illustrated in Fig. 30. As mentioned in Section 12, in solving problems of this type, it is convenient to set $\varepsilon > 0$, taking both electron-like and hole-like states into account. As previously, $\Lambda(\varepsilon) = \exp[-\mathrm{i}\vartheta(\varepsilon)]$ and $\vartheta(\varepsilon) = \arccos(\varepsilon/\Delta)$.

Substituting expressions (307)–(309) in (310), we obtain the quantization condition

$$\cos(S_+ - S_- - 2\vartheta) = \sqrt{R_+R_-}\,\cos\beta + \sqrt{T_+T_-}\,\cos\varphi\,, \tag{311}$$

determining the excitation spectrum ε_ν of Hamiltonian (267) in the SXS system. Here, $\varphi = \varphi_2 - \varphi_1$ is the difference between the superconducting phases of the left and right superconductors and $S_\pm = \chi_\pm^t + k_\pm L$ is the phase gained by electrons and holes in the normal region, where $k_\pm = \sqrt{2m(\bar{\mu} \pm \varepsilon)}/\hbar$ are the corresponding wave vectors. In the case of symmetric barriers, the phase $\beta = (\chi_+^t - \chi_+^r) - (\chi_-^t - \chi_-^r)$ is an integer multiple of π and gives rise to a continuous function $\sqrt{R_+R_-}\cos\beta$ changing its sign at each resonance [234, 235].[53]

The total current in the ground state is $(2e/\hbar)\partial_\varphi U_0$. The ground-state energy U_0 of the system is given by expression (269). We note that the last term in the right-hand side of (269) is the sum of all excitation energies taken with the opposite sign. It is interesting that only this term depends on the superconducting phase difference φ, allowing the calculation of the ground-state Josephson current if the excitation spectrum ε_ν is known. Using this specific feature in the phase dependence of the ground-state energy U_0, we obtain the Josephson current equal to $I = \sum_\nu I_\nu$, where I_ν are found by differentiating the energy ε_ν with respect to the superconducting phase, taken with the opposite sign, $I_\nu = -(2e/\hbar)\partial_\varphi\varepsilon_\nu$.

The total nondissipative current flowing through the SXS junction consists of two parts, one of which originates from discrete energy levels below the gap and the other from the continuous spectrum above the gap. We consider the contribution of only the 'discrete' component, because it typically dominates [234, 253]. After implicit differentiation in (311), we obtain

$$I_\nu = -\frac{2e}{\mathcal{T}_\nu}\sqrt{T_+T_-}\,\sin\varphi\,, \tag{312}$$

where the factor 2 is due to the double spin degeneracy,

$$\mathcal{T}_\nu = \sin(\delta S - 2\vartheta)\,\hbar\partial_\varepsilon[\delta S - 2\vartheta] + \hbar\partial_\varepsilon[\sqrt{T_+T_-}\cos\varphi + \sqrt{R_+R_-}\cos\beta]$$

has the dimension of time and represents the generalized quasiparticle travel time in the normal part of the contact, and $\delta S \equiv S_+ - S_-$.

Expressions (311) and (312) are valid for any scattering matrix. We use them below to describe particular systems.

[53] Equation (311) was obtained in a somewhat simplified form in [252]].

14.2 SNS junction: constriction in a two-dimensional gas

We first consider a multichannel SNS junction with ideal NS boundaries. The simplest (and best known) case is a short SNS junction without inner scatterers. In this case, substituting $T_+ = T_- = 1$, $R_+ = R_- = 0$, and $\delta S = 0$ in (311), we obtain the energy $\varepsilon = \Delta\cos(\varphi/2)$. If the transparency T of the normal part is not equal to unity but weakly depends on the energy in the interval $[\bar{\mu} - \Delta,\ \bar{\mu} + \Delta]$, then the electron and hole transparencies coincide, $T_+ = T_- = T$, and expression (311) gives one level per channel [20]:

$$\varepsilon_n = \Delta\sqrt{1 - T_n\sin^2\frac{\varphi}{2}}\,, \tag{313}$$

where T_n is the transparency of the nth channel.

For example, for a length-L rectangular barrier specifying the effective chemical potential $\bar{\mu}_{x,n}$ (with the chemical potential $\bar{\mu}$ at infinity), the transparency has the form

$$T_n = \frac{4\bar{\mu}\bar{\mu}_{x,n}}{4\bar{\mu}\bar{\mu}_{x,n} + (\bar{\mu} - \bar{\mu}_{x,n})^2\sin^2\left[\sqrt{2m\bar{\mu}_{x,n}/\hbar^2}\,L\right]}\,, \tag{314}$$

where n is the transverse mode number. Below, we omit the subscript n for simplicity.

We consider an SNS junction based on a QPC in a two-dimensional electron gas (Fig. 31a). A one-dimensional contact is formed by two gates determining the electron density of the two-dimensional electron gas. Figure 31b shows the effective one-dimensional chemical potential $\bar{\mu}_x$ corresponding to a channel n. As the 'top' $\bar{\mu}_x(0)$ of this potential increases, the channel n gradually closes: first for holes and then for electrons.

Expression (314), which describes a potential with breaks, is rarely realized in practice. The system outlined in Fig. 31a can be described by the parabolic potential

$$\bar{\mu}_x(x) = \bar{\mu}_x(0) + \frac{m\Omega^2x^2}{2}\,,$$

where $\hbar\Omega = (4/\pi)\sqrt{\varepsilon_L[\bar{\mu} - \bar{\mu}_x(0)]}$ describes the 'curvature' of the potential at $x = 0$ and $\varepsilon_L = \hbar^2\pi^2/2mL^2$ is the quantization energy over the contact length. The value of Ω is selected such that the relation $\bar{\mu}_x(\pm L/2) = \bar{\mu}$ is satisfied. In this case, the transparency T is described by Kemble formula (63) and depends only on the effective chemical potential maximum and its curvature:

$$T = \frac{1}{1 + \exp(-2\pi\bar{\mu}_x(0)/\hbar\Omega)}\,. \tag{315}$$

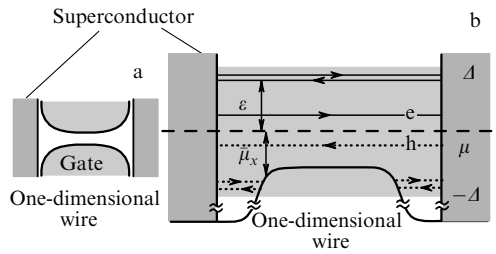

Figure 31. SNS junction. (a) Adiabatic constriction in a normal metal between two superconductors. (b) The corresponding one-dimensional smooth effective potential [235].

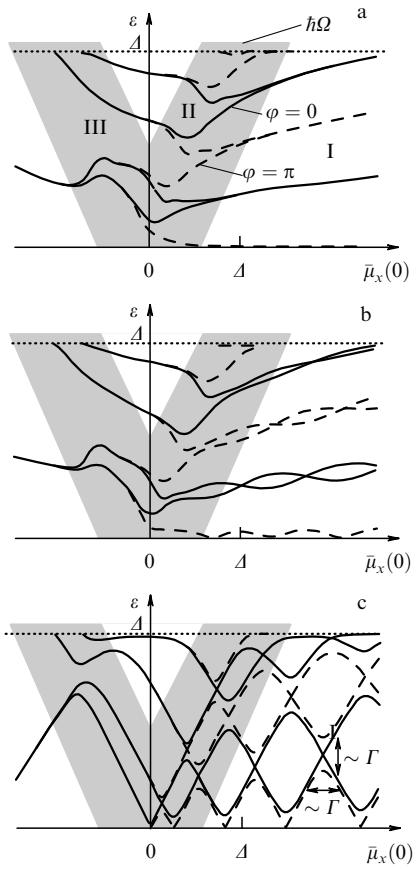

Figure 32. Subgap spectrum for a parabolic potential in the normal part and scatterers with the strength Z on NS boundaries. (a) Ideal NS boundaries ($Z = 0$). (b) Weak scattering ($Z = 0.1$) leads to the appearance of weak resonances and Andreev spectrum splitting. In the case of strong scattering ($Z = 1$), an Andreev quantum dot is formed. In regions I and II, the spectrum depends on the difference between superconducting phases φ (solid curves correspond to the phase $\varphi = 0$ and dashed curves to the phase $\varphi = \pi$) [235].

In the typical case, the expansion of the potential near its maximum can be restricted to the quadratic term because, as the transparency changes according to the Kemble formula from small ($T \ll 1$) to large ($T \approx 1$), scattering is determined by the potential in a rather small vicinity of the potential maximum (see Section 4.3).

For a channel of an arbitrary length, it is necessary to calculate dimensionless actions $S_\pm$ involved in quantization condition (311). The action for a parabolic barrier can be calculated explicitly [234]:

$$\frac{S(E)}{\hbar} = \frac{2E}{\hbar\Omega}\left\{\kappa^2\sqrt{1+\frac{1}{\kappa^2}} + \log\left[|\kappa|\left(1+\sqrt{1+\frac{1}{\kappa^2}}\right)\right]\right\}, \tag{316}$$

where

$$\kappa^2 = Q\,\frac{\hbar\Omega}{E} = \frac{\pi^2\hbar^2\Omega^2}{16E\varepsilon_L}\,. \tag{317}$$

In this case, $S_\pm = S(E = \bar{\mu}_x(0) \pm \varepsilon)$ and $Q \equiv (\pi/4)^2\hbar\Omega/\varepsilon_L$ is a dimensionless parameter, typically, $Q \gg 1$. We also note that the additional change in the action $S(E)$ by π after passing through zero energy in the interval $\hbar\Omega$ cannot be obtained in the semiclassical model.

Figure 32a shows the results of solving quantization equations (311) numerically for the model described above. For a large positive chemical potential $\bar{\mu}_x(0) > \varepsilon + \hbar\Omega$ (region I), the system can be described by expressions (313) and (315). As $\bar{\mu}_x$ decreases (region II), only the electron levels remain, as shown in Fig. 31b; in this case, the energy levels are split, even for $\varphi = 0$. In region III, the channel produced by an electron-like level is closed. In regions with $\bar{\mu}_x(0) < -\varepsilon - \hbar\Omega$, the energy levels no longer depend on the phase and hence represent closed channels. The behavior of the system is described in more detail in [235].

In semiclassical region I, each Andreev level produces a nondissipative current with the amplitude $2|e|/[\tau_+ + \tau_- + 2\hbar/\sqrt{\Delta^2 - \varepsilon^2}]$, where $\tau_\pm = \hbar\,\partial_\varepsilon S_\pm$ are the travel times of electron-like and hole-like quasiparticles in the normal part. For the parabolic potential,

$$\tau(E) = \Omega^{-1} 2\log\left[|\kappa|(1+\sqrt{1+\kappa^{-2}})\right].$$

For small energies, the travel times increase logarithmically, $\tau(E) \approx \Omega^{-1}\log(4Q\hbar\Omega/E)$, in the interval $\hbar\Omega < E < Q\hbar\Omega$ and are saturated at $\tau_0 \approx \Omega^{-1}\log(4Q)$ and energies $E < \hbar\Omega$, at which the system can no longer be considered in the semiclassical approximation.

We find the dependence of the current on the phase difference of superconducting banks. For $\varphi = 0$, double degeneracy occurs, and levels in a pair make contributions to the current with the same modulus but opposite signs; therefore, for $\varphi = 0$, the discrete spectrum makes no contribution to the current. As φ increases, the degeneracy is lifted and each split pair contributes to the nondissipative current, monotonically increasing with increasing φ and reaching the maximum at $\varphi = \pi - 0$. This means that the current takes the critical value at the point $\varphi = \pi - 0$.[54] For $\varphi = \pi - 0$, all the levels except the lowest one become degenerate again and none of the degenerate pairs of levels contributes to the current.

Finally, we obtain a simple expression for the critical current $I_c \equiv \max_\varphi\{I\}$ in semiclassical region I:

$$I_c = \frac{|e|}{\tau_0 + \hbar/\Delta}\,, \tag{318}$$

where τ_0 is the travel time calculated for a parabolic potential, which is constant in an opening channel, and $\tau_0 = \Omega^{-1}\log 4Q$ decays as $\tau_0 = \Omega^{-1}\log 4Q\hbar\Omega/\bar{\mu}_x(0)$ for $\bar{\mu}_x(0) > \hbar\Omega$, and becomes equal to the free-travel time, $\tau_0 = L/v_{\mathrm{F},x}$ for $\bar{\mu}_x(0) > Q\hbar\Omega$. In the last case, for a channel opened at large energies, we obtain the known formula $I_c = |e|v_F/(L + \pi\xi_0)$ for the critical current. The critical current increases by I_c with the appearance of each new open channel (Fig. 33).

[54] It is quite difficult to prove that the contribution of the continuous spectrum to the critical current is insignificant. The discrete and continuous spectra can be simultaneously taken into account by using the Crane theorem, as in [254, 255]. At the same time, it can be shown relatively easily that the contribution from the continuous spectrum vanishes at $\varphi = \pi$ [234]. However, this does not mean that the critical current through the contact, determined by both the discrete and continuous spectra, is then caused only by the discrete spectrum at $\varphi = \pi - 0$. To prove this statement, it is necessary to show that the sum of discrete and continuous spectra reaches a maximum at $\varphi = \pi - 0$. For example, this can be done for the contact length L and the chemical potential $\bar{\mu}_x(0)$ in the middle of the contact distant from the point $(\sqrt{\xi_0/k_F}, \Delta)$ in the $(L, \bar{\mu}_x(0))$ coordinates [234].

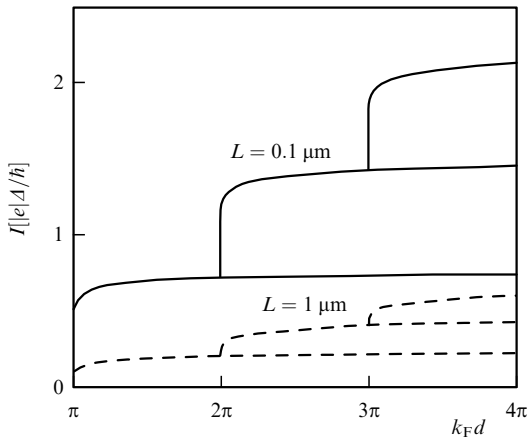

Figure 33. Quantization of the superconducting current. As the width d of the normal channel increases, the superconducting current increases by quanta $|e|/(\tau_0 + \hbar/\Delta)$ [234].

The basic qualitative features of the critical current quantization predicted theoretically were confirmed experimentally in [213].

14.3 SINIS junction: the Andreev quantum dot

In Section 14.2, we considered quantum constriction, assuming that only Andreev reflection occurs on NS boundaries ($Z = 0$). We now consider the case where the boundaries contain scatterers with $Z > 0$. Figure 32b, showing an intermediate case with $Z = 0.1$, demonstrates the appearance of oscillations with a period Δ and an amplitude $\delta\varepsilon$ caused by weak resonances of a double barrier. Figure 32c shows the case of strong normal resonances, $Z = 1$ (the corresponding system based on a carbon nanotube is shown in Fig. 34). We can see the distinct resonance structure of Andreev levels, which is determined by the resonance structure of the normal part. An important parameter is the resonance width Γ given by (106). We restrict our analysis to the case $\bar{\mu}_x(0) \gg Q\hbar\Omega$, where the curvature Ω of the potential no longer plays any role, and the potential only shifts normal resonances.

The excitation spectrum in the Josephson contact with the normal part of any structure can be determined from expression (311). We introduce the quantization condition for a double barrier with $\Omega = 0$. Substituting transmission coefficients (98) and phases (97) in (311), we obtain

$$(R_1 + R_2)\cos\left(2\pi\,\frac{\varepsilon}{\delta}\right) - 4\sqrt{R_1 R_2}\,\cos\left(2\pi\,\frac{\varepsilon_D}{\delta}\right)\sin^2\vartheta + T_1 T_2\cos\varphi = \cos\left(2\vartheta - 2\pi\,\frac{\varepsilon}{\delta}\right) + R_1 R_2\cos\left(2\vartheta + 2\pi\,\frac{\varepsilon}{\delta}\right). \tag{319}$$

Here, we choose the resonance with some number n and energy E_n and omit the index n for brevity. The energy $\varepsilon_D = E_n - \bar{\mu}(0)$ [where $\bar{\mu}(0) = \mu - eV_g$] determines the resonance position $E_n = \varepsilon_L[n - (\chi_1^r + \chi_2^r)/2\pi]^2$ with respect to the chemical potential in the normal part, which is in turn controlled by the external gate potential V_g. We assume that the distance to neighboring resonances $\delta \equiv (E_{n+1} - E_{n-1})/2$ greatly exceeds the superconducting gap Δ.

The dependences of the energy states on the effective chemical potential $\bar{\mu}_x(0)$ are shown in Fig. 32. The parameter Z [see (91)–(93)] specifies the 'strength' of normal scatterers. For a symmetric contact, we have $T_1 = T_2 = 1/(1 + Z^2)$ and $R_1 = R_2 = Z^2/(1 + Z^2)$. For $Z = 0$, expression (319) describes an SNS junction; for $Z = 0.1$, it describes a contact with weak scatterers at the NS boundaries, and for $Z = 1$, it describes a contact with quite strong scatterers at the NS boundaries.

Figure 32 shows that as the scatterer strength increases, a resonance structure appears, as was to be expected. The most interesting case is that of a strong phase dependence of energy, which occurs when some normal resonance passes through the chemical potential. Expression (319) can be simplified in the vicinity of this point and an analytic expression for the Andreev level can be obtained [237, 249, 256] as

$$\varepsilon = \sqrt{\varepsilon_D^2 + \tilde{\Gamma}^2}\,, \tag{320}$$

where

$$\tilde{\Gamma} = \Gamma\sqrt{\cos^2\frac{\varphi}{2} + A^2}\,, \qquad A = \frac{|T_1 - T_2|}{2\sqrt{T_1 T_2}}\,, \tag{321}$$

and $\Gamma = (T_1 + T_2)\delta/4\pi$ is the half-width of the normal resonance. Expression (320) is valid when the resonance E_n approaches the chemical potential $\bar{\mu}$ by a distance of the order of the normal resonance half-width $|\varepsilon_D| \lesssim \Gamma$, while the half-width itself is much smaller than the superconducting gap, $\Gamma \ll \Delta$ (Fig. 32c). In this case, the current through the Andreev quantum dot is

$$I = \frac{2e}{\hbar}\,\frac{\Gamma^2\sin\varphi}{4\sqrt{\varepsilon_D^2 + \tilde{\Gamma}^2}}\,. \tag{322}$$

The critical current is given by

$$I_c = \frac{|e|\Gamma}{\hbar}\left\{\sqrt{1 + A^2 + \frac{\varepsilon_D^2}{\Gamma^2}} - \sqrt{A^2 + \frac{\varepsilon_D^2}{\Gamma^2}}\right\}. \tag{323}$$

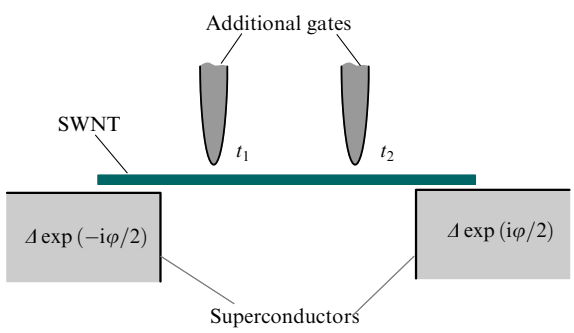

Figure 34. Outline of the experimental realization of the Andreev quantum dot based on a single-wall nanotube (SWNT). Two additional gates form the electron density in certain regions and produce effective barriers with transmission amplitudes t_1 and t_2.

14.4 SGS junction and the Dirac–Bogoliubov–de Gennes equations

This section is devoted to the Josephson current in a superconductor–graphene–superconductor (SGS) junction (Fig. 35a). The method for preparing a graphite (graphene) monolayer was developed a few years ago [257]. Later, a

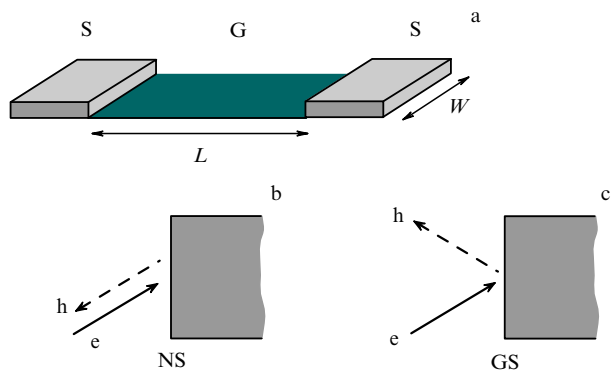

Figure 35. (a) SGS junction: a graphene sheet G of length L and width W connected to two superconductors S. (b) The usual Andreev reflection of an electron to a hole from the ideal NS boundary in the Andreev approximation. The hole repeats the electron trajectory in the opposite direction. (c) Specular reflection from the ideal GS boundary followed by a change in the normal component of the velocity.

current through a graphene Josephson contact was measured [228]. Below, we describe the electron transport and calculate the critical current in the SGS system.

Graphene is described by the relativistic Dirac wave equation. In this case, low-energy quasiparticles have the linear dispersion $\varepsilon = kv$ and zero mass, while the velocity v is independent of energy and is constant. This leads to a number of interesting physical phenomena such as the Klein tunneling [258–260].

Calculations for the SGS junction are quite similar to those for the SNS junction; however, in BdG equations (270), we must now substitute the Dirac Hamiltonian [261–263]

$$\hat{H}_0 = -\mathrm{i}\hbar v(\sigma_x \partial_x + \sigma_y \partial_y)\,, \tag{324}$$

which describes graphene in the absence of superconductors. The resulting system of four first-order differential equations is called the Dirac–Bogoliubov–de Gennes (DBdG) equations.

The coefficients $u = [u_1, u_2]^\top$ and $v = [v_1, v_2]^\top$, as previously, describe the electron and hole parts of the wave function, but now each of them consists of two components, u and v, which have the opposite spin and valley indices related to the two sublattices in the hexagonal graphene lattice. Solving the DBdG equations on ideal GS boundaries, we obtain the coefficients of the scattering matrix responsible for reflection on the graphene side. The coefficients for the left and right boundaries are respectively given by

$$\hat{r}^{(1)}_{\mathrm{GS}} = \begin{bmatrix} 0 & r^{(1)}_{\mathrm{eh}} \\ r^{(1)}_{\mathrm{he}} & 0 \end{bmatrix} = \begin{bmatrix} 0 & \exp(\mathrm{i}\varphi_1 - \mathrm{i}\vartheta\hat{\sigma}_x) \\ \exp(-\mathrm{i}\varphi_1 + \mathrm{i}\vartheta\hat{\sigma}_x) & 0 \end{bmatrix}, \tag{325}$$

$$\hat{r}^{(2)}_{\mathrm{GS}} = \begin{bmatrix} 0 & r^{(2)}_{\mathrm{eh}} \\ r^{(2)}_{\mathrm{he}} & 0 \end{bmatrix} = \begin{bmatrix} 0 & \exp(\mathrm{i}\varphi_2 + \mathrm{i}\vartheta\hat{\sigma}_x) \\ \exp(-\mathrm{i}\varphi_2 - \mathrm{i}\vartheta\hat{\sigma}_x) & 0 \end{bmatrix}. \tag{326}$$

Similarly to matrix (284), reflection matrices (325) and (326) relate the wave functions incident on the GS boundary and reflected wave functions. However due to the presence of the valleys, the matrix size doubles compared to the size of the analogous matrix for the NS boundary. Expressions (325) and (326) describe the subgap scattering, with $\vartheta = \arccos(\varepsilon/\Delta)$ as previously.

We note that Andreev reflection from the ideal NS boundary transforms an electron to a hole (or a hole to an electron) with the opposite velocity vector. This means that the reflected hole (electron) propagates along the same path as the incident electron (or hole), but in the opposite direction (Fig. 35b) [172, 173, 240]. After reflection from the ideal GS boundary, only the normal component of the velocity changes, i.e., specular reflection occurs [261] (Fig. 35c), which is called specular Andreev reflection to distinguish it from the well-known usual Andreev scattering from the NS boundary (retro Andreev reflection).[55]

We assume that a graphene sheet is ideally rectangular and use the boundary condition for transverse quantization [162]

$$k_{y,n} = \left(n + \frac{1}{2}\right)\frac{\pi}{W}\,, \tag{327}$$

where $k_{y,n}$ is the transverse component of the wave vector in the nth channel. The effective chemical potential $\bar{\mu}_{x,n}$ in the nth channel is determined by the relation $\bar{\mu}^2_{x,n} = \bar{\mu}^2 - (\hbar v k_{y,n})^2$, where $\bar{\mu}$ is the chemical potential measured with respect to the Dirac point, i.e., the graphene doping level. A particle with an energy ε has the wave vector $k = (\bar{\mu} + \varepsilon)/\hbar v$ and the corresponding longitudinal component $k_{x,n} = (k^2 - k^2_{y,n})^{1/2}$. Solving the Dirac equation ($\Delta = 0$) for a rectangular potential of length L (with the wave vector equal to $k_{x,n}$ in the potential region and k outside that region), we obtain the scattering matrices describing this potential

$$\mathsf{S}_{\mathrm{e}} = \begin{bmatrix} 0 & \tilde{t}_{\mathrm{ee}} \\ \tilde{t}_{\mathrm{ee}} & 0 \end{bmatrix}, \quad \mathsf{S}_{\mathrm{h}} = \begin{bmatrix} 0 & \tilde{t}_{\mathrm{hh}} \\ \tilde{t}_{\mathrm{hh}} & 0 \end{bmatrix}, \tag{328}$$

where

$$\tilde{t} = \begin{bmatrix} \cos(k_x L) + \dfrac{k_y}{k_x}\sin(k_x L) & \dfrac{\mathrm{i}k}{k_x}\sin(k_x L) \\ \dfrac{\mathrm{i}k}{k_x}\sin(k_x L) & \cos(k_x L) - \dfrac{k_y}{k_x}\sin(k_x L) \end{bmatrix}. \tag{329}$$

The opposite energy signs correspond to electrons and holes, $\tilde{t}_{\mathrm{ee}} = \tilde{t}(\varepsilon)$ and $\tilde{t}_{\mathrm{hh}} = \tilde{t}(-\varepsilon)$. In the general form, the quantization condition for the SGS junction has the form

$$\det\left[1 - \tilde{t}_{\mathrm{ee}}\hat{r}^{(1)}_{\mathrm{eh}}\tilde{t}_{\mathrm{hh}}\hat{r}^{(2)}_{\mathrm{he}}\right] = 0\,. \tag{330}$$

Substituting (325), (326), and (329) in (330), we can obtain the quantization condition determining energy levels in the system under study [262, 263].

In the case of a short contact ($L \ll \Delta, \xi$), the energy levels are described by the simple expression

$$\varepsilon_n = \Delta\sqrt{1 - T_n \sin^2\frac{\varphi}{2}}\,, \tag{331}$$

which completely coincides with expression (313) for a short SNS junction, the only difference being in the definition of the transparency

$$T_n = \frac{k^2_{x,n}}{k^2_{x,n}\cos^2(k_{x,n}L) + (\bar{\mu}/\hbar v)^2\sin^2(k_{x,n}L)}\,. \tag{332}$$

[55] These statements are valid in the Andreev approximation on the NS boundary and a low graphene doping level on the GS boundary.

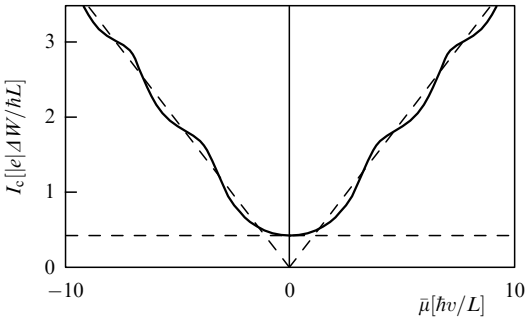

Figure 36. Critical current I_c in an SGS junction as a function of the graphene doping level $\bar{\mu}$ [262].

It follows that transparencies in this case differ considerably from those in (314) for quadratic dispersion.

Each channel makes a contribution to the current, which can be found by differentiating (331) with respect to φ. The total current has the form

$$I = \frac{e\Delta}{\hbar} \sum_{n=0}^{\infty} \frac{T_n \sin\varphi}{\sqrt{1 - T_n \sin^2(\varphi/2)}} \,. \tag{333}$$

We note that unlike the summation in the case of an SNS junction, the summation in (333) extends to infinity over the propagating (real $k_{x,n}$) and evanescent (imaginary $k_{x,n}$) modes. For $L \ll W, \xi$, summation can be replaced by integration.

The numerical results obtained for the critical current are presented in Fig. 36. The main feature is that the critical current does not vanish at the zero doping level, which is confirmed experimentally [228]. For $\bar{\mu} = 0$, the total current is determined by the first nonvanishing term in the expansion of current (333) in the small parameter $|\bar{\mu}| \ll \hbar v/L$ [262]:

$$I = \frac{e\Delta}{\hbar} \frac{2W}{\pi L} \cos\frac{\varphi}{2} \operatorname{artanh}\left(\sin\frac{\varphi}{2}\right) . \tag{334}$$

In this case, the critical current (shown by the horizontal dashed straight line in Fig. 36) is described by the expression

$$I_c = 1.33\, \frac{e\Delta}{\hbar} \frac{W}{\pi L} \,. \tag{335}$$

Away from the Dirac point ($\bar{\mu} \gg \hbar v/L$), the critical current is proportional to the doping level (see the inclined dashed asymptotes in Fig. 36):

$$I_c = 1.22\, \frac{|e|\Delta}{\hbar} \frac{|\bar{\mu}| W}{\pi \hbar v} \,. \tag{336}$$

The case of a nonzero temperature is considered in [264, 265].

15. Shot noise in NS systems at a finite voltage

In this section, we present general expressions for the differential shot noise in a nonideal NS junction in terms of the scattering matrix of the normal part. As mentioned in Section 10, shot noise appears due to the discreteness of the charge carried by a particle and the probabilistic nature of scattering. Shot noise in nonideal NS junctions is produced both in normal scattering processes and in nonideal Andreev scattering [112, 266–268]. The latter process for transport at low temperatures (caused only by the transfer of electron pairs) can be represented as the tunneling of Cooper pairs as a whole, similarly to the tunneling of usual particles. The Andreev scattering leads to fluctuations whose amplitude is proportional to the double electron charge. In this case, the fluctuation amplitude in SNS junctions with applied voltage can increase to a value proportional to the large number of charge quanta [269, 270].

We consider an NXS junction. As above, X denotes a region with an arbitrary normal scattering matrix. The current fluctuation power spectrum at low frequencies is determined by irreducible current–current correlator (183) for $\omega \to 0$. The time-dependent current operator is defined as

$$\hat{I}(\tau) = \exp\left[\mathrm{i}(\hat{H} - \mu\hat{N})\tau\right] \hat{I} \exp\left[-\mathrm{i}(\hat{H} - \mu\hat{N})\tau\right] , \tag{337}$$

where $\hat{N}$ is the particle number operator. Expression (337) differs from formula (179) used previously in that the Hamiltonian determining the time evolution is replaced by an effective Hamiltonian that can be diagonalized in the mean-field approximation via a Bogoliubov transformation. This approach neglects order parameter fluctuations in the superconducting region and assumes that Bogoliubov quasiparticles coherently propagate through the entire system, not changing their energy.

Time-dependent current operator (337) can be expressed in terms of solutions of BDG equations (268) and the Bogoliubov creation and annihilation operators,

$$\hat{I}(t) = -\frac{\mathrm{i}e}{m} \sum_{\nu',\nu} \int \mathrm{d}y\, \mathrm{d}z \left(u^*_{\nu'} \hat{\partial}_x u_\nu \hat{a}^\dagger_{\nu'} \hat{a}_\nu - v^*_{\nu'} \hat{\partial}_x v_\nu \hat{a}_\nu \hat{a}^\dagger_{\nu'}\right) \exp\left[\mathrm{i}(\varepsilon_{\nu'} - \varepsilon_\nu)t\right] , \tag{338}$$

where the new operator $u\hat{\partial}_x v \equiv u\partial_x v - v\partial_x u$ is introduced. As before, we take only states with the positive energy $\varepsilon_\nu > 0$ into account, omitting the channel number n where it is insignificant. For simplicity, we calculate expression (338) in the normal region.

For voltages smaller than the superconducting gap ($|eV| < \Delta$), quasiparticles can appear only from a normal reservoir, and the wave functions are still dependent only on the parts of the scattering matrix responsible for scattering (r_{ee}, r_{he}, r_{eh}, and r_{hh}). Each of these $N \times N$ matrices describes the NXS junction as a whole.

The noise power is determined by transitions (due to the operator $\hat{I}$) between the states

$$|\mathrm{s}\rangle = |f_{\beta,\nu,n} = 1,\, f_{\beta',\nu',m} = 0\rangle \,,$$
$$|\mathrm{i}\rangle = |f_{\beta,\nu,n} = 0,\, f_{\beta',\nu',m} = 1\rangle$$

that differ only by the occupation of two one-particle states with the energy subscripts ν and ν' in the respective nth and mth channel. The subscripts β and β' indicate the electron (e) of hole (h) states. For example, a transition between the incident electron ($\beta = \mathrm{e}$) from the nth channel and the incident hole ($\beta = \mathrm{h}$) from the mth channel occurs due to the presence of a nonzero matrix element describing the interaction between reflected electrons (and holes), $\langle \mathrm{s}|\hat{I}|\mathrm{i}\rangle \propto f_{\mathrm{e}}(1 - f_{\mathrm{h}})(r^\dagger_{\mathrm{eh}} r_{\mathrm{ee}} - r^\dagger_{\mathrm{hh}} r_{\mathrm{he}})_{mn}$. Here, the occupation numbers f_β for electrons and holes are given by the Fermi distribution $f_{\mathrm{e/h}} = f(\varepsilon \mp eV)$; the voltage is measured relative

to the electrostatic potential in the superconductor. Summation over the channels gives the contribution to fluctuations

$$\sum_{m,n} \left|\langle \mathrm{s}|I|\mathrm{i}\rangle\right|^2 \propto f_\mathrm{e}(1-f_\mathrm{h}) \times \mathrm{Tr}\left\{(r_\mathrm{ee}^\dagger r_\mathrm{eh} - r_\mathrm{he}^\dagger r_\mathrm{hh})(r_\mathrm{eh}^\dagger r_\mathrm{ee} - r_\mathrm{hh}^\dagger r_\mathrm{he})\right\} = f_\mathrm{e}(1-f_\mathrm{h})\,\mathrm{Tr}\left\{r_\mathrm{he}^\dagger r_\mathrm{he}(1-r_\mathrm{he}^\dagger r_\mathrm{he})\right\}.$$

Considering similar processes, allows obtaining the expression for the low-frequency power spectrum [19, 271] valid for $\Theta \ll |eV| < \Delta$:

$$S = \frac{4e^2}{h}\int_0^\Delta \mathrm{d}\varepsilon \left\{\left[f_\mathrm{e}(1-f_\mathrm{h}) + f_\mathrm{h}(1-f_\mathrm{e})\right] \times \mathrm{Tr}\left[r_\mathrm{he}^\dagger r_\mathrm{he}(1-r_\mathrm{he}^\dagger r_\mathrm{he})\right] + \left[f_\mathrm{e}(1-f_\mathrm{e}) + f_\mathrm{h}(1-f_\mathrm{h})\right]\,\mathrm{Tr}\left[(r_\mathrm{he}^\dagger r_\mathrm{he})^2\right]\right\}. \tag{339}$$

The first term in the right-hand side of (339) describes transitions between the states making contributions to the current with opposite signs, while the second term describes transitions making contributions with the same signs. At zero temperature, the second term vanishes and the shot noise is determined by the first term. At a nonzero temperature, both terms contribute, in particular, to the Johnson–Nyquist noise [272, 273] due to thermal fluctuations.

As in the calculation of the NXS junction conductance, we express the scattering matrix $r_\mathrm{he}(\varepsilon)$ in terms of the scattering matrix of the normal part X and the Andreev scattering amplitude. Substituting the result in (339), we obtain the general expression for shot noise in a multichannel NXS junction. We restrict ourselves to the case where the contact has a constant cross section, with the differential conductance $G_n(\varepsilon) = (4e^2/h)[r_\mathrm{he}^\dagger r_\mathrm{he}]_{nn}$ described by expression (298). At zero temperature, the power spectrum of shot noise takes the form

$$S = \frac{1}{|e|}\int_0^{|eV|} \mathrm{d}\varepsilon \sum_n \zeta_n(\varepsilon)\,,$$

where ζ_n is the differential shot noise in the nth channel,

$$\zeta_n(\varepsilon) = \frac{2|e|^3}{h}\,4\left[r_\mathrm{he}^\dagger r_\mathrm{he}(1-r_\mathrm{he}^\dagger r_\mathrm{he})\right]_{nn} = \frac{2|e|^3}{h}\,4T_n(\varepsilon)\,T_n(-\varepsilon)\Big\{R_n(\varepsilon) + R_n(-\varepsilon) - 2\,\mathrm{Re}\left[\Lambda^2(\varepsilon)\,r_n(\varepsilon)\,r_n^*(-\varepsilon)\right]\Big\}\Big\{T_n(\varepsilon)\,T_n(-\varepsilon) + R_n(\varepsilon) + R_n(-\varepsilon) - 2\,\mathrm{Re}\left[\Lambda^2(\varepsilon) r_n(\varepsilon)\,r_n^*(-\varepsilon)\right]\Big\}^{-2}. \tag{340}$$

In the limit as $\varepsilon \to 0$ ($\Lambda \to -\mathrm{i}$), the dependence on the phases gained by quasiparticles between the scatterer X and the NS boundary disappears, and we obtain the linear response [274]

$$\zeta_n(0) = \frac{2|e|^3}{h}\,\frac{16\,T_n^2(0)\,\left[1-T_n(0)\right]}{\left[2-T_n(0)\right]^4}\,. \tag{341}$$

Now, again using the Dorokhov distribution function, we can find the total noise in a dirty contact as [197]

$$S = \frac{2}{3}\,|e|I\,. \tag{342}$$

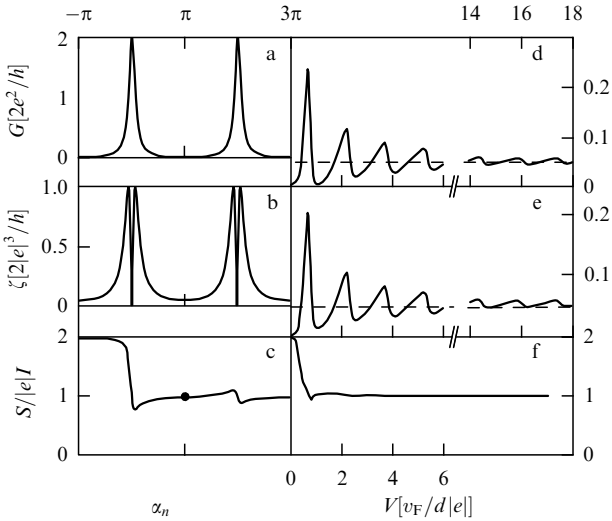

Figure 37. (a, d) Conductance at zero temperature, (b, e) shot noise, and (c, f) noise power spectrum for the NINS junction (solid curves) with $\int \mathrm{d}x\,V(x) = 3\hbar v_\mathrm{F}$, mean transparency $T = 0.05$, $E_\mathrm{F} = 500\Delta$, and $d = 20v_\mathrm{F}/\Delta$, $v_\mathrm{F}/d \ll \Delta \ll E_\mathrm{F}$. Plots in Figs a–c are determined by Eqns (343) and (344) for one channel, and in Figs d–f by Eqns (298) and (340) averaged over 8×10^4 channels. The conductance (d) and noise (e) asymptotically approach the corresponding values (dashed straight lines) in the NIN junction. The ratio $S/|e|I$ shown in Figs 37c, f approaches the classical value $S/|e|I = 1$ at high voltages [278].

We can see that the Fano factor $F = 2/3$ is twice the Fano factor for noise in a normal dirty conductor (see Section 10.3), which, of course, indicates the presence of the charge $2e$ in the system. This effect was observed in experiments [275, 276].

15.1 Noise in an NINS junction

We consider a strong scatterer I ($T \ll 1$) without the internal resonance structure, located at a distance d from the NS boundary, X = NIN.[56] In this case, the reflection amplitude $r(\varepsilon) = \sqrt{R}\exp\left(\mathrm{i}\chi^r(\varepsilon)\right)$ depends on energy weakly, the energy dependence being completely determined by the phase $\chi^r(\varepsilon) \approx 2(k+\varepsilon/v)d + \chi_0$ that is gained between the scatterer I and the NS boundary; k and v are the wave vector and velocity in a quasi-one-dimensional channel. Differential shot noise (340) in the nth channel, which takes the form

$$\zeta_n(\varepsilon) = \frac{2|e|^3}{h}\,\frac{4T^2 2R\left[1-\cos\alpha_n(\varepsilon)\right]}{\left\{T^2 + 2R\left[1-\cos\alpha_n(\varepsilon)\right]\right\}^2}\,, \tag{343}$$

depends only on the phase difference $\alpha_n(\varepsilon) = \chi_n^r(\varepsilon) - \chi_n^r(-\varepsilon) - 2\vartheta(\varepsilon)$. The resonance structure of ζ_n is reflected in the differential conductance

$$G_n(\varepsilon) = \frac{4e^2}{h}\,\frac{T^2}{T^2 + 2R\left[1-\cos\alpha_n(\varepsilon)\right]}\,. \tag{344}$$

Figures 37a and b show the dependences of the conductance and spectral noise on the phase difference α_n. The minimal value of the denominator in (343) and (344), reached at $\varepsilon_{v,n} = v_n/2d\left[n\pi + \arccos\left(\varepsilon_{v,n}/\Delta\right)\right]$, corresponds to the resonances shown in these figures. Differential shot noise ζ_n

[56] This model describes, for example, a thin NS film and a metal needle brought near it — the system in which Rowell–McMillan resonances were observed [277].

in (343) vanishes at these resonances and reaches a maximum at $\cos\alpha_n = (2R - T^2)/2R$, when energies are still close to resonances.

It is remarkable that such a nontrivial structure is preserved even in the multichannel case,[57] which is shown in Figs 37d, e. This can be explained by the fact that levels 'adhere' to the electrochemical potential (of the superconductor). Comparing Figs 37b and e, we see that a sharp double peak in the noise (Fig. 37b) disappears in the multichannel case (Fig. 37e), while the noise S takes the maximum value (instead of the minimal) at the resonance, repeating the corresponding conductance curve (Fig. 37d).

For large voltages $|eV| \gg v_F/d$, the noise and conductance can be estimated by averaging the phase α_n in Eqns (343) and (344),

$$\bar{\zeta} = \frac{1}{2\pi}\int_0^{2\pi} \mathrm{d}\alpha\, \zeta(\alpha) = \frac{2|e|^3}{h}\, T, \qquad \bar{G} = \frac{2e^2}{h}\, T. \tag{345}$$

The sum over channels is replaced by the integral in (345), $(1/N)\sum_n \to (1/2\pi)\int_0^{2\pi}\mathrm{d}\alpha$. This means that both the noise and the conductance reach their normal values (in the corresponding NIN junction) at the voltages $v_F/d \ll |eV| \ll \Delta$.

We now consider the Fano factor $F = S/|e|I$, where $S = \int_0^{|eV|}\mathrm{d}\varepsilon\,\zeta(\varepsilon)$, $I = \int_0^{|eV|}\mathrm{d}\varepsilon\, G(\varepsilon)$. At low voltages, $F = 2$, which reflects the fact that charge carriers are Cooper pairs. At high voltages ($v_F/d \ll |eV| \ll \Delta$), the Fano factor decreases to the normal value $F = 1$. Such a decrease in F, which occurs immediately after the first Andreev resonance (as shown in Figs 37c, f), is caused by the noise suppression in the resonance region. A similar noise suppression was observed in [120].

15.2 Noise in the NINIS junction

As mentioned in Section 13, the NINIS junction can be interpreted as a qualitative model of a disordered conductor [34, 206].

The resonance structure appearing in an INI scatterer leads to the bimodal distribution of the transparency T. For a symmetric INI scatterer ($T_1 = T_2 \ll 1$), the transparency distribution is given by [274]

$$\rho(T) = \frac{1}{\pi}\frac{T_1}{2}\frac{1}{\sqrt{T^3(1-T)}}, \qquad T \in \left[\frac{T_1^2}{\pi^2}, 1\right]. \tag{346}$$

Expression (346) has an analogue in the case of a disordered conductor [34, 206]. The structure of $\rho(T)$ in the NININ junction does not affect macroscopic transport properties. The differential shot noise and linear conductance that can be calculated for bimodal transparency distribution (346),

$$\zeta = \frac{2|e|^3}{h}\int \mathrm{d}T\,\rho(T)\,T(1-T) = \frac{2|e|^3}{h}\frac{T_1}{4}, \tag{347}$$

$$G = \frac{2e^2}{h}\int \mathrm{d}T\,\rho(T)\,T = \frac{2e^2}{h}\frac{T_1}{2}, \tag{348}$$

describe coherent transport [279]. In the incoherent case, the resistance is a sum of two resistances determined by barriers I, connected in series. In this case, $\zeta/|e|G = 1/2$, as a consequence of charge conservation [85]. In the coherent case, the linear response of the NINIS junction can be found from expressions (298), (340), and (346):

$$\zeta(0) = \frac{2|e|^3}{h}\int \mathrm{d}T\,\rho(T)\,\frac{16T^2(1-T)}{(2-T)^4} = \frac{2|e|^3}{h}\frac{T_1}{2}\frac{3}{4\sqrt{2}}, \tag{349}$$

$$G(0) = \frac{2e^2}{h}\int \mathrm{d}T\,\rho(T)\,\frac{2T^2}{(2-T)^2} = \frac{2e^2}{h}\frac{T_1}{2}\frac{1}{\sqrt{2}}. \tag{350}$$

The ratio of the spectral noise density to the conductance in this case is $\zeta(0)/|e|G(0) = 3/4$ [274]. The noise-to-conductance ratios in the coherent case for X = I and X = IN and for a contact with X = D (where D is a diffusion conductor) are compared in Table 1. The transparency distribution for a unit barrier has a maximum at $T \ll 1$. The ratios $\zeta_N/|e|G_N = 1$ in the NIN junction and $\zeta_S/|e|G_S = 2$ in the NIS junction characterize the carrier as an electron or a Cooper pair. In the presence of disorder, superconductivity in the NDS junction produces twice the noise determined by the normal NDN junction. However, in the case of a double barrier, noise in the NINIS junction increases 3/2 times compared with that in the NININ junction (see Table 1). Therefore, we can conclude that noise doubling is not universal and can depend on the features of the transparency distribution function. This is explained by the fact that noise is caused by channels with mean transparencies $0 \lesssim T \lesssim 1$, while the current is related to open channels with $T \to 1$.

Table 1. The ratio $\zeta/|e|G$ of the spectral noise density to the conductance for NXN and NXS junctions. Results are valid [85, 112, 274, 279] for a weak transparency $T \ll 1$ and many channels $N \to \infty$.

	Single barrier*	Double barrier**	Disorder***
NXN $\zeta_N/\lvert e\rvert G_N$	1	1/2	1/3
NXS $\zeta_S/\lvert e\rvert G_S$	2	3/4	2/3

* Single barrier without an internal structure, X = I.
** Symmetric coherent double barrier, X = INI.
*** X = D.

At finite voltages, the differential noise is determined by Eqn (340) with reflection amplitudes (306) of the double INI barrier. This noise for a symmetric barrier, $T_1 = T_2 = 0.05$, is shown in Fig. 38. For voltages of the order of the Andreev level, $|eV| \sim v_F/d$, the resonance structure is independent of the number of channels, while the resonance peaks are reflected in both the noise and conductance. At higher voltages, $|eV| \gg v_F/d$, resonances disappear due to dephasing of electrons and holes. In this case, the difference between NIN and NIS junctions also disappears.

16. Conclusions

We have considered mainly all basic aspects of the scattering matrix application for electron transport description. However, because of the unavoidable size limitations, topics such as multichannel cases, the transparency statistics for dirty conductors, the integer quantum Hall effect, and some others have only barely been discussed or simply mentioned, as, for example, problems with time-dependent fields. Although the fundamentals of the method described here are presented in books (see, e.g., [72, 73] and handbook [65]), a number of issues have been mentioned only in articles, while some have

[57] For example, the resonance structure of a normal double barrier is not preserved in the multichannel case.

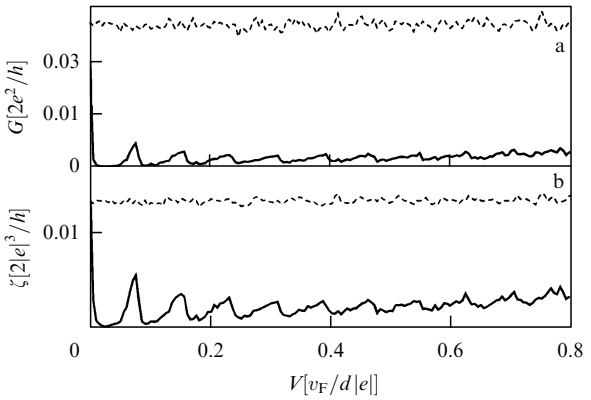

Figure 38. (a) Differential conductance and (b) shot noise in the NINIS junction with many channels (8×10^4). The transparencies of scatterers are the same, $T_1 = T_2 \approx 0.05$, the distance between scatterers is $d = 20v_F/\Delta$, and $\int dx\, V(x) = 3\hbar v_F$. Averaged shot noise per channel (340) has local maxima at conductance resonances (solid curves). The conductance and shot noise for the corresponding nonsuperconducting NININ structure are shown by dashed curves [278].

not been considered at all. We hope that this review compensates at least partially for this deficiency, especially as regards the Russian literature. We note in conclusion that the possibilities inherent in the approach initiated by Landauer in 1957 [5] are far from being exhausted, especially concerning the description of systems with interacting particles, while at the same time this approach has already become a convenient tool in solving electron transport problems in the noninteracting case.

Acknowledgements
This work was supported by the Russian Foundation for Basic Research [grant no. 11-02-00744-a (GBL)] and NSF ECS-0608842, ARO W911NF-09-1-0395, and DARPA HR0011-09-1-0009 grants (IAS). We thank M V Suslov, I S Burmistrov, L I Glazman, V I Fal'ko, and L E Fedichkin for reading the manuscript and for their useful remarks.

We also thank their co-authors D E Khmel'nitskii, L B Ioffe, L S Levitov, V I Fal'ko, C Presilla, Th Martin, G Blatter, F Hassler, M V Suslov, G M Graf, N M Chtchelkatchev, and A V Lebedev and colleagues A I Larkin, B L Al'tshuller, D A Ivanov, K A Matveev, R Landauer, V V Ryazanov, C Glattli, M Sanquer, V Bouchiat, and M Reznikov, who helped us in discussions to understand many aspects of quantum electron transport. The review is partially based on the lecture course read by GBL at the Eidgenössische Technische Hochschule Zürich in 2008, and the lecture notes prepared by IAS and F Hassler. The plan of lectures proposed by G Blatter also affected the structure of this review.

17. Appendix: properties of scattering matrices

A.1 Properties of scattering states

The basic properties of scattering states both in the purely one-dimensional and in the multichannel and multilead cases are obtained by the same methods as in the three-dimensional case, which is usually considered in textbooks. However, the orthonormalization and completeness of a set of scattering states can also be found from the following (not very rigorous) considerations: we create scattering states from plane waves, e.g., at an instant $t = t_{\rm in}$ [the set of wave functions $\psi_k(x, t_{\rm in}) = \exp(ikx)$ at that instant] by adiabatically increasing the scattering potential (localized in some region) up to a specified value. Then both the orthonormalization and the completeness of the set $\{\psi_k(x,t)\}$ in the subsequent instants automatically follow from the unitarity of the evolution of the wave packets because the initial set of plane waves had these properties (for plane waves, this can be proved by direct explicit calculations). Because the states $\psi_k(x,t)$ transform into Lieppmann–Schwinger scattering states as $t \to \infty$ (it is this statement that should be proved more rigorously), we have obtained the orthonormalization and completeness for them.

We note that these properties can be used only in the region of wave packets that have already experienced scattering from a potential with the required accuracy close to the specified potential, i.e., $|x| \ll v_k\tau$, where τ is the time elapsed from the instant at which the potential was close to the specified potential, with the required accuracy.[58] It also follows from these considerations that the type of normalization (for example, to the energy delta function) of scattering states can be determined from their asymptotic forms: the flow density in the incident wave can be related to a plane wave, for which the normalization can be done easily.

A.2 Unitarity of the scattering matrix

The scattering matrix S is parameterized as

$$\mathsf{S} = \begin{bmatrix} r & t' \\ t & r' \end{bmatrix}. \tag{351}$$

The scattering matrix is unitary,

$$\mathsf{S}\mathsf{S}^\dagger = 1\,, \tag{352}$$

which means that the amplitudes t, t', r, and r' are not independent quantities:

$$r^\dagger r + t'^\dagger t' = t^\dagger t + r'^\dagger r' = 1\,, \tag{353}$$

$$tr^\dagger + r't'^\dagger = 0\,. \tag{354}$$

For example, if t, t', and r are known, we can find from (354) that

$$r' = -tr^\dagger[t'^\dagger]^{-1}\,. \tag{355}$$

The Hermitian conjugation symbol † is used here instead of the complex conjugation symbol $*$ to emphasize that scattering amplitudes can be matrices in the multichannel case.[59] In the one-dimensional spatially symmetric case (with the time reversal symmetry assumed), it follows from (354) that

$$tr^* = \pm i\sqrt{TR}\,. \tag{356}$$

[58] The possible appearance of coupled states requires some modification of our arguments; however, we do not consider this question here because such states rarely contribute to the transport phenomena under study.

[59] In addition, scattering amplitudes are not always described by scattering matrices. For example, the numbers of channels on the left and right sides of the barriers can be different. The scattering amplitudes are also matrices in the spin space in general. These matrices become nondiagonal in the case of spin-flip scattering, which can be caused by the spin–orbital interaction in the barrier or the action of an inhomogeneous exchange field (caused by ferromagnetic barriers) on the electron spin.

In the case of scattering from the delta function, the plus sign in (356) corresponds to the attractive potential in which a bound state exists, while the minus sign corresponds to the repulsive potential I in which only a continuous spectrum exists [see (91)]. In the case of scattering from a double barrier, the sign changes after passing through the (ideal) resonance. Such a behavior of the phase affects the general interference pattern in the INIS structure (see Section 13.4).

A.3 Symmetry of the Hamiltonian under time reversal

When the system Hamiltonian is invariant under a symmetry transformation, this invariance is extended in a certain way to the scattering matrix. If the Hamiltonian in invariant under time reversal, then the scattering matrix satisfies the relation

$$\mathsf{S} = \mathsf{S}^{\top} . \tag{357}$$

It follows from (357) that $t = t'$. Using relations (353) and (354), we can also find that $|r| = |r'|$ and that the usual relation exists between reflection ($R = |r|^2 = |r'|^2$) and transmission ($T = |t|^2 = |t'|^2$) probabilities:

$$R + T = 1 . \tag{358}$$

If we take a magnetic field into account, then, because time reversal changes the direction of the magnetic field **B** to the opposite [72, 280], we have

$$\mathsf{S}_{-\mathbf{B}} = \mathsf{S}_{\mathbf{B}}^{\top} . \tag{359}$$

For the transmission amplitude for a scatterer inside which the magnetic field acts nontrivially on the orbital (one-dimensional) motion of particles, we have $t_{\mathbf{B}} = t'_{-\mathbf{B}}$.

References

1. Born M *Z. Phys.* **37** 863 (1926)
2. Wheeler J A *Phys. Rev.* **52** 1107 (1937)
3. Heisenberg W *Z. Phys.* **120** 513 (1943)
4. Heisenberg W *Z. Phys.* **120** 673 (1943)
5. Landauer R *IBM J. Res. Dev.* **1** 223 (1957)
6. Anderson P W et al. *Phys. Rev. B* **22** 3519 (1980)
7. Fisher D S, Lee P A *Phys. Rev. B* **23** 6851 (1981)
8. Economou E N, Soukoulis C M *Phys. Rev. Lett.* **46** 618 (1981)
9. v. Klitzing K, Dorda G, Pepper M *Phys. Rev. Lett.* **45** 494 (1980)
10. Imry Y, in *Directions in Condensed Matter Physics* (Eds G Grinstein, G Mazenko) (Singapore: World Scientific, 1986) p. 101
11. Büttiker M *Phys. Rev. Lett.* **57** 1761 (1986)
12. Büttiker M *IBM J. Res. Dev.* **32** 63 (1988)
13. Büttiker M *IBM J. Res. Dev.* **32** 317 (1988)
14. Büttiker M *Phys. Rev. B* **38** 9375 (1988)
15. Takane Y, Ebisawa H *J. Phys. Soc. Jpn.* **61** 1685 (1992)
16. Takane Y, Ebisawa H *J. Phys. Soc. Jpn.* **61** 2858 (1992)
17. Lambert C J *J. Phys. Condens. Matter* **3** 6579 (1991)
18. Lambert C J, Hui V C, Robinson S J *J. Phys. Condens. Matter* **5** 4187 (1993)
19. Anantram M P, Datta S *Phys. Rev. B* **53** 16390 (1996)
20. Beenakker C W J *Phys. Rev. Lett.* **67** 3836 (1991); "Erratum" *Phys. Rev. Lett.* **68** 1442 (1992)
21. Lesovik G B *Pis'ma Zh. Eksp. Teor. Fiz.* **49** 513 (1989) [*JETP Lett.* **49** 592 (1989)]
22. Büttiker M *Phys. Rev. Lett.* **65** 2901 (1990)
23. Martin Th, Landauer R *Phys. Rev. B* **45** 1742 (1992)
24. Levitov L S, Lesovik G B *Pis'ma Zh. Eksp. Teor. Fiz.* **58** 225 (1993) [*JETP Lett.* **58** 230 (1993)]
25. Landauer R *Philos. Mag.* **21** 863 (1970)
26. Hassler F et al. *Phys. Rev. B* **78** 165330 (2008)
27. Sukhorukov E V, Levinson I B *Zh. Eksp. Teor. Fiz.* **97** 1384 (1990) [*Sov. Phys. JETP* **70** 782 (1990)]
28. Sharvin Yu V *Zh. Eksp. Teor. Fiz.* **48** 984 (1965) [*Sov. Phys. JETP* **21** 655 (1965)]
29. Glazman L I, Khaetskii A V *Pis'ma Zh. Eksp. Teor. Fiz.* **48** 546 (1988) [*JETP Lett.* **48** 591 (1988)]
30. Glazman L I, Khaetskii A V *Europhys. Lett.* **9** 263 (1989)
31. Patel N K et al. *J. Phys. Condens. Matter* **2** 7247 (1990)
32. Patel N K et al. *Phys. Rev. B* **44** 13549 (1991)
33. Matveev K A, Glazman L I *Phys. Rev. Lett.* **70** 990 (1993)
34. Dorokhov O N *Pis'ma Zh. Eksp. Teor. Fiz.* **36** 259 (1982) [*JETP Lett.* **36** 318 (1982)]
35. Mello P A, Pereyra P, Kumar N *Ann. Physics* **181** 290 (1988)
36. van Wees B J et al. *Phys. Rev. Lett.* **60** 848 (1988)
37. Wharam D A et al. *J. Phys. C* **21** L209 (1988)
38. Thornton T J et al. *Phys. Rev. Lett.* **56** 1198 (1986)
39. Fal'ko V I, Lesovik G B, in *Coulomb and Interference Effects in Small Electronic Structures: XIVth Moriond Workshop, Switzerland, January 22–29, 1994* (Eds D C Glattli, M Sanquer, J Trân Thanh Vân) (Gif-sur-Yvette: Editions Frontieres, 1994) p. 389
40. Glazman L I et al. *Pis'ma Zh. Eksp. Teor. Fiz.* **48** 218 (1988) [*JETP Lett.* **48** 238 (1988)]
41. Kemble E C *Phys. Rev.* **48** 549 (1935)
42. Landau L D, Lifshitz E M *Kvantovaya Mekhanika: Nerelyativistskaya Teoriya* (Quantum Mechanics: Non-Relativistic Theory) (Moscow: Fizmatlit, 2004) [Translated into English (Oxford: Pergamon Press, 1977)]
43. Kawabata A *J. Phys. Soc. Jpn.* **58** 372 (1989)
44. Fertig H A, Halperin B I *Phys. Rev. B* **36** 7969 (1987)
45. Büttiker M *Phys. Rev. B* **41** 7906 (1990)
46. Frank S et al. *Science* **280** 1744 (1998)
47. Poncharal Ph et al. *Eur. Phys. J. D* **9** 77 (1999)
48. Martel R et al. *Appl. Phys. Lett.* **73** 2447 (1998)
49. Olesen L et al. *Phys. Rev. Lett.* **72** 2251 (1994)
50. Krans J M et al. *Nature* **375** 767 (1995)
51. Scheer E et al. *Phys. Rev. Lett.* **78** 3535 (1997)
52. Rodrigues V, Fuhrer T, Ugarte D *Phys. Rev. Lett.* **85** 4124 (2000)
53. Peres N M R, Castro Neto A H, Guinea F *Phys. Rev. B* **73** 195411 (2006); "Erratum" *Phys. Rev. B* **73** 239902(E) (2006)
54. Tombros N et al. *Nature Phys.* **7** 697 (2011)
55. Patel N K et al. *Phys. Rev. B* **44** 10973 (1991)
56. Thomas K J et al. *Phys. Rev. Lett.* **77** 135 (1996)
57. Glazman L I, Khaetskii A V *J. Phys. Condens. Matter* **1** 5005 (1989)
58. Laughlin R B *Phys. Rev. B* **23** 5632 (1981)
59. Halperin B I *Phys. Rev. B* **25** 2185 (1982)
60. Devyatov E V *Usp. Fiz. Nauk* **177** 207 (2007) [*Phys. Usp.* **50** 197 (2007)]
61. Aharonov Y, Bohm D *Phys. Rev.* **115** 485 (1959)
62. Yacoby A et al. *Phys. Rev. Lett.* **74** 4047 (1995)
63. Fano U *Phys. Rev.* **124** 1866 (1961)
64. Ji Y et al. *Nature* **422** 415 (2003)
65. Chtchelkatchev N M, Lesovik G B *Odnomernoe Rasseyanie v Kvantovoi Mekhanike i Ego Prilozheniya* (One-dimensional Scattering in Quantum Mechanics and Its Applications) (Moscow: MFTI, 2011)
66. Moskalets M, Büttiker M *Phys. Rev. B* **66** 205320 (2002)
67. Moskalets M, Büttiker M *Phys. Rev. B* **70** 245305 (2004)
68. Lesovik G B, Levitov L S *Phys. Rev. Lett.* **72** 538 (1994)
69. Levitov L S, Lee H, Lesovik G B *J. Math. Phys.* **37** 4845 (1996)
70. Ivanov D A, Levitov L S *Pis'ma Zh. Eksp. Teor. Fiz.* **58** 450 (1993) [*JETP Lett.* **58** 461 (1993)]
71. Ivanov D A, Lee H W, Levitov L S *Phys. Rev. B* **56** 6839 (1997)
72. Datta S *Electronic Transport in Mesoscopic Systems* (Cambridge: Cambridge Univ. Press, 1995)
73. Demikhovskii V Ya, Vugal'ter G A *Fizika Kvantovykh Nizkorazmernykh Struktur* (Physics of Quantum Low-dimensional Structures) (Moscow: Logos, 2000)
74. Azbel M Ya, in *Localization, Interaction, and Transport Phenomena: Proc. of the Intern. Conf., August 23–28, 1984, Braunschweig, Germany* (Springer Series in Solid-State Sciences, Vol. 61, Eds B Kramer, G Bergmann, Y Bruynseraede) (Berlin: Springer-Verlag, 1985) p. 162

75. Al'tshuler B L *Pis'ma Zh. Eksp. Teor. Fiz.* **41** 530 (1985) [*JETP Lett.* **41** 648 (1985)]
76. Lee P A, Stone A D *Phys. Rev. Lett.* **55** 1622 (1985)
77. Al'tshuler B L, Khmel'nitskii D E *Pis'ma Zh. Eksp. Teor. Fiz.* **42** 291 (1985) [*JETP Lett.* **42** 359 (1985)]
78. Larkin A I, Khmel'nitskii D E *Zh. Eksp. Teor. Fiz.* **91** 1815 (1986) [*Sov. Phys. JETP* **64** 1075 (1986)]
79. Petrashov V T, Reinders P, Springford M *Pis'ma Zh. Eksp. Teor. Fiz.* **45** 565 (1987) [*JETP Lett.* **45** 720 (1987)]
80. Washburn S *IBM J. Res. Dev.* **32** 335 (1988)
81. Ghosh A, Raychaudhuri A K *Phys. Rev. Lett.* **84** 4681 (2000)
82. Kubo R *J. Phys. Soc. Jpn.* **12** 570 (1957)
83. Greenwood D A *Proc. Phys. Soc. London* **71** 585 (1958)
84. Dorokhov O N *Solid State Commun.* **51** 381 (1984)
85. Beenakker C W J, Büttiker M *Phys. Rev. B* **46** 1889 (1992)
86. Prange R E, Girvin S M (Eds) *The Quantum Hall Effect* (New York: Springer-Verlag, 1987) [Translated into Russian (Moscow: Mir, 1989)]
87. Brouwer P W, Frahm K *Phys. Rev. B* **53** 1490 (1996)
88. Efetov K B, Larkin A I *Zh. Eksp. Teor. Fiz.* **85** 764 (1983) [*Sov. Phys. JETP* **58** 444 (1983)]
89. Efetov K B *Adv. Phys.* **32** 53 (1983)
90. Pruisken A M M, Škorić B, Baranov M A *Phys. Rev. B* **60** 16838 (1999)
91. Lesovick G B *Mod. Phys. Lett. B* **3** 611 (1989)
92. Anisovich A V et al. *Pis'ma Zh. Eksp. Teor. Fiz.* **45** 237 (1987) [*JETP Lett.* **45** 295 (1987)]
93. Lesovik G B, Khmel'nitskii D E *Zh. Eksp. Teor. Fiz.* **94** (5) 164 (1988) [*Sov. Phys. JETP* **67** 957 (1988)]
94. Franz R, Wiedemann G *Ann. Physik* **165** 497 (1853)
95. Lifshitz E M, Pitaevskii L P *Fizicheskaya Kinetika* (Physical Kinetics) (Moscow: Fizmatlit, 2007) [Translated into English (New York: Pergamon Press, 1981)]
96. Engquist H-L, Anderson P W *Phys. Rev. B* **24** 1151 (1981)
97. Landauer R *Physica D* **38** 226 (1989)
98. Landauer R, Martin Th *Physica B* **175** 167 (1991)
99. Landauer R, Martin Th *Physica B* **182** 288 (1992)
100. Schönhammer K *Phys. Rev. B* **75** 205329 (2007)
101. Stone A D, Szafer A *IBM J. Res. Dev.* **32** 384 (1988)
102. Keldysh L V *Zh. Eksp. Teor. Fiz.* **47** 1515 (1964) [*Sov. Phys. JETP* **20** 1018 (1965)]
103. Landau L D, Lifshitz E M *Statisticheskaya Fizika* (Statistical Physics) Vol. 1 (Moscow: Fizmatlit, 2010) [Translated into English (Oxford: Pergamon Press, 1980)]
104. Lesovik G B, Loosen R *Pis'ma Zh. Eksp. Teor. Fiz.* **65** 280 (1997) [*JETP Lett.* **65** 295 (1997)]
105. Gavish U, Levinson Y, Imry Y *Phys. Rev. B* **62** R10637 (2000)
106. Aguado R, Kouwenhoven L P *Phys. Rev. Lett.* **84** 1986 (2000)
107. Basset J, Bouchiat H, Deblock R *Phys. Rev. Lett.* **105** 166801 (2010)
108. Onac E et al. *Phys. Rev. Lett.* **96** 176601 (2006)
109. Gustavsson S et al. *Phys. Rev. Lett.* **99** 206804 (2007)
110. Deblock R et al. *Science* **301** 203 (2003)
111. Gavish U et al., cond-mat/0211646
112. Khlus V A *Zh. Eksp. Teor. Fiz.* **93** 2179 (1987) [*Sov. Phys. JETP* **66** 1243 (1987)]
113. Reznikov M et al. *Phys. Rev. Lett.* **75** 3340 (1995)
114. Kumar A et al. *Phys. Rev. Lett.* **76** 2778 (1996)
115. Steinbach A, Martinis J, Devoret M H *Bull. Am. Phys. Soc.* **40** 400 (1995)
116. Liefrink F et al. *Phys. Rev. B* **49** 14066 (1994)
117. Lesovik G B, Loosen R *Z. Phys. B* **91** 531 (1993)
118. Saminadayar L et al. *Phys. Rev. Lett.* **79** 2526 (1997)
119. de-Picciotto R et al. *Nature* **389** 162 (1997)
120. Lefloch F et al. *Phys. Rev. Lett.* **90** 067002 (2003)
121. Reznikov M et al. *Nature* **399** 238 (1999)
122. Blanter Ya M, Büttiker M *Phys. Rep.* **336** 1 (2000)
123. Martin T, in *Nanophysics*: *Coherence and Transport*: *Lecture Notes of the Les Houches Summer School 2004, Session LXXXI* (Eds H Bouchiat et al.) (Amsterdam: Elsevier, 2005) p. 283
124. Levitov L S, Lesovik G B *Pis'ma Zh. Eksp. Teor. Fiz.* **55** 534 (1992) [*JETP Lett.* **55** 555 (1992)]
125. Lesovik G B *Pis'ma Zh. Eksp. Teor. Fiz.* **60** 806 (1994) [*JETP Lett.* **60** 820 (1994)]
126. Falci G, Paladino E, Fazio R, in *Quantum Phenomena in Mesoscopic Systems*: *Proc. of the Intern. School of Physics "Enrico Fermi", 2002, Varenna, Italy, Course 151* (Eds B Altshuler, A Tagliacozzo, V Tognetti) (Amsterdam: IOS Press, 2003)
127. Galperin Y M et al. *Phys. Rev. Lett.* **96** 097009 (2006)
128. Neder I et al. *Nature Phys.* **3** 534 (2007)
129. Averin D V, Sukhorukov E V *Phys. Rev. Lett.* **95** 126803 (2005)
130. Levitov L S, Lesovik G B, cond-mat/9401004
131. Bachmann S, Graf G M, Lesovik G B *J. Stat. Phys.* **138** 333 (2010)
132. Shelankov A, Rammer J *Europhys. Lett.* **63** 485 (2003)
133. Lesovik G B, Hassler F, Blatter G *Phys. Rev. Lett.* **96** 106801 (2006)
134. Muzykantskii B A, Adamov Y *Phys. Rev. B* **68** 155304 (2003)
135. Avron J E et al. *Commun. Math. Phys.* **280** 807 (2008)
136. Hassler F, Lesovik G B, Blatter G *Phys. Rev. Lett.* **99** 076804 (2007)
137. Büttiker M *Phys. Rev. B* **46** 12485 (1992)
138. Lesovik G B, Thesis of Doctor of Physical Mathematical Sciences (Chernogolovka: Institute of Solid State Physics, RAS, 1997)
139. Burkard G, Loss D, Sukhorukov E V *Phys. Rev. B* **61** R16303 (2000)
140. Fève G et al. *Science* **316** 1169 (2007)
141. Mahé A et al. *Phys. Rev. B* **82** 201309(R) (2010)
142. Keeling J, Klich I, Levitov L S *Phys. Rev. Lett.* **97** 116403 (2006)
143. Lebedev M V, Shchekin A A, Misochko O V *Kvantovaya Elektron.* **38** 710 (2008) [*Quantum Electron.* **38** 710 (2008)]
144. Abanov A G, Ivanov D A *Phys. Rev. Lett.* **100** 086602 (2008)
145. Abanov A G, Ivanov D A *Phys. Rev. B* **79** 205315 (2009)
146. Roothaan C C J *Rev. Mod. Phys.* **23** 69 (1951)
147. Kambly D, Ivanov D A *Phys. Rev. B* **80** 193306 (2009)
148. Courant R, Hilbert D *Methoden der mathematischen Physik* 4th ed. (Berlin: Springer-Verlag, 1993) [Translated into English *Methods of Mathematical Physics* (New York: Interscience Publ., 1989)]
149. Bayandin K V, Lebedev A V, Lesovik G B *Pis'ma Zh. Eksp. Teor. Fiz.* (submitted)
150. Bayandin K V, Lebedev A V, Lesovik G B *Zh. Eksp. Teor. Fiz.* **133** 140 (2008) [*JETP* **106** 117 (2008)]
151. Bomze Yu et al. *Phys. Rev. Lett.* **95** 176601 (2005)
152. Gershon G et al. *Phys. Rev. Lett.* **101** 016803 (2008)
153. Timofeev A V et al. *Phys. Rev. Lett.* **98** 207001 (2007)
154. Reulet B et al., in *Perspectives of Mesoscopic Physics*: *Dedicated to Yoseph Imry's 70th Birthday* (Eds A Aharony, O Entin-Wohlman) (Singapore: World Scientific, 2010) p. 211
155. Gustavsson S et al. *Phys. Rev. Lett.* **96** 076605 (2006)
156. Petersson K D et al. *Phys. Rev. Lett.* **105** 246804 (2010)
157. Lesovik G B, Suslov M V, Blatter G *Phys. Rev. A* **82** 012316 (2010)
158. Ivanov D A, Abanov A G *Europhys. Lett.* **92** 37008 (2010)
159. Jalabert R A, Pichard J-L, Beenakker C W J *Europhys. Lett.* **27** 255 (1994)
160. Lee H, Levitov L S, Yakovetz A Yu *Phys. Rev. B* **51** 4079 (1995)
161. Danneau R et al. *Phys. Rev. Lett.* **100** 196802 (2008)
162. Tworzydlo J et al. *Phys. Rev. Lett.* **96** 246802 (2006)
163. Katsnelson M I *Eur. Phys. J. B* **51** 157 (2006)
164. Lebedev A V, Lesovik G B, Blatter G *Phys. Rev. Lett.* **100** 226805 (2008)
165. Goorden M C, Büttiker M *Phys. Rev. Lett.* **99** 146801 (2007)
166. Gogolin A O et al. *Ann. Physik* **16** 678 (2007)
167. Beenakker C W J, Schomerus H *Phys. Rev. Lett.* **86** 700 (2001)
168. Lebedev A V, Lesovik G B, Blatter G *Phys. Rev. B* **81** 155421 (2010)
169. de Gennes P G *Rev. Mod. Phys.* **36** 225 (1964)
170. de Gennes P G *Superconductivity of Metals and Alloys* (New York: W. A. Benjamin, 1966) [Translated into Russian (Moscow: Mir, 1968)]
171. Svidzinskii A V *Prostranstvenno-Neodnorodnye Zadachi Teorii Sverkhprovodimosti* (Spatially Inhomogeneous Problems of the Superconductivity Theory) (Moscow: Nauka, 1982)
172. Andreev A F *Zh. Eksp. Teor. Fiz.* **46** 1823 (1964) [*Sov. Phys. JETP* **19** 1228 (1964)]
173. Andreev A F *Zh. Eksp. Teor. Fiz.* **47** 2222 (1964) [*Sov. Phys. JETP* **20** 1490 (1965)]
174. Andreev A F *Zh. Eksp. Teor. Fiz.* **49** 655 (1965) [*Sov. Phys. JETP* **22** 455 (1966)]
175. Blonder G E, Tinkham M, Klapwijk T M *Phys. Rev. B* **25** 4515 (1982)
176. Lesovik G B, Martin T, Blatter G *Eur. Phys. J. B* **24** 287 (2001)
177. Recher P, Sukhorukov E V, Loss D *Phys. Rev. B* **63** 165314 (2001)

178. Chtchelkatchev N M et al. *Phys. Rev. B* **66** 161320(R) (2002)
179. Bayandin K V, Lesovik G B, Martin T *Phys. Rev. B* **74** 085326 (2006)
180. Beenakker C W J *Phys. Rev. B* **46** 12841 (1992)
181. Büttiker M et al. *Phys. Rev. B* **31** 6207 (1985)
182. Anderson P W *J. Phys. Chem. Solids* **11** 26 (1959)
183. Nazarov Yu V, Stoof T H *Phys. Rev. Lett.* **76** 823 (1996)
184. Stoof T H, Nazarov Yu V *Phys. Rev. B* **53** 14496 (1996)
185. Hekking F W J, Nazarov Yu V *Phys. Rev. B* **49** 6847 (1994)
186. Volkov A F, Zaitsev A V, Klapwijk T M *Physica C* **210** 21 (1993)
187. Petrashov V T et al. *Phys. Rev. Lett.* **74** 5268 (1995)
188. Courtois H et al. *Phys. Rev. Lett.* **76** 130 (1996)
189. Lesovik G B, Fauchère A L, Blatter G *Phys. Rev. B* **55** 3146 (1997)
190. Leadbeater M, Lambert C J *J. Phys. Condens. Matter* **8** L345 (1996)
191. Magnée P H C et al. *Phys. Rev. B* **50** 4594 (1994)
192. Poirier W, Mailly D, Sanquer M, unpublished
193. Christen T, Büttiker M *Europhys. Lett.* **35** 523 (1996)
194. Giaever I *Phys. Rev. Lett.* **5** 147 (1960)
195. Giaever I, Hart H R (Jr.), Megerle K *Phys. Rev.* **126** 941 (1962)
196. Giaever I *Rev. Mod. Phys.* **46** 245 (1974)
197. Beenakker C W J *Rev. Mod. Phys.* **69** 731 (1997)
198. Artemenko S N, Volkov A F, Zaitsev A V *Solid State Commun.* **30** 771 (1979)
199. Pothier H et al. *Phys. Rev. Lett.* **73** 2488 (1994)
200. Marmorkos I K, Beenakker C W J, Jalabert R A *Phys. Rev. B* **48** 2811 (1993)
201. Yip S *Phys. Rev. B* **52** 15504 (1995)
202. Kastalsky A et al. *Phys. Rev. Lett.* **67** 3026 (1991)
203. Nguyen C, Kroemer H, Hu E L *Phys. Rev. Lett.* **69** 2847 (1992)
204. Nitta J, Akazaki T, Takayanagi H *Phys. Rev. B* **49** 3659 (1994)
205. Bakker S J M et al. *Phys. Rev. B* **49** 13275 (1994)
206. Melson J A, Beenakker C W J *Physica B* **203** 219 (1994)
207. Chaudhuri S, Bagwell P F *Phys. Rev. B* **51** 16936 (1995)
208. Edwards J T, Thouless D J *J. Phys. C* **5** 807 (1972)
209. Altland A, Gefen Y, Montambaux G *Phys. Rev. Lett.* **76** 1130 (1996)
210. van Wees B J et al. *Phys. Rev. Lett.* **69** 510 (1992)
211. Josephson B D *Phys. Lett.* **1** 251 (1962)
212. van Wees B J, Lenssen K-M H, Harmans C J P M *Phys. Rev. B* **44** 470 (1991)
213. Takayanagi H, Akazaki T, Nitta J *Phys. Rev. Lett.* **75** 3533 (1995)
214. Akazaki T et al. *Appl. Phys. Lett.* **68** 418 (1996)
215. Schäpers Th et al. *Appl. Phys. Lett.* **73** 2348 (1998)
216. Sutton A P *Curr. Opin. Solid State Mater. Sci.* **1** 827 (1996)
217. Morpurgo A F, Klapwijk T M, van Wees B J *Appl. Phys. Lett.* **72** 966 (1998)
218. Baselmans J J A et al. *Nature* **397** 43 (1999)
219. Krans J M et al. *Phys. Rev. B* **48** 14721 (1993)
220. Muller C J, van Ruitenbeek J M, de Jongh L J *Phys. Rev. Lett.* **69** 140 (1992)
221. Scheer E et al. *Nature* **394** 154 (1998)
222. Kasumov A Yu et al. *Science* **284** 1508 (1999)
223. Jarillo-Herrero P, van Dam J A, Kouwenhoven L P *Nature* **439** 953 (2006)
224. Cleuziou J-P et al. *Nature Nanotech.* **1** 53 (2006)
225. Eichler A et al. *Phys. Rev. B* **79** 161407(R) (2009)
226. Roch N et al. *Nature* **453** 633 (2008)
227. Winkelmann C B et al. *Nature Phys.* **5** 876 (2009)
228. Heersche H B et al. *Nature* **446** 56 (2007)
229. Du X, Skachko I, Andrei E Y *Phys. Rev. B* **77** 184507 (2008)
230. Ojeda-Aristizabal C et al. *Phys. Rev. B* **79** 165436 (2009)
231. Ohta H, Ishii C (Eds) *Physics and Applications of Mesoscopic Josephson Junctions* (Tokyo: The Physical Society of Japan, 1999)
232. Furusaki A, Takayanagi H, Tsukada M *Phys. Rev. Lett.* **67** 132 (1991)
233. Furusaki A, Takayanagi H, Tsukada M *Phys. Rev. B* **45** 10563 (1992)
234. Chtchelkatchev N M, Lesovik G B, Blatter G *Phys. Rev. B* **62** 3559 (2000)
235. Kuhn D D et al. *Phys. Rev. B* **63** 054520 (2001)
236. Sadovskyy I A, Lesovik G B, Blatter G *Phys. Rev. B* **75** 195334 (2007)
237. Sadovskyy I A, Lesovik G B, Blatter G *Pis'ma Zh. Eksp. Teor. Fiz.* **86** 239 (2007) [*JETP Lett.* **86** 210 (2007)]
238. Sadovskyy I A et al. *Phys. Rev. B* **82** 235310 (2010)
239. Beenakker C W J, van Houten H *Phys. Rev. Lett.* **66** 3056 (1991)
240. Schmidt V V *Vvedeine v Fiziku Sverkhprovodnikov* (Introduction to the Physics of Superconductors) (Moscow: MTsNMO, 2000); *The Physics of Superconductors: Introduction to Fundamentals and Applications* (Berlin: Springer, 1997)
241. Clarke J, in *Superconductor Applications*: *SQUIDs and Machines* (Eds B B Schwartz, S Foner) (New York: Plenum Press, 1977) p. 67
242. Clarke J, Braginski A I (Eds) *The SQUID Handbook* Vol. 1 *Fundamentals and Technology of SQUIDs and SQUID Systems* (Berlin: Wiley-VCH, 2004)
243. Clarke J, Braginski A I (Eds) *The SQUID Handbook* Vol. 2 *Applications of SQUIDs and SQUID Systems* (Berlin: Wiley-VCH, 2004)
244. Kleiner R et al. *Proc. IEEE* **92** 1534 (2004)
245. Kulik I O *Zh. Eksp. Teor. Fiz.* **57** 1745 (1969) [*Sov. Phys. JETP* **30** 944 (1970)]
246. Ishii C *Prog. Theor. Phys.* **44** 1525 (1970)
247. van Houten H *Appl. Phys. Lett.* **58** 1326 (1991)
248. Chrestin A, Matsuyama T, Merkt U *Phys. Rev. B* **49** 498 (1994)
249. Wendin G, Shumeiko V S *Superlat. Microstruct.* **20** 569 (1996)
250. Wendin G et al. *Jpn. J. Appl. Phys.* **38** 354 (1999)
251. Wendin G, Shumeiko V S, Samuelsson P *Superlat. Microstruct.* **25** 983 (1999)
252. Wendin G, Shumeiko V S *Phys. Rev. B* **53** R6006 (1996)
253. Chtchelkatchev N M, Ph.D. Thesis of Physics and Mathematical Sciences (Moscow: Landau Institute for Theoretical Physics, RAS, 2002)
254. Krichevsky A et al. *Phys. Rev. B* **61** 3723 (2000)
255. Akkermans E et al. *Phys. Rev. Lett.* **66** 76 (1991)
256. Beenakker C W J, van Houten H, in *Single-Electron Tunneling and Mesoscopic Devices*: *Proc. of the 4th Intern. Conf., SQUID'91, Berlin, Germany, June 18–21, 1991* (Eds H Koch, H Lübbig) (Berlin: Springer, 1992) p. 175
257. Novoselov K S et al. *Science* **306** 666 (2004)
258. Katsnelson M I, Novoselov K S, Geim A K *Nature Phys.* **2** 620 (2006)
259. Cheianov V V, Fal'ko V I *Phys. Rev. B* **74** 041403(R) (2006)
260. Beenakker C W J *Rev. Mod. Phys.* **80** 1337 (2008)
261. Beenakker C W J *Phys. Rev. Lett.* **97** 067007 (2006)
262. Titov M, Beenakker C W J *Phys. Rev. B* **74** 041401(R) (2006)
263. Cuevas J C, Yeyati A L *Phys. Rev. B* **74** 180501(R) (2006)
264. González J, Perfetto E *J. Phys. Condens. Matter* **20** 145218 (2008)
265. Hagymási I, Kormányos A, Cserti J *Phys. Rev. B* **82** 134516 (2010)
266. Muzykantskii B A, Khmelnitskii D E *Phys. Rev. B* **50** 3982 (1994)
267. de Jong M J M, Beenakker C W J *Phys. Rev. B* **49** 16070 (1994)
268. Hessling J P et al. *Europhys. Lett.* **34** 49 (1996)
269. Averin D, Imam H T *Phys. Rev. Lett.* **76** 3814 (1996)
270. Dieleman P et al. *Phys. Rev. Lett.* **79** 3486 (1997)
271. Martin T *Phys. Lett. A* **220** 137 (1996)
272. Johnson M B *Phys. Rev.* **29** 367 (1927)
273. Nyquist H *Phys. Rev.* **32** 110 (1928)
274. de Jong M J M, Beenakker C W J, in *Mesoscopic Electron Transport* (Eds L L Sohn, L P Kouwenhoven, G Schön) (Dordrecht: Kluwer Acad. Publ., 1997) p. 225
275. Jehl X et al. *Phys. Rev. Lett.* **83** 1660 (1999)
276. Jehl X et al. *Nature* **405** 50 (2000)
277. Rowell J M, McMillan W L *Phys. Rev. Lett.* **16** 453 (1966)
278. Fauchère A L, Lesovik G B, Blatter G *Phys. Rev. B* **58** 11177 (1998)
279. Chen L Y, Ting C S *Phys. Rev. B* **43** 4534 (1991)
280. Landau L D, Lifshitz E M *Teoriya Polya* (The Classical Theory of Fields) (Moscow: Fizmatlit, 2006) [Translated into English (Oxford: Pergamon Press, 1980)]